Dissertation

Quantum Gravity, Extra Dimensions
and the Exact Renormalisation Group

Ausgeführt zum Zwecke der Erlangung des akademischen Grades eines
Doktors der technischen Wissenschaften
unter der Leitung von

em.o.Univ.Prof.DI.Dr. Wolfgang Kummer
Institut 136
Institut für Theoretische Physik

Eingereicht an der Technischen Universität Wien
Fakultät für Physik
von

Dipl.Ing. Peter Fischer
e9625103
Hormayrgasse 23, A-1170 Wien

Wien, 23.Mai 2005

Peter Fischer

Kurzfassung

Quanteneffekte der Schwerkraft, bereits an sich ein Feld tiefgehender und langandauernder Arbeiten, erfahren seit kurzem weiter verstärktes phänomenologisches Interesse. Dies rührt von kürzlich vorgeschlagenen feldtheoretischen Modellen mit großen zusätzlichen Dimensionen der Raumzeit her, Grund für die Untersuchung der quantisierten Theorie der Schwerkraft in diesem Zusammenhang.

Ein großes Hindernis für die erfolgreiche Quantisierung der Schwerkraft stellt ihre störungstheoretische Nichtrenormierbarkeit dar. Ein weit verbreiteter Ansatz zur Lösung dieses Problems besteht darin, über lokale feldtheoretische Grundlagen hinaus zu gehen, wie zum Beispiel in der String–Theorie. Ein alternativer Ansatz besteht in der Möglichkeit der nicht-störungstheoretischen Renormierbarkeit. Diese Möglichkeit wurde erstmals von Weinberg 1979 aufgezeigt und als asymptotische Sicherheit (asymptotic safety) im Rahmen der Renormierungsgruppe formuliert. In diesem Verständnis entspricht die nicht-störungstheoretische Renormierbarkeit einer Theorie dem Auftreten eines nicht-trivialen Fixpunktes ihrer Renormierungsgruppengleichungen.

Solch ein Fixpunkt wurde kürzlich für die vierdimensionale Schwerkraft gefunden. Dies wurde durch das Verwenden von Methoden der Exakten Renormierungsgruppe in der Näherung der Einstein–Hilbert Trunkierung möglich. Dieser Fixpunkt findet sich auch in erweiterten Trunkierungen, woraus sich Anzeichen für die asymptotische Sicherheit der vollen Quantentheorie der Schwerkraft in vier Dimensionen ergeben.

In dieser Dissertation wird nach entsprechenden Fixpunkten in höheren Dimensionen gesucht. Sie werden für einen weiten Bereich verschiedener technischer Hilfsgrößen, sogenannter cutoff-Funktionen, und Eichungen, gefunden. Ihre Stabilitätseigenschaften und universellen Eigenwerte werden untersucht. Die künstlichen Abhängigkeiten der physikalischen Ergebnisse von den genannten Hilfsgrößen stammt von der verwendeten Näherung, in diesem Falle der Einstein–Hilbert–Trunkierung. Ihre Analyse erlaubt eine Bewertung der Verläßlichkeit der erlangten Ergebnisse. Aufbauend auf diesen künstlichen Abhängigkeiten wird eine Methode zur Optimierung der cutoff-Funktionen vorgeschlagen. Es wird gezeigt, das sie zu erhöhter Verläßlichkeit der Ergebnisse führt. Sollten die Fixpunkte auch in erweiterten Trunkierungen erhalten bleiben, bedeutet dies die asymptotische Sicherheit und damit nichtperturbative Renormierbarkeit der Quantentheorie der Schwerkraft in höheren Dimensionen. Im Laufe dieser Fixpunktstudien zeigte sich, daß eine bestimmte cutoff-Funktion zu besonders hoher Verläßlichkeit führt. Diese optimierte cutoff-Funktion wird im weiteren dazu verwendet, um Lösungskurven der Renormierungsgruppengleichungen zu finden, die den gesamten Phasenraum der Kopplungen durchlaufen. Die so erhaltenen Phasenraumbilder werden explizit in vier Dimensionen diskutiert und klassifiziert. Dadurch lassen sich die universalen Eigenschaften des gesamten Flusses erschließen. Sowohl der Fixpunkt als auch die phänomenologisch relevante Lösungskurve befinden sich in einem Bereich des Phasenraumes, der zuverlässig in der Einstein–Hilbert Trunkierung beschrieben wird.

Ein Ausblick auf mögliche phänomenologische Folgen der asymptotischen Sicherheit der Schwerkraft für Modelle mit zusätzlichen Dimensionen der Raumzeit beschließt diese Arbeit.

Abstract

Quantum gravity has recently been brought into phenomenological focus by the advent of field theoretic models with large extra dimensions. This provides a motivation for its investigation in more than four dimensions in a field theoretic context.

A major obstruction to such a description has been the perturbative non-renormalisability of gravity. A prevalent resolution to this issue consists in going beyond local field theoretic concepts, most prominently in string theory. An alternative solution would be provided by gravity's *non*perturbative renormalisability. This notion has been formulated in the framework of the renormalisation group as "asymptotic safety" by Weinberg in 1979. It corresponds to the existence of a non-trivial fixed point in the renormalisation group equations of a theory.

Such a fixed point has recently been detected for gravity in four dimensions. This was achieved by using exact renormalisation group methods in a certain approximation, the Einstein–Hilbert truncation. It was reproduced in more general settings and shows evidence for the asymptotic safety of the full theory.

In this thesis we search for non-trivial fixed points in higher dimensions. They are reported for a wide range of regulators, the cutoff functions, and gauges. Their stability properties and universal eigenvalues are studied. The artificial dependence of physical results on these auxiliary quantities results from working in the approximation of the Einstein–Hilbert truncation. We study these dependences to analyse the reliability of the obtained results. A cutoff optimisation procedure is proposed and demonstrated to yield increased reliability of the fixed point results. If the fixed point persists within extended truncations, quantum gravity in extra dimensions is asymptotically safe, i.e. non-perturbatively renormalisable.

During the fixed point studies one particular cutoff function is seen to lead to particularly enhanced stability of the flow. This optimised cutoff function is used to find renormalisation group flows spanning the entire phase space of couplings. These phase space portraits are discussed and classified for four dimensions explicitly. This allows to extract the universal features of the flows. The fixed point and physical trajectory is seen to lie in a sector of phase space with good reliability of the Einstein–Hilbert truncation.

Phenomenological implications of the asymptotic safety scenario for models with extra dimensions are indicated.

Acknowledgements

Contents

List of Figures

List of Tables

Chapter 1

Introduction

In this introduction, we will briefly give some physical motivations for the study of higher dimensional quantum gravity and outline one key obstacle for the perturbative description, non-renormalisability, and a possible non-perturbative solution to that issue. An outline of the further content of this work concludes this introduction.

1.1 Motivation for Quantum Gravity

Nowadays it is common belief that our world is governed by the principles of quantum mechanics. This belief is founded on nearly a century of confirmation by experiment throughout physics and chemistry, and by commercial applications omnipresent in every-day life. All of matter and its interactions is ultimately described by fields obeying quantum theory. The standard model of particle physics gathers the principles, tools and (so far) basic constituents allowing the understanding of physical observations until now.

One force of Nature, however, has not yet received its quantum description. It is that part of Nature which is most prominent in every-day observation, from the falling of an apple to the rising of the Sun. It was the first, historically, to be investigated in what we now call modern science sense, in this sense giving birth to all of natural science. It seems that, as it was the first, gravity is also intent on being the last purely classical theory. It can be safely stated that to date no quantum theory of gravity has entered the textbooks as *the* universally accepted and experimentally confirmed one.

So far our search for a quantum theory of gravity is purely motivated by theoretical reasons: in contrast to the beginnings of quantum mechanics, where experiments were unexplainable with the theories then available, no experiment has yet detected any gravitational effects necessitating a quantum description. Nor did it seem probable until recently that such a test could be within reach in the near or intermediate future. This experimental inaccessibility is caused by the huge value of the energy for which quantum effects are expected to become important. This scale is given by the Planck mass, defined as $M_4 = \sqrt{\hbar c / G_N} = 1.22 \times 10^{19}$ GeV. Reverberations of the Big Bang seemed the only source of experimental evidence potentially accessible. In section 1.2 a novel set of models, raising hopes for the experimental accessibility of quantum gravity

in the nearest future, is described.

The expectation of the quantum Nature of gravity is, however, substantiated beyond a simple "rule of majority" [1] (3:1 for quantum) by the many incompatibilities the junction of an unquantised theory with a quantised one would entail. The possible violations of Heisenberg's principle of uncertainty would lead to unsurmountable paradoxes in that case. It is common belief that a successful union of quantum theory and gravity would require some notions and principles on one or both sides to be given up. The previous paragraphs took the point of view that gravity alone had to be adapted to quantum theory. But the reverse notion is entertained as reasonable.

Many attempts have been made to achieve a reconciliation of gravity with the other, already quantised theories. The most prominent one is without doubt string theory, but many other approaches have been investigated. Although much has been accomplished, none has yet achieved a true breakthrough into the textbooks as *the* correct one. The number of people and works investigating this topic is, although certainly finite, barely countable. For some references, see for instance [1], [2], [3]. In the end, experiment alone has to decide what description of gravitational phenomena ultimately is correct.

The approach followed in this thesis is that of an exact renormalisation group formulation of gravity. One main topic of this work is to apply it to more than four spacetime dimensions, a motivation for this being given in the following section.

1.2   Extra Dimensions

It was mentioned above that tests for the quantum nature of gravity seemed to be restricted to the realm of cosmology. Recently a class of models has been proposed, which opens the possibility for the detection of direct quantum gravitational effects in realistic collider experiments. For the most optimistic choices of parameters of these models, the LHC (due for completion in 2007) could turn into a veritable tool to investigate the basic structure of spacetime (in this context it has been called a "black-hole machine" [4], [5], [6]).

The new ingredient of these quantum field-theoretic models is the presence of large dimensions in addition to our observed four. Higher dimensional spacetimes have already been considered before. In physical models, they date back to the work of Kaluza and Klein. Most prominently, higher dimensions are inherent in (super)string theory, which requires ten spacetime dimensions. To reproduce the observed four-dimensional nature of spacetime, these universal extra dimensions are compactified at sufficiently small lengths. Hence these extra dimensions are small with respect to typical distances in particle physics.

Introducing four-dimensional *branes* [7] allows an increase in the size of extra dimensions considerably. A brane is a four-dimensional domain-wall configuration of a classical scalar field. Other fields, scalars, fermions and gauge bosons [8], can be bound to the brane by appropriate couplings. They show a four-dimensional behaviour at energies lower than the typical scale of the branes (brane width, binding energy), which has to be sufficiently above the energies of particle physics to comply with experimental constraints. The other dimensions can hence extend to sizes far larger than the

tested distances on the brane. Gravity must naturally extend into the entire bulk, since it describes the dynamics of spacetime itself. The experimental constraints on its higher-dimensional behaviour are weaker than those for the other elementary particles, confirming Newton's four-dimensional force law down to the hundred micrometre range [9].

Branes also emerge naturally in string theory and as solitons in its low energetic supergravity limit [10]. In that case, the characteristic scale of the brane is set by the string scale, related to the Planck mass.

Since the origin of the brane can only be resolved at energies at and above the brane scale, phenomenological field-theoretic models describing physics below this scale are equally valid for an underlying high energy field or string theory. The fundamental theory is only resolved at and above this scale.

The first model making use of these features was introduced in 1998 by Arkani-Hamed, Dvali and Dimopolous (the famous ADD model) [11]. In that setting, the extra dimensions are flat and compactified to a torus. One non-flat, "warped", compact extra dimension was introduced by Randall and Sundrum in 1999 (RSI model) [12], and shortly afterwards a version with an infinite extra dimension (RSII) [13] but, because of the warp factor, a finite extra volume. Extra dimensions with infinite volume have also been considered, starting with [14]. For other models, see for instance [15].

These models have many new, exciting physical consequences. One of the main motivations for the setup outlined above is that it can provide a natural solution to *the hierarchy problem*[1] [11]. This term refers to the large difference between the mass scale of the standard model of particle physics, which lies around 115 GeV and is set by the mass of the scalar Higgs field, and the scale of the unknown, fundamental theory which seems to lie at the Planck mass. The Higgs mass receives large quantum corrections which would increase it to the scale of the more fundamental theory expected to set in at the Planck scale, cf. section 1.1. To keep it as low as, e.g., 115 GeV requires a large amount of fine tuning of the bare parameters of the theory. One of the most prominent attempts to solve this problem is supersymmetry.

The key observation for its resolution in models with large extra dimensions is that gravity extending into dimensions forbidden to the other fields is diluted by the extra volume available. Its true scale of coupling, denoted by the fundamental Planck mass M_d in d-dimensional bulk space, is related to the observed, effective four-dimensional scale of gravitational coupling, given by the four-dimensional Planck mass $M_4 \approx 10^{19}$ GeV, in the ADD model, by [11]

$$(M_4)^2 = L^{d-4} (M_d)^{d-2} . \tag{1.1}$$

L is the size of the flat, compact extra dimensions. This relation is obtained by comparing the actions of four-dimensional gravity and the higher-dimensional one for distances far larger than L, or, alternatively, the point mass potentials in the two cases for the

---

[1]Unnatural differences in scales within one physical theory are referred to as *a* hierarchy problem. The article *the* is usually reserved to the one outlined in the main text. Other well-known issues of this type compromise the large differences in fermionic masses or, the largest hierarchy yet observed, the sixty orders of magnitude difference between the Planck mass and the cosmological constant.

same limit. If L is significantly larger than M_d^{-1}, (1.1) yields a large apparent hierarchy for moderate d. With two flat extra dimensions, M_d can be as low as a few TeV for L close to the experimental bounds. Hence, there is no large hierarchy between particle physics and gravity: the typical scales of both can be brought to the same one or two orders of magnitude around a TeV.

The arising issue of the freshly introduced hierarchy between L and M_d is addressed in the Randall–Sundrum models [12], [13]. There, curvature of the single extra dimension induces an exponential "warp factor" between M_4 and M_5. The large hierarchy between them can hence result from a moderate exponent, avoiding the introduction of large ratios.

As in four dimensions, the fundamental, high energy theory of gravity is expected to become important at this "true" Planck scale, M_d. Accordingly, it may give rise to new phenomena already at the TeV scale, which will be opened to experimental research in the very near future. This exciting possibility has sparked off great phenomenological interest into models of extra dimensions. Further theoretical developments have increased interest even more.

For example, for energies approaching M_d, the fields localised on the brane start to experience the extra dimensions. The gauge couplings accordingly change their running behaviour [16] and unification of the standard model gauge couplings is possible near M_d [17]. Electroweak symmetry can be broken dynamically if the standard model gauge fields and third-generation quarks propagate in TeV size extra dimensions [18]. The recently observed accelerated expansion of the Universe, usually attributed to a cosmological constant of very small value, and hence causing the cosmological constant (hierarchy) problem, can be explained in models of infinite-size extra dimensions as a higher-dimensional effect [14].

The arising phenomenology of the proposed models includes astrophysical, cosmological, and accelerator-physics effects, see for example [15], [19], [6], [139]. Gravity enters these phenomenological considerations as a classical field theory, since its quantum theory is wanting, as discussed in section 1.1. Although string theory is a possible candidate for it, the lack of a definite version containing the standard model prevents its application to these phenomenological studies. Hence, field-theoretic calculations in this setting are only trusted for relevant energies below M_d [20], [136], [139]. High energy corrections due to gravity are incalculable. But tree-level virtual graviton exchanges at lower energies, too, necessitate the introduction of an ultraviolet regulator of the order of M_d. Real graviton emission shows unbounded growth of cross sections with energy [20].

It can be concluded that the introduction of models with large extra dimensions and TeV-range Planck mass have greatly enhanced the phenomenological need for a field-theoretic description of gravity that would be valid beyond the Planck scale.

However, it must be mentioned that the increased formation of black holes is expected to dominate for centre-of-mass energies above M_d [4], [5]. This is widely considered as a (perhaps even fundamental) veil, hiding the direct signs of trans-Planckian physics [5]. Nevertheless, even if the high energetic manifestations of the fundamental theory of spacetime remain hidden, their M_d effects should still be important.

1.3 Perturbative Non-Renormalisability

The main obstacle for a field-theoretic formulation of quantum gravity is that gravity is perturbatively not renormalisable. This means that at each order in perturbation theory divergences with new analytic and tensorial structures arise. To remove these infinities, new interactions and couplings have to be introduced at each order. Completing the perturbative expansion yields an infinite number of interactions and coupling constants. Since these constants have to be fixed by experiment, the theory looses predictive power.

The perturbative non-renormalisability of gravity had already been suspected by Heisenberg (1939) from a power counting argument and the negativity of Newton's constants mass dimension [21], [22]. The confirmation by explicit quantum field-theoretic calculations was only possible after the covariant Feynman rules for gravity were found by Feynman [23] and DeWitt [24] in the 1960's. The one-loop diagrams of pure gravity and gravity coupled to matter were calculated in the following decade by 't Hooft, Veltman, Deser, Nieuwenhuizen and others [25], [26], [27], [28]. The divergences in pure gravity could still be removed. In the presence of matter degrees of freedom, this is no longer possible. However, pure gravity is also found to be non-renormalisable at the two-loop level, see Goroff and Sagnotti (1985) [29], [30] and [31].

The long span of time between each of the above results bears witness to the tremendous technical and conceptual effort involved to establish the validity of the initial suspicion. Hence, we will restrict ourselves to a short, heuristic power counting argument [32] to further explicate gravity's perturbative non-renormalisability.

For an interacting theory with coupling g, the maximal, superficial degree of divergence of the nth order perturbative contribution G_N^n to the correlator of fields $\phi(x)$ at N points x_i, $G_N := \langle \phi(x_1) \dots \phi(x_N) \rangle$, can be determined by counting the power of momenta to be integrated over in the corresponding expression. Since this result is potentially divergent, the integrals have to be regularised. This is done by the common upper momentum cutoff Λ. For an expression to be finite, the limit $\Lambda \to \infty$ has to be defined. The result of these standard textbook considerations [33], [34] is that the maximal degree of divergence of the Fourier transform $\tilde{G}_N^n$ of the N-point correlator is given by

$$\tilde{G}_N^n \sim g^n \, \Lambda^{c_N - n \, d_g} \, . \tag{1.2}$$

Here c_N is a number independent of the order n: it depends only on the dimension d of spacetime and the considered type of amplitude. In the simplest case of a scalar theory it equals $d - N(d-2)/2$. Generally, c_N is positive only for a finite number of $\tilde{G}_N$'s; d_g is the mass dimension of the coupling, $d_g := [g]$, and its sign is of critical importance: if d_g is positive, the exponent $c_N - n\,d_g$ will be negative for all orders $n > \max(c_N, 0)/d_g$. The cutoff can be removed in these cases without yielding any divergences, these $\tilde{G}_N^n$ are finite. Hence only a finite number of correlator functions (those for which $c_N > 0$) will receive a finite number of divergent contributions. The divergences of these correlators can be absorbed by redefining – normalising – a finite number of couplings. Only these couplings have to enter the theory as free parameters. Such theories are consequently renormalisable.

For the case $d_g = 0$ (e.g. QED, QCD), div- or convergence of (1.2) is independent of

the order and depends solely on c_N. Since it is positive for a finite number of amplitudes only, their divergences can be absorbed into a finite number of couplings and these theories are also perturbatively renormalisable.

The third possible case, $d_g < 0$, is realised for gravity in any spacetime with more than two dimensions, since the mass dimension of Newton's constant is $[G_N] = 2 - d$. Here, the exponent of the cutoff will grow monotonically with order n. Regardless of c_N it will become positive for sufficiently high n. Hence any correlator G_N will eventually receive divergent contributions. This infinity of infinities would necessitate an equal number of couplings to be renormalised in the limit $\Lambda \to \infty$, rendering the theory meaningless in this limit. Any theory with couplings of negative mass dimensions, in particular gravity, is considered as perturbatively not renormalisable.

A derivation of (1.2) alternative to the standard one is given in appendix 1.3. A more detailed discussion of some subtleties arising for gravity are discussed, e.g., in a pedagogical work by Deser [35]. The conclusion of gravity's power counting non-renormalisability is not affected by these modifications.

However, the simple power counting estimate neglects the symmetries of the theory that generically lower the degree of divergence. Whereas for renormalisable theories it guarantees the success of the full calculation, failure of perturbative renormalisability does not necessarily follow from power counting non-renormalisability. A good example for the impact of symmetries provides gravity itself: as mentioned above, general relativity without matter fields is found to be perturbatively renormalisable at one loop. Only at two loops do divergent terms not absorbable by the original action appear. It is, however, highly unlikely for a finite number of symmetries to take care of infinitely many divergences. So even though they improve the situation at each order, it is very probable that the power counting estimate will prevail in the end.

1.4   Asymptotic Safety

Even though gravity is perturbatively not renormalisable, it is still an excellent effective theory at energy scales far below the Planck mass, gravity's "natural" scale. It describes Nature exceptionally well at the large scales of the solar system, stars and apples, down to the experimentally tested submillimetre range. Augmented with the appropriate matter and energy contents of the Universe, it allows a consistent description of the entire cosmos. At these very large distances (with respect to the Planck length), the higher-derivative interactions generated by local quantum effects are vanishingly small. Effective field theory [36], [37] techniques yield reliable predictions for non-local quantum effects at these scales; see [38], [39], [40], [41] and references therein. Such an understanding and treatment is believed to hold up to the scale set by Newton's constant, the Planck mass, $M_{\text{Planck}} \approx 10^{19}$ GeV. Up to this energy Einstein's equation should describe gravitational interactions with very high precision.

The properties of a supposed "more fundamental" quantum theory of gravity are hidden in the parameters of the effective theory, general relativity. It is only at energies nearing the Planck scale that this fundamental theory can be experimentally resolved.

This way of reasoning reflects precisely the way science ascended the energy ladder

of matter's nature – from molecules to atoms to nuclei to nucleons to quarks to . . . – in the last one and a half centuries; however, even the first step is very much higher for gravity than for matter[2]. In this sense, gravity is an extremely good effective field theory [40].

Until experimental evidence pertaining to the next step is procured, no judgement as to its nature can be made and all consistent possibilities can be, should be and are investigated. One hope is that already the first step leads to *the* fundamental theory of gravity, which holds true for arbitrarily high and ultimately infinite energies being truly renormalisable.

Most candidates for such a UV completion of gravity, such as string theory, loop quantum gravity, field theory on non-commutative spacetime, supergravity, composite gravitons, etc., have in common that they alter some of the concepts of gravity as a perturbatively treatable local quantum field theory of the metric (or equivalent) degrees of freedom. Locality, degrees of freedom of gravitational interaction, procedure of quantisation or the nature of spacetime itself are often abandoned or modified. In this thesis we follow a conceptually quite conservative scenario, originally proposed by Weinberg in 1979 [42]. All of the underlying concepts used in the perturbative and effective description of gravity are kept unchanged. It is the perturbative treatment that is generalised to a non-perturbative one. Before introducing the tool used to this end, the exact renormalisation group, in section 2.1, and applying it to gravity in section 2.2, we give Weinberg's [42] generalisation of perturbative renormalisability, *asymptotic safety*. Having formulated such a notion is paramount to judging whether a possible UV completion of gravity has been detected.

The first key observation [42] is that the running, energy dependent couplings of consistent perturbatively renormalisable theories tend to zero in the UV-limit of asymptotically high energies. The energy dependence of the couplings is described by the equations of the *renormalisation group* (RG) [43], [44]. Accordingly, this vanishing of the couplings corresponds to the existence of a UV *fixed point* (FP) of the RG equations of the couplings, their β-functions, at vanishing couplings. This behaviour is known as *asymptotic freedom*, the theory becomes non-interacting, a.k.a. free, for asymptotically high energies (renormalisation scales). The FP of such a free theory is called a trivial or *Gaussian* one[3].

The second key observation is that from the RG point of view, there exists no conceptual difference between Gaussian and non-Gaussian FPs. A theory with such a non-Gaussian UV FP remains well-defined to arbitrarily high energies. Its FP limit is a candidate for its UV completion. If the FP is furthermore attractive for a finite number of (linear combinations of) couplings in the UV, only a finite number of free parameters remain. The theory can than be considered renormalisable in the general sense; it is called asymptotically safe [42].

The non-perturbative renormalisability of perturbatively non-renormalisable quantum field theories has been shown for several examples where non-Gaussian UV FPs

---

[2]This discrepancy in scales can be seen as one of the manifestations of the hierarchy problem.

[3]For vanishing couplings, the action is only quadratic in the degrees of freedom. The corresponding path integral is hence Gaussian.

according to asymptotic safety were discovered. The asymptotic safety scenario was applied to gravity in $2 + \varepsilon$ dimensions in the same work where it was introduced [42]. This allows – via dimensional continuation – to use perturbative calculations near two dimensions. A non-Gaussian UV FP [4] complying with asymptotic safety is discovered.

Also in $2 + \varepsilon$ dimensions, the non-linear σ-model was shown to be renormalisable by Brezin and Zinn-Justin [45]. It was found to possess a non-Gaussian FP, in accordance with asymptotic safety. In addition to small-ε expansion, Wilsonian RG methods were employed.

A third example is provided by the Gross–Neveu model [46]. Its non-perturbative renormalisability in $2 + \varepsilon$ spacetime dimensions is demonstrated in [47] and in $2 + 1$ in [48]. Again, Wilsonian RG methods lead to the detection of a non-Gaussian FP.

In all four instances a small parameter was available, allowing for analytic treatment different from perturbation theory in the coupling. The importance of Wilsonian RG techniques for the detection of the FP became apparent in the last three applications.

The rest of this section is dedicated to illustrating the asymptotic safety scenario with Weinberg's original derivation. This gives us the opportunity to introduce the concept of the stability matrix and fix some notation. We will also convince ourselves that the asymptotic safety scenario indeed allows us to extend the scientific method – to yield falsifiable predictions for future experiments from past measurements – into the non-perturbative regime.

Considering some effective field theory, one assumes to know the infinitely many RG β_i-functions describing the renormalisation scale μ dependence of the infinitely many couplings G_i. Since the renormalisability of the theory has yet to be established, an effective field-theoretic description containing all local operators constructable from the given fields and consistent with demanded symmetries must be the starting point. The coefficients of these operators are the couplings G_i, which carry appropriate mass dimension d_i. Let us introduce the corresponding dimensionless couplings and β-functions by separating out this momentum scale:

$$g_i(\mu) := \mu^{-d_i} G_i(\mu) \quad , \quad \beta_i(g_j(\mu)) := \mu \, \partial_\mu g_i(\mu) = (-d_i + \mu \, \partial_\mu) G_i(\mu) \, . \tag{1.3}$$

The FPs of this system of equations are found by solving the (infinite) system of FP equations, i.e. demanding the simultaneous vanishing of the β-functions of the dimensionless couplings at the FP values g_i^*:

$$\beta_i(g_j^*) = 0 \quad \forall i \, . \tag{1.4}$$

At a FP, the dimensionless coupling constants are scale-independent. This allows well defined calculations even in the limit $\mu \to \infty$, i.e. to take the UV limit of the theory. Why do we search for a FP of the dimensionless couplings and not of the original, dimensionful ones? Ultimately we want to take the limit of infinitely high momenta or infinitely small wavelengths. In a local theory, all other scales become irrelevant in this limit. Hence μ remains the only dimensionful quantity in the theory in its so-called

---

[4]With Newton's constant at the fixed point $G^{\mathrm{FP}}_{\mathrm{Newton}} \sim \varepsilon$ being perturbative in dimension.

scaling regime[5]: all quantities have an energy dependence determined by their mass dimension. Thus it must be the dimensionless couplings, that attain a fixed value, and not the dimensionful ones, which behave like $G^i(\mu) = \mu^{d_i} g^i_*$ in the scaling FP regime.

Having identified one (or more) FP we ask for its relevance to couplings at finite scales, off their FP values. Since they are scale-dependent, they may approach the FP for a certain set of initial values. If this is the case, these RG *trajectories* in coupling space connect couplings at low, IR scales to well-defined UV values in the FP. Each such trajectory corresponds to a theory with a well-defined and predictive UV limit. Such theories are renormalisable in the general sense.

To determine the set of initial conditions of trajectories attracted to the FP, we must investigate the stability properties of the β-function system around it. In perturbative theories with one coupling (e.g. QED, QCD), this is determined by the sign of $\partial\beta/\partial g$ evaluated at the FP. A negative sign implies that the coupling is attracted toward its FP value for increasing μ, the FP is UV-attractive. This is the case in QCD whereas the positive sign in QED indicates a UV-repulsive but IR attractive-FP. Only the Gaussian UV-attractive FP of QCD guarantees the consistent perturbative renormalisability of the theory.

In case of more than one coupling, the corresponding quantity to be studied is the *stability matrix* at the FP:

$$\theta_{ij} := -\left.\frac{\partial\,\beta_i}{\partial\,g^j}\right|_{g^i_*}.$$ (1.5)

The minus sign is convention. In terms of the stability matrix, in the neighbourhood of the FP the couplings behave to first order as

$$\mu\,\partial_\mu\,g^i(\mu) \approx \sum_j \theta_{ij}(g^j_* - g^j_k)\,.$$ (1.6)

These linearised equations have the general solutions

$$g^i(\mu) \approx g^i_* + \sum_n C_n\,V^n_i\,\mu^{-\theta_n}\,,$$ (1.7)

where V^n_i and θ_n are the eigenvectors and eigenvalues of θ_{ij},

$$\sum_j \theta_{ij}\,V^n_j = \theta_n\,V^n_i\,.$$ (1.8)

The C_n are constants of integration to be fixed, ultimately, by experiment. If the theory is to have predictive power, the number of these constants must be finite. This reduction of the constants of integration of an infinite system of linear differential equations to a finite number is effected by imposing auto-consistency of the solutions in the UV limit of μ: if we demand $\lim_{\mu\to\infty} g^i(\mu) = g^i_*$, the constants C_n corresponding to negative

---

[5]Locality of the theory is essential for this to hold. In fundamentally non-local theories such as field theories on non-commutative spacetime, this argument fails and UV–IR mixing phenomena occur. Since our aim is to formulate a local quantum field theory of gravity, we are are safe from this per telum.

eigenvalues $\theta_n < 0$ have to vanish identically. For all non-zero values, the couplings would otherwise diverge instead of approaching their FP values. Only the C_n's corresponding to non-negative θ_n's have to be fixed by hand (experiment). If the number of such eigenvalues is finite, a finite number of experiments suffices to completely define the theory. This is the non-perturbative version of renormalisability introduced by Weinberg as asymptotic safety. It is assumed to hold for the rest of the discussion.

The eigenvectors V_i^n of positive stability matrix eigenvalues θ_n, together with the FP, define a hyperplane in the infinite-dimensional "theory space" spanned by all allowed operators. The dimension of this *UV-critical surface* is equal to the number $\mathcal{D}$ of such $\theta_n \geq 0$. The linearised solutions of the RG trajectories (1.7) hold only infinitesimally close to the FP. However, the dimension of the hypersurface spanned by those trajectories, which asymptotically approach the FP, is necessarily equal to $\mathcal{D}$, that of its tangent plane through the FP.

Asymptotic safety can be restated as the existence of a finite-dimensional UV-critical surface (which implies the existence of a FP defining this surface) in a given theory space. All trajectories on this surface correspond to non-perturbatively renormalisable theories, in a theory space defined in turn by its degrees of freedom and the imposed symmetries.

Note that the above argument can also be applied with reversed signs to the IR limit $\mu \to 0$ of the theory, identifying a stable IR FP of the theory, which allows an analysis of the phase transitions of the full quantum effective action. This will not be further discussed in the present work.

Let us briefly restate an argument of Weinberg [42] showing how perturbative power-counting renormalisability is contained in the framework of the general FP analysis.

The β-functions and the stability matrix have the general form

$$\beta_i = -d_i g^i(\mu) + \text{quantum corrections} \tag{1.9}$$

$$\theta_{ij} = d_i \delta_{ij} + \text{quantum corrections}. \tag{1.10}$$

In perturbation theory the quantum corrections of (1.10) are just the loop contributions. For perturbation theory to hold, they must be bounded and small with respect to the first term. At a perturbative, i.e. Gaussian, FP, all couplings vanish simultaneously. Hence the loop contributions, which are polynomials in the couplings, vanish too. The eigenvectors of $\theta_{ij} \equiv d_i \delta_{ij}$ are orthonormal and parallel to the axes of the couplings. Stability is solely governed by the mass dimension of the couplings: for $d_i > 0$ the direction is UV-stable and the corresponding coupling requires fixing by experiment whereas, for $d_i < 0$, the unstable coupling is forced to its Gaussian FP value zero. These are precisely the perturbatively relevant and irrelevant couplings. In a perturbatively renormalisable theory lying on the UV-critical surface, only couplings relevant and marginal at the FP can occur [6].

From (1.10) one can also construct a heuristic argument for the finiteness of the dimensions of the UV-critical surface of theories endowed with a non-Gaussian FP, again

---

[6]For marginal couplings $d_i = 0$, stability is purely quantum governed and requires treatment beyond linear order. Since our application, quantum gravity, contains only perturbatively relevant and irrelevant couplings, we omit the discussion that this important case deserves.

following Weinberg. In this case the quantum corrections in (1.10) do not vanish. For local theories, $d_i \leq d$, but not bounded from below. For asymptotic safety to fail, an infinite number of stability matrix eigenvalues must be positive. This would require the quantum corrections to infinitely many θ_{ij}'s to cancel d_i, which decreases unboundedly, ultimately diverging. One would have to imagine a quite pathological theory for this to happen. Hence the UV-critical surface is generically expected to have a finite number of dimensions. Given the existence of a FP, asymptotic safety can be viewed rather as the rule than the exception.

An important notion is that of *universal quantities*. These quantities are independent of the regularisaion used, i.e. the way μ is defined. An important example for such a universal quantity is that of the eigenvalues of the stability matrix, θ_n. The β_i, and accordingly their FP solutions g_*^i and the stability matrix θ_{ij}, depend on the definition of μ. The eigenvalues, however, are independent of transformations of the couplings and hence changes of the flow. This follows straightforwardly from the definition of θ_{ij} and the properties of the determinant.

1.5 Outline of the Thesis

The main aim of this thesis is to demonstrate that evidence for gravity's non-perturbative renormalisability, discussed previously in four dimensions, can be procured in higher dimensions too. This property is crucial with a view to a reliable description of gravity at energies above the Planck mass.

Some motivation for the field-theoretic formulation of quantum gravity in higher dimensions was provided in sections 1.1 and 1.2. In section 1.3 the main obstacle for a quantum field formulation of gravity, perturbative non-renormalisability, is illustrated by a short power-counting argument. The notion of non-perturbative renormalisability is introduced as asymptotic safety à la Weinberg, see section 1.4. It requires the existence of fixed points of the renormalisation group.

The renormalisation group formulation of gravity used throughout this thesis is provided by the *exact renormalisation group* (ERG). The formulation of an ERG description of quantum gravity is the main topic of chapter 2. After describing ERG in section 2.1 and defining a cutoff optimisation procedure in section 2.1.1, we repeat the original application of the ERG to Einstein–Hilbert gravity in section 2.2. Fixed points, indicating asymptotic freedom, detected so far in this framework are discussed in section 2.3. The phenomenological, cosmological implications of these previous results are listed in section 2.4.

Our own results are given in chapters 3, 4 and 5. In chapter 3, the cutoff dependence of fixed points is studied in dimensions 4 to 10. Previous extra-dimensional FP results suffered from a large dependence on the implementation of the cutoff. We demonstrate how these spurious dependences can be removed by our cutoff optimisation scheme in section 3.1 and show that the physical results obtained in this way are maximally reliable in section 3.2. These conclusions are further confirmed by comparing different types of cutoff, see section 3.3.

In chapter 4 we demonstrate that the spurious dependence on the gauge fixing parameter present in the approximation we used only has a quantitative impact and is further reduced by cutoff optimisation. After repeating the FP analysis for now general gauge fixing in section 4.1, the gauge dependence of universal quantities is studied in section 4.3. The large gauge dependence of the dimensionless combinations of couplings for large values of the gauge-fixing parameter is noted, explained, discussed and interpreted as an indication for a possibly profitable extension of the approximation. The good independence of the type of cutoff used is presented in section 4.4; it further strengthens our confidence in the reliability of the obtained results in higher dimensions.

During the analysis of the previous two chapters, one specific cutoff has proved maximally reliable in a consistent fashion. This cutoff furthermore allows analytic studies of the system of equations. In chapter 5 these advantageous properties are used to present a detailed analysis of the entire four-dimensional phase space. This is preluded by an analytic study of fixed points in arbitrary dimensions and gauge fixings in section 5.2, supplementing the numerical findings presented in the previous parts of this thesis. The explicit numerical solution and analytical discussion of the entire phase space is performed in section 5.3 for one choice of gauge fixing and in section 5.4 for another. A similar study has been done previously, and we compare its results with our own findings in section 5.5.

Chapter 6 contains the summary of our results together with indications of their implications. Furthermore, possible directions for future research are mentioned.

Appendix A gives a more detailed version of the power-counting argument presented in section 1.3. There, we give a derivation of the superficial degree of divergence alternative to the textbook variant. To the best of our knowledge, this argument has not been presented anywhere else. Appendix B lists the classes of cutoff functions used in this work. In appendix C the lengthy general flow equations of Einstein–Hilbert ERG gravity are given.

Chapter 2

Non-perturbative Quantum Gravity

2.1 Exact Renormalisation Group

The instances for asymptotic safety mentioned in section 1.4 already indicated that Wilsonian RG methods are well suited for the study of theories with non-trivial UV structure. In the Wilsonian RG [49], [50], [51], [52], the quantum fluctuations of field modes with euclidean momenta belonging to successive momentum-shells are included into the coupling constants of a theory. This coarse-graining procedure generates a Wilsonian flow of the action. The renormalisation scale is given by the euclidean momentum-radius of the shells.

One formulation of this method particularly apt for non-perturbative applications [53] is the *exact renormalisation group* (ERG). ERG was obtained by Wetterich by coarse-graining an effective average action [54] as a continuous analog of the discrete Kadanoff block-spin transformation [55]. It generates an exact flow for the action which interpolates between an initial, bare action and the full quantum action, which contains all quantum effects induced by the fluctuations of the degrees of freedom of the theory at hand. The ERG flow equation can be obtained from the path integral (PI) by successively integrating out the momentum-modes of the degrees of freedom [56]. This is effected by introducing a cutoff-term quadratic in the fields into the PI, which acts as an IR regulator. A comparison of ERG and other Wilsonian RGs, among them Polchinski's RG [57], can be found in [58] and [53].

Let us briefly repeat the PI derivation of the ERG flow equation [56] for the simplest case, a one component, real scalar field ϕ. The starting point is some bare microscopic action Γ_Λ, which describes physics at the high energy (small distance) scale Λ. For a renormalisable theory one can remove the UV cutoff $\Lambda \to \infty$ and identify the bare action with the classical one, $\lim_{\Lambda\to\infty} \Gamma_\Lambda = S_{\mathrm{cl}}$. Otherwise, Γ_Λ can be a microscopic effective action, given by a local operator expansion with dimensionful coefficients of the appropriate order of Λ. It contains all quantum fluctuations from unspecified physics above Λ, but those from lower momenta have not yet been included.

ERG describes how to obtain an effective action Γ_k at finite renormalisation scale $0 \le k \le \Lambda$ from Γ_Λ. For Γ_k to describe an effective field theory at scale k, all quantum effects from energies between k and Λ have to be included into it. In the PI, this

corresponds to integrating out all momentum modes of the fields with momenta between these two scales, whereas those with momenta lower than k remain unintegrated as the effective degrees of freedom. This separation of the degrees of freedom into high-momentum ones to be integrated out and unintegrated low-momentum ones is effected by adding a term quadratic in the fields to Γ_Λ in the (euclidean) PI:

$$\Gamma_\Lambda \rightarrow \Gamma_\Lambda + \Delta S_k\,, \qquad \Delta S_k := \frac{1}{2} \int d^D q\, \phi(-q) R_k(q^2) \phi(q)\,. \tag{2.1}$$

The momentum cutoff function $R_k(q^2) > 0$ serves as an IR cutoff at the scale k. It is large for $q^2 < k^2$ and small for $q^2 > k^2$. More precisely, we impose

$$\lim_{q^2/k^2 \rightarrow \infty} R_k(q^2) \sim e^{-q^2/k^2} \rightarrow 0\,, \tag{2.2}$$

$$\lim_{q^2/k^2 \rightarrow 0} R_k(q^2) > 0\,. \tag{2.3}$$

The UV cutoff Λ of the bare action can be included into R by further demanding

$$\lim_{k \rightarrow \Lambda} R_k(q^2) \rightarrow \infty\,. \tag{2.4}$$

This allows to formally extend the path integral integration to modes of infinitely high momenta, since ΔS_k will reduce the contribution of all modes above Λ to zero by virtue of (2.4). In the case of renormalisable theories, condition (2.4) can be implemented implicitly by $R_k(q^2 \ll k^2) \sim k^2$. Since Λ is removed in that case, it does not enter explicitly. This is the case for the topic of this thesis and hence Λ does not appear in the perused cutoff functions, cf. appendix B.

The PI of the effective action with the cutoff term and the usual source term $j \cdot \phi = \int d^D q\, j(-q) \phi(q)$ defines the generating functional $Z_k[j]$ with a finite IR-cutoff:

$$Z_k[j] := \int \mathcal{D}\phi\, e^{-\Gamma_\Lambda - \Delta S_k + j \cdot \phi}\,. \tag{2.5}$$

From (2.2) it follows that the high momentum modes contribute unsuppressed to the PI, whereas (2.3) leads to a damping for the low momentum ones with $\exp(-\Delta S_k)$. Hence, in Z_k the quantum fluctuations with momenta above k are integrated out, while those with lower momenta do not contribute, implementing the Wilsonian RG concept.

(2.2) implies $\lim_{k \rightarrow 0} Z_k = Z$, the full generating functional containing all quantum effects. The logarithm of Z_k is the (cutoff) generating functional of the connected Green functions, $W_k[j]$. The effective expectation values $\bar\phi_k(q)$ of the fields are obtained by varying $W_k[j]$ after the source

$$\bar\phi_k(q) = \langle \phi(q) \rangle_k = \frac{\delta W_k[j]}{\delta j(q)}\,, \tag{2.6}$$

and the (cutoff) two-point function $G_k(q, q')$ is given by

$$G_k(q, q') = \frac{\delta^2 W_k[j]}{\delta j(q)\, \delta j(q')} = \langle \phi^T(q) \phi(q') \rangle - \bar\phi_k(q) \bar\phi_k(q')\,. \tag{2.7}$$

The high momentum modes of $\bar{\phi}_k(q)$ are essentially identical to the usual mean fields obtained from the full generating functional Z, whereas the low momentum modes remain quantum, $\bar{\phi}_k(q < k) \approx \phi(q < k)$.

The (cutoff) generating functional of the one-point-irreducible Green functions $\bar{\Gamma}_k[\bar{\phi}_k]$ is defined as the Legendre transform of W_k with respect to the sources:

$$\bar{\Gamma}_k[\bar{\phi}_k] := -W_k[j] + j \cdot \bar{\phi}_k. \tag{2.8}$$

Varying $\bar{\Gamma}_k$ twice after the effective fields, multiplying it with (2.7) and using (2.6) yields the cutoff version of a well-known identify, where $\delta^d(x)$ is the d-dimensional Dirac-delta functional:

$$\int d^d q' \, G_k(q, q') \, \frac{\delta^2 \bar{\Gamma}_k}{\delta \bar{\phi}_k(q') \, \delta \bar{\phi}_k(q'')} = \delta^D(q + q''). \tag{2.9}$$

After these adaptations of usual definitions to the case with the cutoff, the actual derivation of the ERG flow equation is straightforward. Let us take the derivative of $\bar{\Gamma}_k$ with respect to the IR-cutoff k for fixed $\bar{\phi}_k$ and trace the k-dependence back to its source $R_k(q^2)$:

$$\frac{\partial}{\partial k} \bar{\Gamma}_k \Big|_{\bar{\phi}_k} = -\frac{\partial}{\partial k} W_k[j] = -\frac{\partial}{\partial k} \ln Z_k[j] = Z_k^{-1} \int \mathcal{D}\phi \left(\frac{\partial}{\partial k} \Delta S_k \right) e^{-\Gamma_\Lambda - \Delta S_k - j \cdot \phi}$$

$$= \frac{\partial}{\partial k} \langle \Delta S_k \rangle = \langle \frac{1}{2} \int d^D q \, \phi(-q) \phi(q) \frac{\partial}{\partial k} R_k(q^2) \rangle$$

$$= \frac{1}{2} \int d^D q \left[G_k(-q, q) + \bar{\phi}_k(-q) \bar{\phi}_k(q) \right] \frac{\partial}{\partial k} R_k(q^2). \tag{2.10}$$

Defining the *effective (average) action* $\Gamma_k[\bar{\phi}_k]$ as

$$\Gamma_k[\bar{\phi}_k] := \bar{\Gamma}_k[\bar{\phi}_k] - \frac{1}{2} \int d^D q \bar{\phi}_k(-q) \bar{\phi}_k(q) R_k(q^2), \tag{2.11}$$

and using (2.9) we finally arrive at the ERG equation

$$\boxed{\frac{\partial}{\partial k} \Gamma_k = \frac{1}{2} \mathrm{Tr} \left(\Gamma_k^{(2)} + R_k \right)^{-1} \cdot \frac{\partial}{\partial k} R_k.} \tag{2.12}$$

$\Gamma_k^{(2)}$ is the second derivative of the effective action with respect to the fields. The inverse of the full cutoff propagator, $\Gamma_k^{(2)} + R_k$, has to be understood through (2.9). In the case of a one component, real scalar field the Trace stands for equating the two momentum arguments in $\Gamma_k^{(2)}$ and integrating over the remaining one, $\int d^d q$.

Before turning to generalisations to other fields, we discuss the universal structural properties of (2.12). It is a one-loop equation for the full non-perturbative propagator and differential in the cutoff k. Integrating (2.12) with respect to k corresponds to re-summing the complete loop expansion in the perturbative calculation. By expanding the denominator in the couplings, one re-obtains perturbation theory [59], [60]. The nominator renders it local in momenta: due to the properties (2.2) and (2.3) the derivative $\partial_k R_k$ vanishes for momenta much lower and higher than the cutoff scale k. It acts

as a kind of smeared-out delta-function. Hence it is necessarily UV-finite, the UV cutoff Λ does not enter (2.12) explicitly. As long as $k > 0$, it remains also IR-finite even for gap-less theories. Since (2.12) is differential in the cutoff, it can be used to go to higher as well as lower k. It allows to integrate modes "in" and "out". (2.12) is an exact equation, no approximations have entered so far. It generates an *exact flow* for the effective action Γ_k. This means that the limits $k \to 0$ and $k \to \Lambda$ yield the full effective quantum and the bare action, respectively:

$$\lim_{k \to 0} \Gamma_k = \Gamma \quad , \quad \lim_{k \to \Lambda} \Gamma_k = \Gamma_\Lambda . \tag{2.13}$$

That the present scheme fulfils these requirements follows from the properties of the momentum cutoff function, (2.2) and (2.4). (2.2) implies that ΔS_k vanishes in the limit $k \to 0$. All definitions and calculations turn to usual ones without a IR-cutoff and one obtains the definition of the full effective quantum action Γ. On the other hand, (2.4) makes the classical saddle point approximation of the PI exact in the limit $k \to \Lambda$. This yields the validity of the second limit (2.13) for ERG.

ERG flows connect the bare action continuously to the full quantum action [60]. This mapping is independent of the implementation of $R_k(q^2)$, which has not been specified further than by (2.2)–(2.4). For different functions R_k, R_k', however, the effective actions at any intermediate scale $0 < k < \Lambda$ can, and generally will, differ. For different cutoffs, the trajectories of actions through theory space differ, only their endpoints must coincide.

The properties of ERG discussed in the previous paragraphs hold independently of the field content. Its concrete implementation for fields other than the exemplary one scalar field above requires, however, appropriate adaptations in the application of (2.12).

For more than one degree of freedom – different field types, internal indices, spinor- or vector components – the formal inverse, product and Trace in (2.12) include the appropriate matrix operations [56]. The cutoff function has to be an appropriate tensor so that ΔS_k is again scalar with respect to external and internal indices [61]. The application to gauge theories requires some extra care. It is discussed in section 2.1.2.

ERG has been applied to a wide range of problems. Questions in scalar and fermionic models [62], [63], [64], [65], [66], [67], spontaneous symmetry breaking [69], [70], [68], [71], [72], the standard model (or parts or extensions of it) [73] , [75], [74] and thermal field theory [76], [77] have already been investigated with ERG. Its non-perturbative nature makes it especially attractive for the study of low-energy QCD and the problem of confinement, [78], [79]. Due to the intricate relation of statistical physics to quantum field theory in the Wilsonian RG, ERG has also been employable in this field, cf. the reviews [80] and [81] and references therein. This short list of references is by no means comprehensive and only intends to illustrate the versatility of ERG.

2.1.1 Truncation and optimisation

So far no approximations have been made. For any concrete application, however, it will be inevitable to introduce some approximation scheme. As mentioned above, a perturbative expansion in the couplings reproduces perturbation theory and the usual

termination at finite order in the couplings constitutes a perturbative approximation. The non-perturbative properties of (2.12) are of course lost in this way. Different schemes are the local potential (in powers of the fields) and derivative (in powers of momenta) expansions of the effective action [82], [80]. An approximation scheme retaining non-perturbativity is given by *truncation* of the effective action: only a finite number of operators is retained. In terms of theory space, only a finite dimensional subspace is considered. In general, the trajectories resulting from flows of truncated actions differ from the projections of the trajectories of the same, full flows onto the truncation subspace. A good truncation is clearly one for which this deviation is small. Especially the (projections of the) physical endpoints of the trajectories, the full quantum theory in the IR and the bare action in the UV, must be correctly reproduced by the truncated flow if it should constitute a good approximation.

How can one know whether a truncation reliably resembles the full theory? One method is to include more and operators into the truncation and study the influence of this extension on the solutions. If at a certain step no relevant modification occurs, one can terminate the process with some confidence in the results. The method which will be employed in this work is to study the stability of the flow [83], [84], [85], [86], [87] under variations of the implementation and type of the cutoff employed. Since the universal features and quantities of the full theory must be independent of the cutoff, their low cutoff dependence in some truncation can be interpreted as a sign for its reliability and physical relevance. The artificial cutoff dependence is caused by having left out relevant terms in the truncation. It can hence be interpreted as a measure for the reliability of a given truncation.

This argument can be turned around and used to *improve* the reliability of a truncation. By minimising the cutoff dependence, the influence of the left-out terms is simultaneously reduced, yielding a more stable flow. If the truncated flow is meant to reproduce the dominant features of the exact theory, its finitely many terms must be the ones which govern the flow. Respectively, the infinitely many truncated operators must be sub-dominant. The relative importance of the retained and of the truncated terms on the flow depends on the cutoff. Hence, the extremum of this dependence is also one of this partitioning of influence. Assuring that it is a maximum, one has detected the most stable flow for a given truncation. It yields physical quantities with minimal artificial cutoff dependence. The practical working of these considerations has been demonstrated already in a variety of cases [82], [85], [88], [89].

Let us illustrate the philosophy of optimisation briefly with an experimental analog. The full, untruncated action would correspond to the physical system to be studied. Truncation corresponds to the finite choice of quantities to be measured, and the cutoff function R_k to the experimental means taken to measure them. Optimisation in this picture means to design the best measurement processes yielding maximal signal from the desired quantities. For an optical experiment, for example, this would mean to adapt the slit or grid spacing to the wavelength one is interested in with the required accuracy, simultaneously maximising the detected amplitude. This is precisely what tuning R_k achieves: a sharper cutoff function picks up a smaller band of momenta with "higher resolution" and accordingly "lower amplitude", while a smoother one achieves

the contrary. To find the optimal compromise for a set of given operators is the aim of cutoff optimisation. But even the best measurement does not further the understanding of a physical system if a quantity sub-relevant to that system has been measured. The correct choice of truncation still requires a "guess", educated by available data, previous understanding and physical intuition.

How can these considerations be implemented quantitatively in truncated exact flows? The main ingredient of the non-perturbative flow equation (2.12) is the full, non-perturbative propagator with IR cutoff. Its scalar part is of the general form

$$G_k(z, \phi) = \frac{k^{-2}}{z + z r_k(z) + w(z, \phi)} , \qquad (2.14)$$

where w depends generally on both the fields and the (generalised) momenta[1] $q^2 = z \, k^2$. The dimensionless cutoff function $r_k(z)$ is related to the previously introduced one in by $R_k(z) =: k^2 \, z \, r_k(z)$. Within a certain truncation only a part w_0 of $w = w_0 + \delta w$ is taken into account, whereas the truncated-away part δw contains all the neglected terms.

Since the topic of this work is the study of the Einstein–Hilbert truncation of quantum gravity, cf. section 2.2, it will be used presently as a concrete example in the following. This allows to fix of some notation to be used later. In the Einstein–Hilbert truncation with cutoffs of type A (see section 2.2.4 and appendix C.1), w_0 is given by -2λ, where λ is the dimensionless cosmological constant, a real number. We will restrict our notation from hereon to this example, the generalisation to general w is obvious and straightforward.

In [84] a leading order (LO) cutoff optimisation procedure yielding (LO) maximal stability of the flow was introduced. This procedure is independent of the concrete theory, w does not enter. It consists in maximising the minimal value of the cutoff propagator $z(1 + r)$. Its contribution to the flow is maximal around its minimum which we define as

$$\lambda_{\text{bound}} := \frac{1}{2} \min_{z > 0} z \left(1 + r(z) \right) . \qquad (2.15)$$

Although this definition holds independently of the actual theory, we have chosen the notation on the l.h.s. to fit the case at hand. Identifying an optimal cutoff means to maximise λ_{bound}:

$$\max_{r} \lambda_{\text{bound}} . \qquad (2.16)$$

This criterion reduces the space of admissible cutoffs by one dimension. In practice one uses families of cutoff functions, which are parametrised by one parameter, and identifies their optimal member with (2.16). There is still a plenitude of such optimal cutoffs for which cutoff optimisation provides no further selection criterion. Furthermore, (2.16) makes sense only for sets of normalised cutoff functions. The most common normalisation is $r(1) = 1$. The cutoffs used in this work are normalised in this way, except where especially mentioned. More details and applications of LO optimisation can be found in the original literature [84].

---

[1]The widely used local potential approximation neglects the z-dependence of w.

In this work we introduce a next-to-leading-order (NLO) optimisation criterion taking into account the content of the truncation. For the case studied throughout this work $w_0 = -2\lambda$, and to identify the NLO optimal cutoff one searches for maximal

$$\max_r \left(\lambda_{\text{bound}} - \lambda \right) . \tag{2.17}$$

This corresponds to maximising the "mass gap" in the truncated propagator for fixed value of λ. The outcome of this procedure depends on the value of λ. In the rest of this work we will investigate UV FPs, the value of interest is the FP solution λ_*. Due to truncation it depends itself artificially on the cutoff. This cutoff dependence enters the NLO procedure.

The numerical values of the dimensionless couplings can be altered arbitrarily by rescaling the auxiliary renormalisation scale k. This can in turn be absorbed into a redefinition of the cutoff function. It is hence preferable to consider a quantity invariant under such rescalings. As a third optimisation procedure we propose the maximisation of the normalised next-to-leading-order (NNLO) gap

$$\max_r \xi \quad , \quad \xi := 1 - \frac{\lambda}{\lambda_{\text{bound}}} . \tag{2.18}$$

To abbreviate the notation, we introduce ξ for further extensive use. For NNLO optimisation, the normalisation of the cutoff is not required. This has the practical advantage that one-parameter families of cutoff functions can be compared directly without prior rescalings to a common normalisation. The value of ξ at its maximum, ξ_m, can be interpreted as a semi-quantitative measure for the maximal NNLO stability of a solution and hence its "reliability".

In chapter 3 and 4 we apply all three optimisation procedures in the Einstein-Hilbert truncation and compare their results. All three criteria yield quantitatively well agreeing results, although differences grow with space-time dimension. This can be expected from the perturbative consideration that increasing the dimension also increases the number of perturbatively relevant (whose mass dimension is lower than the dimension of space-time) and marginal (whose mass dimension is equal to the dimension of space-time) operators which have been omitted and the truncation becomes less and less reliable. Nevertheless all three procedures continue to stabilise the universal properties of the flow for all investigated numbers of space-time dimensions.

In [86] the cutoff function

$$r^{\text{opt}}(z) = \left(\frac{1}{z} - 1 \right) \Theta(1 - z) \tag{2.19}$$

was introduced. It is a LO optimised cutoff [84]. Indeed it is an optimal cutoff for all arguments $z < 1$ simultaneously, since the cutoff propagator $z(1 + r) \equiv \Theta(1 - z)$ is independent of $z < 1$. The cutoff (2.19) is thus called *the optimised cutoff*. It has many advantageous features discussed and employed in [86], [85], [82], [88] [87], among which the increased stability of its flows will be underlined by the results of chapters 3 and 4. Hence it is employed in chapter 5 to study the entire flow over all of phase space. The analytic simplicity of (2.19) plays a pivotal role for the systematic study presented there.

2.1.2   Gauge theories and background field method

The application of ERG to local gauge theories requires extra care. The key issue is to preserve gauge invariance in the presence of the momentum cutoff.

Gauge invariance of the full effective action $\Gamma[A]$ of some gauge field A (all indices are suppressed in this section) is controlled by the respective Ward identities, see for instance [37]. In turn, the effective action $\Gamma_k[A]$ for finite k has to fulfil *modified Ward identities* [90], [91]. They contain a contribution from the cutoff term, which vanishes for $k \to 0$, restoring the original Ward identities for the full effective action. The flow equation for gauge theories [92] commutes with the modified Ward identities: if they are fulfilled by the original, bare action $\Gamma_\Lambda[A]$, they are also fulfilled for all k [90], [91], guaranteeing the validity of the normal Ward identities for the full effective action. Note that $\Gamma_k[A]$, which obeys the modified Ward identities, may contain gauge-non-invariant terms for $k > 0$ and must revert to physical gauge invariance only for $k = 0$. Control over these terms is also possible in practical applications, i.e. approximation schemes, see, e.g.,[93], [94]. Nevertheless, physical gauge invariance throughout the flow would be of great conceptual and practical value. One possibility to ensure the validity of the normal Ward identities is provided in the background field approach [91], [95].

In the background field formalism [96], the quantum field $\mathcal{A}$ is split into a fixed background field $\bar{A}$ and dynamical degrees of freedom a. Only the latter are integrated over in the PI. Accordingly, also the effective, classical, mean fields decompose as $A = \bar{A} + \bar{a}$, where $\bar{a}$ is the expectation value of a in the presence of the background field. The gauge transformation acts on a only. It encodes the physics of gauge invariance for the quantum effects of the theory. To fix this gauge freedom, a gauge condition, conveniently linear in a but depending on $\bar{A}$ through background covariant derivatives [95], is used. Ghosts are introduced with respect to this gauge fixing. The sources couple to a (and the ghosts) only.

The key point of the background field formalism is that the background dependent, full effective action $\Gamma[A, \bar{A}]$ is invariant under a simultaneous background gauge transformation of $\bar{A}$ and a homogeneous, tensorial transformation of $\bar{a}$ [96] (some issues concerning the gauge invariance of the S-matrix have been discussed in [97]). By identifying the effective field A with the background field $\bar{A}$, i.e. $\bar{a} = 0$, the original, physical gauge invariance is recovered from this à priori auxiliary transformation. Hence, gauge invariance is guaranteed for the usual full effective action $\bar{\Gamma}[A] := \Gamma[A, \bar{A} = A]$ too, if $\Gamma[A, \bar{A}]$ fulfils the Ward identities for the physical gauge transformations of the quantum fields.

This property can be extended to hold for $\Gamma_k[A, \bar{A}]$ in the ERG approach: by using appropriate cutoff functions for a and the ghosts, which are quadratic in the dynamical fields and contain $\bar{A}$ through background covariant derivatives serving as discriminators between low- and high-momentum modes, the cutoff-terms can be made invariant under the background field transformation of all fields. Hence, $\Gamma_k[A, \bar{A}]$ is also invariant under this background transformation. This is of great practical value since truncations can be restricted to terms according with this invariance. For the above to hold, $\Gamma_k[A, \bar{A}]$ must obey the modified Ward identities for the physical gauge transformations of the quantum fields [93], [98].

A second set of background Ward identities can be generated by considering an auxiliary background gauge transformation acting only on $\bar{A}$ [95]. The cutoff functions lead to a contribution to these background Ward identities equal in size to that to the physical ones, but with opposite sign. Hence, the combined action of the two gauge transformations on $\Gamma_k[A, \bar{A}]$ leads to homogeneous identities without explicit cutoff-terms. These identities also commute with the flow [95]. As a consequence, $\bar{\Gamma}_k[A] :=$ $\Gamma_k[A, \bar{A}]$ is invariant under the physical gauge transformation and fulfils the usual Ward identities. Physical gauge invariance can thus be recovered for finite k. That of Γ follows explicitly [99].

However, the flow is only exact for $\Gamma_k[A, \bar{A}]$: identifying the fields $\bar{A} \equiv A$ in the flow leads to extra contributions on the r.h.s. of the flow equation, since the full propagator is obtained by deriving $\Gamma_k[A, \bar{A}]$ twice with respect to A, not $\bar{A}$. To remain exact, the full background dependence has to be tracked throughout the flow [100]. Cf. [97] for a related issue in the perturbative approach.

2.2 Einstein–Hilbert Quantum Gravity

ERG was made accessible to euclidean quantum gravity in 1996 by Reuter, [101]. In the present section we repeat the essential steps of the derivation of the flow equations for the Einstein–Hilbert truncation, albeit in shortened form. The original calculations were performed in harmonic gauge. In [102], [103] they were extended to general gauge fixings.

The non-perturbative nature of ERG and the presence of the IR cutoff are welcome features when treating gravity. Use of background field methods allows for an effective action invariant under general coordinate transformations. We restrict ourselves to the Einstein–Hilbert truncation, which contains the two invariant operators corresponding to Newton's constant and the cosmological constant. This choice is motivated both from the experimental situation as well as from the theoretical consideration that they are the invariant operators of lowest mass-dimension. To extract the β-functions for these two couplings, a weak-curvature projection of the flow is employed.

The major steps in finding the flow equations of Einstein–Hilbert gravity for harmonic gauge are summarised in sections 2.2.1 to 2.2.4, following [101] closely. The general gauge case is shortly discussed in section 2.2.5, repeating the achievements of [103].

In this work, the results of [101] are used throughout chapter 3, those of [103] in chapters 4 and 5.

2.2.1 Background field gauge fixing

Background field methods are employed for the ERG formulation of quantum gravity. They guarantee the physical gauge invariance of the full effective action, restraining the choice of truncation to invariant operators. Furthermore, they allow for the simple implementation of the cutoff term and convenient structure of the cutoff functions, cf. section 2.1.2.

The full metric $\gamma_{\mu\nu}$ is split into a fixed, unphysical, auxiliary background metric $\bar{g}_{\mu\nu}$ and the quantum fluctuations $h_{\mu\nu}$

$$\gamma_{\mu\nu} = \bar{g}_{\mu\nu} + h_{\mu\nu}\,. \tag{2.20}$$

Indices are lowered and raised by the background metric from now on. Barred quantities are defined with respect to the background metric. In analogy to (2.5), the cutoff generating functional of the connected Green functions is

$$\exp\left(W_k[t^{\mu\nu}, \sigma^\mu, \bar{\sigma}^\mu; \bar{g}_{\mu\nu}]\right) :=$$

$$\int \mathcal{D}h_{\mu\nu}\mathcal{D}C^\mu\mathcal{D}\bar{C}^\mu\exp\Big(- S[\bar{g} + h] - S_{\rm gf}[h; \bar{g}] - S_{\rm gh}[h, C, \bar{C}; \bar{g}] - \Delta S_k[h, C, \bar{C}; \bar{g}]$$

$$- S_{\rm source}[h, C, \bar{C}; t, \sigma, \bar{\sigma}; \bar{g}]\Big)\,. \tag{2.21}$$

The various terms and arguments are explained in the following.

The classical action S depends on the full metric $\gamma_{\mu\nu}$ only. It will be kept general until section 2.2.2. In accordance with the principle of general relativity, S must be invariant under local coordinate transformations. Hence the Lie derivatives of the full metric with respect to some vector field v^μ can be interpreted as the local gauge transformations leaving the classical action invariant:

$$\delta\gamma_{\mu\nu} = \mathcal{L}_v\gamma_{\mu\nu} \equiv v^\rho\partial_\rho\gamma_{\mu\nu} + \partial_\mu v^\rho\gamma_{\rho\nu} + \partial_\nu v^\rho\gamma_{\mu\rho}\,. \tag{2.22}$$

In the background field formalism, see, e.g., [92], [91] and section 2.1.2, the physical gauge transformation acts on the quantum fields $h_{\mu\nu}$, leaving the background metric unchanged:

$$\delta\bar{g}_{\mu\nu} = 0 \quad , \quad \delta h_{\mu\nu} = \mathcal{L}_v\,\gamma_{\mu\nu}\,. \tag{2.23}$$

It carries the physical information on the local symmetries of the theory. This gauge freedom is fixed by $S_{\rm gf}$ (augmented by $S_{\rm gh}$). Under the background gauge transformation, all tensors, including the background metric, transform under general coordinate transformations according to their rank. This will guarantee the gauge invariance of the full effective action, a major advantages of the background field formalism [94], as explained in section 2.1.2.

Gauge fixing of the physical gauge transformation is cared for by $S_{\rm gf}$, which contains the gauge fixing function $F_\mu(\bar{g}, h)$,

$$S_{\rm gf}[h; \bar{g}] = \frac{1}{2\alpha} \int d^d x\, \sqrt{\bar{g}}\, \bar{g}^{\mu\nu}\, F_\mu\, F_\nu\,, \tag{2.24}$$

where α is the *gauge-fixing parameter*.

The action of the Fadeev–Popov ghosts C^μ and anti-ghosts $\bar{C}^\mu$ is determined via the Fadeev–Popov determinant as for vectorial Yang–Mills theories, see, e.g., [37], it reads

$$S_{\rm gh}[h, C, \bar{C}; \bar{g}] = -\kappa^{-1} \int d^d x\, \bar{C}_\mu\bar{g}^{\mu\nu}\frac{\partial F_\nu}{\partial h_{\rho\lambda}}\mathcal{L}_C(\bar{g}_{\rho\lambda} + h_{\rho\lambda})\,, \tag{2.25}$$

where $\kappa^{-1} = \sqrt{32\pi G_N}$, with G_N the bare Newton's constant.

For the harmonic gauge condition

$$F_\mu = \sqrt{2}\kappa \left(\delta_\mu^\lambda \bar{g}^{\rho\nu} \bar{D}_\nu - \frac{1}{2} \bar{g}^{\rho\lambda} \bar{D}_\mu \right) h_{\rho\lambda} \,, \tag{2.26}$$

the ghost action is

$$S_{\mathrm{gh}}[h, C, \bar{C}; \bar{g}] = -\sqrt{2} \int d^d x \sqrt{\bar{g}}\, \bar{C}_\mu \Big(\bar{g}^{\mu\rho} \bar{g}^{\sigma\lambda} \bar{D}_\lambda \left((\bar{g}_{\rho\nu} + h_{\rho\nu}) D_\sigma + (\bar{g}_{\sigma\nu} + h_{\sigma\nu}) D_\rho \right)$$
$$- \bar{g}^{\rho\sigma} \bar{g}^{\mu\lambda} \bar{D}_\lambda \left(\bar{g}_{\sigma\nu} + h_{\sigma\nu} \right) D_\rho \Big) C^\nu \,. \tag{2.27}$$

F_μ, and hence S_{gh}, vanishes identically for $g_{\mu\nu} = \bar{g}_{\mu\nu}$. The case $\alpha = 1$ in (2.24) is the harmonic gauge, the analog in gravity to Feynman gauge for vectorial gauge theories.

The cutoff term ΔS_k has to be quadratic in the dynamical fields. The cutoff functions have to transform as tensors of the appropriate rank under the background gauge transformation [95]. Their arguments (replacing q^2 of the scalar case) are chosen as the background field Laplacians, which are seen below to yield a convenient form of the cutoff propagator:

$$\Delta S_k[h, C, \bar{C}; \bar{g}] = \frac{\kappa^2}{2} \int d^d x \sqrt{\bar{g}}\, h_{\mu\nu} R_k^h [-\bar{D}^2]^{\mu\nu\rho\lambda} h_{\rho\lambda}$$
$$+ \sqrt{2} \int d^d x \sqrt{\bar{g}}\, \bar{C}_\mu R_k^C [-\bar{D}^2] C^\mu \,. \tag{2.28}$$

The eigenvalues of the covariant background Laplacian, $\bar{D}^2 = \bar{g}^{\mu\nu} \bar{D}_\mu \bar{D}_\nu$, separate the low- and the high-energy modes. The cutoff functions have to fulfil the conditions (2.2)–(2.4). For some one-parameter families of cutoff-functions used in this work, see appendix B.

The source term

$$S_{\mathrm{source}}[h, C, \bar{C}; t, \sigma, \bar{\sigma}; \bar{g}] = - \int d^d x \sqrt{\bar{g}} \left(t^{\mu\nu} h_{\mu\nu} + \bar{\sigma}_\mu C^\mu + \sigma^\mu \bar{C}_\mu \right) \tag{2.29}$$

contains the sources $t^{\mu\nu}, \bar{\sigma}_\mu, \sigma^\mu$ for the metric variations, the ghosts and the antighosts.

Given the functional W_k at fixed k, the effective or classical fields $\bar{h}_{\mu\nu}^k, \xi_k^\mu, \bar{\xi}_\mu^k$ (for readability's sake, the index k will be left out for the effective fields from now on) are given by the variation of the generating functional with respect to the sources

$$\bar{h}_{\mu\nu} = \frac{1}{\sqrt{\bar{g}}} \frac{\delta W_k}{\delta t^{\mu\nu}} \,, \quad \xi^\mu = \frac{1}{\sqrt{\bar{g}}} \frac{\delta W_k}{\delta \bar{\sigma}_\mu} \,, \quad \bar{\xi}_\mu = \frac{1}{\sqrt{\bar{g}}} \frac{\delta W_k}{\delta \sigma^\mu} \,. \tag{2.30}$$

The effective action $\Gamma_k[\bar{h}, \xi, \bar{\xi}; \bar{g}]$ is defined as for scalar case (2.11) as the Legendre transform of $W_k[t, \sigma, \bar{\sigma}; \bar{g}]$:

$$\Gamma_k[\bar{h}, \xi, \bar{\xi}; \bar{g}] := -W_k[t, \sigma, \bar{\sigma}; \bar{g}] - \Delta S_k[\bar{h}, \xi, \bar{\xi}; \bar{g}] + \int d^d x \sqrt{\bar{g}} \left(t^{\mu\nu} \bar{h}_{\mu\nu} + \bar{\sigma}_\mu \xi^\mu + \sigma^\mu \bar{\xi}_\mu \right) \,. \tag{2.31}$$

Introducing the classical metric as

$$g_{\mu\nu} := \langle \gamma_{\mu\nu} \rangle = \bar{g}_{\mu\nu} + \bar{h}_{\mu\nu} , \tag{2.32}$$

the arguments of the effective action are reordered, $\Gamma_k[g, \bar{g}, \xi, \bar{\xi}]$.

The derivation of the ERG flow equation proceeds like in (2.10). The cutoff terms for the metric and the ghosts give rise to two terms in the flow equation, where an opposite sign is due to the fermionic nature of the ghosts:

$$\partial_k \, \Gamma_k[g, \bar{g}, \xi, \bar{\xi}] = \frac{1}{2} \text{Tr} \left(\left(\kappa^{-2} \Gamma^{(2)}_{k,gg} + R_k^h \right)^{-1} \cdot \partial_k \left(R_k^h \right) \right)$$

$$- \frac{1}{2} \text{Tr} \left(\left(\frac{1}{2} \Gamma^{(2)}_{k,\xi\bar{\xi}} + R_k^C \right)^{-1} \cdot \partial_k \, R_k^C \right) . \tag{2.33}$$

Here we reverted to the representation space independent Trace-notation, which contains the trace over indices and integrals over position or momentum. In this Trace, the differential operator $-D^2$ has yet to be evaluated through the sum of its eigenvalues.

The inverse of the second derivatives of the effective action with respect to the fields is to be understood through their relation with the two point functions

$$G^{(tt)}_{\mu\nu\rho\lambda}(x,y) = \frac{1}{\sqrt{\bar{g}(x)}\sqrt{\bar{g}(y)}} \frac{\delta^2 W_k[t, \sigma, \bar{\sigma}; \bar{g}]}{\delta t^{\mu\nu} \, \delta t^{\rho\lambda}} \tag{2.34}$$

$$G^{(\sigma\bar{\sigma})\nu}_{\mu}(x,y) = \frac{1}{\sqrt{\bar{g}(x)}\sqrt{\bar{g}(y)}} \frac{\delta^2 W_k[t, \sigma, \bar{\sigma}; \bar{g}]}{\delta \sigma^{\mu} \, \delta \bar{\sigma}_{\nu}} \tag{2.35}$$

$$\frac{\delta^d(y-z)}{\sqrt{\bar{g}(z)}} \delta^{\alpha}_{\mu} \delta^{\beta}_{\nu} = \int d^d x \sqrt{\bar{g}} G^{(tt)}_{\mu\nu\rho\lambda}(y, x) \left(\Gamma^{(2)}_{k,gg} + \kappa^2 R_k^h \right)^{\rho\lambda\alpha\beta} \tag{2.36}$$

$$\frac{\delta^d(y-z)}{\sqrt{\bar{g}(z)}} \delta^{\nu}_{\mu} = \int d^d x \sqrt{\bar{g}} G^{(\sigma\bar{\sigma})\rho}_{\mu}(y, x) \left(\Gamma^{(2)}_{k,\xi\bar{\xi}} + 2 \, R_k^C \right)^{\nu}_{\rho} . \tag{2.37}$$

The effective action and the flow equation (2.33) have the general structural properties discussed for the scalar case. For properly defined cutoff functions, the r.h.s. of (2.33) is both UV and IR finite. By taking the limit $\lim_{k\to 0} \Gamma_k[g, \bar{g}, 0, 0]$ *and then* equating background and classical metric consistently, the full effective quantum action is recovered. On the other hand, for $k \to \Lambda$ the bare effective action reads

$$\Gamma_\Lambda[g, \bar{g}, \xi, \bar{\xi}] = S[g] + S_{\text{gf}}[g - \bar{g}; \bar{g}] + S_{\text{gh}}[g - \bar{g}, \xi, \bar{\xi}; \bar{g}] . \tag{2.38}$$

It is essential that these two steps – flow evolution and background identification – do not commute, see section 2.1.2. The corresponding issue is also of importance in the perturbative approach, [97].

One further remark, concerning the conformal factor problem, has to be made at this place. Although the occurrence of scalar conformal modes with negative kinetic terms renders the euclidean PI divergent, the flow equation (2.33) remains finite and allows for well defined calculations.

2.2.2 Einstein–Hilbert truncation

So far, no approximations have been made. A first restriction consists in making the following Ansatz:

$$\Gamma_k[g, \bar{g}, \xi, \bar{\xi}] = \bar{\Gamma}_k[g] + \hat{\Gamma}_k[g, \bar{g}] + S_{\text{gf}}^k[g - \bar{g}; \bar{g}] + S_{\text{gh}}[g - \bar{g}, \xi, \bar{\xi}; \bar{g}]. \tag{2.39}$$

The gauge fixing and ghost terms keep their classical operator structure, the suffix k is meant to express that the bare couplings G_N appearing in S_{gf} is replaced by the running coupling G_k (factors of G_N in the ghost action cancel each other out). The two flowing terms are defined as

$$\bar{\Gamma}_k[g] := \Gamma_k[g, \bar{g} = g, 0, 0]. \tag{2.40}$$

Consequently, $\hat{\Gamma}_k[g, \bar{g}] = 0$. (2.39) has to fulfil (2.38) in the limit $k \to \Lambda$, yielding

$$\lim_{k \to \Lambda} \bar{\Gamma}_\Lambda[g] = S[g] \quad , \quad \lim_{k \to \Lambda} \hat{\Gamma}_\Lambda[g - \bar{g}; \bar{g}] = 0. \tag{2.41}$$

The second approximation consists in setting $\hat{\Gamma}_k[g, \bar{g}] = 0$. A similar truncation turned out to work well for Yang–Mills theories [92], [104]. In this approximation, the flow equation (2.33) fails to remain exact, even in the absence of further truncations [100]. Furthermore, the corresponding modified Ward identities [101] are violated, cf. section 2.1.2 and [101]. In turn, this truncation fulfils homogeneous identities, i.e. the violation of the modified ones is given by the cutoff-induced, inhomogeneous term of the modified Ward identity. For the explicit form of the modified Ward identities, we refer to the original work [101], since they will not be used in the present work.

The final step is to specify the operators and couplings building up $\bar{\Gamma}_k$. In the Einstein–Hilbert truncation, the effective action contains the same operators as the euclidean, classical Einstein–Hilbert action:

$$S_{\text{EH}} = -\frac{1}{16\pi G_N} \int d^d x \sqrt{g} \left(R(g) - 2\bar{\lambda} \right). \tag{2.42}$$

The Ricci scalar R is obtained by contracting the indices of the curvature tensor $R_{\rho\mu\sigma\nu}$ given in terms of the Christoffel symbols $\Gamma^\rho_{\mu\nu}$:

$$\begin{aligned}
R &= g^{\mu\nu} R_{\mu\nu} = g^{\mu\nu} g^{\rho\sigma} R_{\rho\mu\sigma\nu} \\
&= g^{\mu\nu} g^{\rho\sigma} g_{\rho\alpha} \left(\frac{\partial \Gamma^\alpha_{\mu\sigma}}{\partial x^\nu} - \frac{\partial \Gamma^\alpha_{\mu\nu}}{\partial x^\sigma} + \Gamma^\alpha_{\beta\nu} \Gamma^\beta_{\mu\sigma} - \Gamma^\alpha_{\beta\nu} \Gamma^\beta_{\mu\nu} \right),
\end{aligned} \tag{2.43}$$

$$\Gamma^\rho_{\mu\nu} = \frac{g^{\rho\sigma}}{2} \left(\frac{\partial g_{\nu\rho}}{\partial x^\mu} + \frac{\partial g_{\mu\rho}}{\partial x^\nu} - \frac{\partial g_{\nu\mu}}{\partial x^\sigma} \right). \tag{2.44}$$

The two couplings are Newton's constant G_N and the cosmological constant $\bar{\lambda}$. Varying S_{EH} after the metric yields the Einstein equations with a cosmological term. In the effective action, the coupling constants are replaced by the respective scale dependent quantities $G_k, \bar{\lambda}_k$. In Einstein–Hilbert truncation, the effective action reads

$$\begin{aligned}
\Gamma_k[g, \bar{g}, \xi, \bar{\xi}] = &-\frac{1}{16\pi G_k} \int d^d x \sqrt{g} \left(R(g) - 2\bar{\lambda}_k \right) + \frac{1}{2\alpha} \int d^d x \sqrt{\bar{g}} \, \bar{g}^{\mu\nu} F_\mu^k F_\nu^k \\
&- \sqrt{32\pi G_k} \int d^d x \bar{C}_\mu \bar{g}^{\mu\nu} \frac{\partial F_\nu^k}{\partial h_{\rho\lambda}} \mathcal{L}_C (\bar{g}_{\rho\lambda} + h_{\rho\lambda}).
\end{aligned} \tag{2.45}$$

The suffixes k to the gauge fixing conditions F indicate that they contain each a factor $G_k^{-1/2}$. In the case of the ghost action this cancels G_k in the pref-actor.

2.2.3 Background identification

Γ_k given by (2.45) is now inserted into the flow equation (2.33). *After* evaluating the r.h.s. (i.e. determining $\Gamma_k^{(2)}$), metric consistency $g_{\mu\nu} = \bar{g}_{\mu\nu}$ is demanded and the ghosts are exorcised $\xi = \bar{\xi} = 0$. The l.h.s of the flow equation then takes the form

$$\partial_k \Gamma_k[g, g, 0, 0] = \frac{1}{16\pi} \int d^d x \sqrt{g} \left((R(g) - 2\bar{\lambda}_k) \frac{\partial_k G_k}{G_k^2} + \frac{2}{G_k} \partial_k \bar{\lambda}_k \right) . \tag{2.46}$$

Since only $\Gamma_k^{(2)}$ enters the r.h.s., it suffices to determine the part of the effective action quadratic in $h_{\mu\nu}$, Γ_k^{qu}, since all higher orders vanish upon background-identification. The classical ghost action is already purely quadratic in the ghosts.

In the next step, the r.h.s. is projected onto the operators appearing on the l.h.s., $\sqrt{g} R(g)$ and $\sqrt{g}$. This is necessary to obtain explicit expressions for the β-functions of the couplings appearing on the l.h.s., $\partial_k G_k$ and $\partial_k \bar{\lambda}$. The r.h.s of the flow equation is thus expanded in R around zero curvature, the zeroth and first term yielding the sought for β-functions. These steps are performed explicitly in section 2.2.4.

The background metric remained unfixed so far. To obtain the needed first order in R, it is possible to fix $\bar{g}_{\mu\nu}$ to the technically most advantageous choice permitting to extract $\sqrt{g}$, $\sqrt{g} R$ (flat background, $\bar{g}_{\mu\nu} = \eta_{\mu\nu}$, for example, would not permit to extract the curvature). We assume henceforth the background space-time to be a *maximally symmetric space*. The curvature and Ricci tensor in terms of dimension d and a scalar curvature $\bar{R}$ are

$$R_{\mu\nu\rho\lambda} = \frac{1}{d(d-1)} \left(\bar{g}_{\mu\rho} \bar{g}_{\nu\lambda} - \bar{g}_{\mu\lambda} \bar{g}_{\nu\rho} \right) \bar{R} \quad , \quad R_{\mu\nu} = \frac{1}{d} \bar{g}_{\mu\nu} \bar{R} . \tag{2.47}$$

In the full theory, physical results are independent of the choice of the auxiliary background field. Truncation may induce an artificial dependence.

2.2.4 Harmonic gauge

Using the harmonic gauge condition (2.26) and working in harmonic gauge $\alpha = 1$ and maximally symmetric space (2.47), the quadratic part of the action can be written as

$$\Gamma_k^{\mathrm{qu}}[g, \bar{g}, \xi, \bar{\xi}] = \frac{1}{16\pi G_k} \int d^d x \sqrt{\bar{g}} \, \bar{h}_{\mu\nu} \left\{ -K^{\mu\nu\rho\lambda} \bar{D}^2 + U^{\mu\nu\rho\lambda} \right\} \bar{h}_{\rho\lambda}$$

$$- \sqrt{2} \int d^d x \sqrt{\bar{g}} \, \bar{\xi} \, M^\mu_\nu \, \xi^\nu , \tag{2.48}$$

with the metric dependent tensors

$$K^{\mu\nu\rho\lambda} = \frac{1}{4}\left(\bar{g}^{\mu\rho}\bar{g}^{\nu\lambda} + \bar{g}^{\mu\lambda}\bar{g}^{\nu\rho} - \bar{g}^{\mu\nu}\bar{g}^{\rho\lambda}\right),$$

$$U^{\mu\nu\rho\lambda} = \frac{1}{4}\bar{g}^{\mu\nu}\bar{g}^{\rho\lambda}\left(\frac{d-4}{d}\bar{R} + 2\bar{\lambda}_k\right) + \frac{1}{4}\bar{g}^{\mu\rho}\bar{g}^{\nu\lambda}\left(\frac{d(d-3)+2}{d(d-1)}\bar{R} - 2\bar{\lambda}_k\right) \quad (2.49)$$

$$+ \frac{1}{4}\bar{g}^{\mu\lambda}\bar{g}^{\nu\rho}\left(\frac{d(d-3)+6}{d(d-1)}\bar{R} - 2\bar{\lambda}_k\right),$$

$$M^\mu_\nu = \delta^\mu_\nu\left(\bar{D}^2 + \bar{R}\right). \qquad (2.50)$$

The metric is decomposed into a traceless, $\hat{h}^\mu_\mu = 0$, and a trace part ϕ:

$$\bar{h}_{\mu\nu} = \hat{h}_{\mu\nu} + \frac{1}{d}\bar{g}_{\mu\nu}\phi. \qquad (2.51)$$

This decomposition is only sufficient in harmonic gauge. For general α, the non-diagonal terms like $\bar{D}^\mu \bar{h}_{\mu\nu}$ appear in (2.48)'s equivalence. This necessitates a more involved field decomposition to prepare the field for the heat-kernel evaluation of $-\bar{D}^2$ [102], [103]. We will discuss that case briefly in section 2.2.5.

With this metric decomposition, the quadratic part of the effective action takes the form

$$\Gamma^{\mathrm{qu}}_k[\hat{h}, \phi, , \bar{g}, \xi, \bar{\xi}] = \frac{1}{32\pi G_k}\int d^d x\sqrt{\bar{g}}\frac{1}{2}\Big[\hat{h}_{\mu\nu}\left(-\bar{D}^2 - 2\bar{\lambda}_k + C_T\bar{R}\right)\hat{h}^{\mu\nu}$$

$$- \frac{d-2}{2d}\phi\left(-\bar{D}^2 - 2\bar{\lambda}_k + C_S\bar{R}\right)\phi + 2\sqrt{2}(16\pi G_k)\bar{C}_\mu\left(-\bar{D}^2 + C_V\bar{R}\right)C^\mu\Big], \quad (2.52)$$

where the tensorial, vectorial and scalar coefficients are

$$C_T = \frac{d(d-3)+4}{d(d-1)}, \quad C_V = -\frac{1}{d}, \quad C_S = \frac{d-4}{d}. \qquad (2.53)$$

The three types of fields in (2.52) do not mix to second order. Hence the r.h.s of the flow equation (2.33) splits into three separate parts if the cutoff functions are chosen appropriately. Their tensorial structure is fixed by the fields they are meant to regularise, while their normalisation is chosen so that each kinetic term $-\bar{D}^2$ is augmented by the IR cutoff $+k^2$. The scalar cutoff function $R^0(-\bar{D}^2/k^2)$ is still unspecified:

$$\left(R^h_k(-\bar{D}^2/k^2)\right)^{\mu\nu\rho\lambda} = \left(R^T_k(-\bar{D}^2/k^2)\right)^{\mu\nu\rho\lambda} + \frac{1}{d}R^S_k(-\bar{D}^2/k^2)\bar{g}^{\mu\nu}\bar{g}^{\rho\lambda}, \qquad (2.54)$$

$$\left(R^T_k(-\bar{D}^2/k^2)\right)^{\mu\nu\rho\lambda} = \frac{G_N}{G_k}\left(\frac{1}{2}\bar{g}^{\mu\rho}\bar{g}^{\nu\lambda} + \frac{1}{2}\bar{g}^{\mu\lambda}\bar{g}^{\nu\rho} - \frac{1}{d}\bar{g}^{\mu\nu}\bar{g}^{\rho\lambda}\right)R^0_k(-\bar{D}^2/k^2), (2.55)$$

$$R^S_k(-\bar{D}^2/k^2) = -\frac{G_N}{G_k}\frac{d-2}{2d}R^0_k(-\bar{D}^2/k^2), \qquad (2.56)$$

$$R^C_k(-\bar{D}^2/k^2) = \sqrt{2}R^0_k(-\bar{D}^2/k^2). \qquad (2.57)$$

This tensorial structure of the cutoffs is determined by the field decomposition. This, in turn, is established by restraining the gauge fixing to the harmonic gauge, $\alpha = 1$. The

cutoffs in (2.54) are hence appropriate to this choice of gauge fixing. They are called *cutoffs of type A*, since they were introduced historically prior to those of *type B*, which pertain to the general case of arbitrary gauge fixing, discussed in section 2.2.5.

Inserting the second derivative of (2.52) and the cutoffs (2.54) into (2.33) and setting $\bar{g}_{\mu\nu} = g_{\mu\nu}$, $\xi = \bar{\xi} = 0$, the flow equation reads

$$
\partial_k \Gamma_k[g] = \frac{1}{2}\frac{(d-1)(d+2)}{2}\, Tr\, \frac{\partial_k R_k^0(-D^2/k^2) - R_k^0(-D^2/k^2)\partial_k \ln G_k}{-D^2 + R_k^0(-D^2/k^2) - 2\,\bar{\lambda}_k + C_T \bar{R}}
$$
$$
+ \frac{1}{2} Tr\, \frac{\partial_k R_k^0(-D^2/k^2) - R_k^0(-D^2/k^2)\partial_k \ln G_k}{-D^2 + R_k^0(-D^2/k^2) - 2\,\bar{\lambda}_k + C_S \bar{R}}
$$
$$
- d\,Tr\, \frac{\partial_k R_k^0(-D^2/k^2)}{-D^2 + R_k^0(-D^2/k^2) + C_V \bar{R}}\,. \qquad (2.58)
$$

The functional traces Tr over the functionals of the covariant Laplacian $-D^2$ still remain to be evaluated. The traces over the tensor indices have already been performed and yield the corresponding coefficients. These coefficients $(d-1)(d+2)/2, 1, d$ in front of these functional traces stem from evaluating the tensor products between the denominators and nominators and are equal to the number of independent traceless symmetric, scalar and vector field components.

The functional traces are evaluated by using the heat kernel expansion [105]:

$$
Tr[e^{-isD^2}] = \left(\frac{i}{4\pi s}\right)^{d/2} \int d^d x \sqrt{g}\left(1 - \frac{is}{6}\bar{R} + O(\bar{R}^2)\right)\,. \qquad (2.59)
$$

A trace over a function $W(-D^2)$ can be expressed through its Fourier transform

$$
\begin{aligned}
Tr[W(-D^2)] &= \int_{-\infty}^{\infty} ds\,\tilde{W}(s)\, Tr[e^{-isD^2}]\\
&= (-4\pi i)^{-d/2}\left(\int ds\, s^{-d/2}\tilde{W}(s)\right) \times \left(\int d^d x \sqrt{g}\right) \qquad (2.60)\\
&\quad - (-4\pi i)^{-d/2}\frac{i}{6}\left(\int ds\, s^{1-d/2}\tilde{W}(s)\right) \times \left(\int d^d x \sqrt{g}\bar{R}\right) + O(\bar{R}^2)
\end{aligned}
$$

In the present case, the functions W are the three expressions under the traces in (2.58). They contain the scalar curvature in the denominator. To finally extract the β-functions of the couplings, the denominators are expanded to first order in R. This allows us to collect all terms proportional to $\int d^d x \sqrt{g}$ and $\int d^d x \sqrt{g}\,R$ on the r.h.s. of the flow equation. By comparing the coefficients of these operators on both hands of (2.33), one finally arrives at the β-functions of G_k, λ_k. We re-express them for dimensionless quantities, which are defined from the dimensionful ones:

$$
t := \ln(k/k_0)\,, \quad z := s/k^2\,, \quad R^0(s/k^2) =: k^2\, z\, r(z)\,, \quad g_k(z) := k^{d-2}\,G_k\,, \quad \lambda_k := k^{-2}\bar{\lambda}_k\,, \qquad (2.61)
$$

k_0 is an arbitrary unit of momentum.

For these dimensionless couplings, the resulting b-functions describing their dependence on the RG-scale are

$$\partial_t g_k = [d - 2 + \eta_N(k)] g_k \,, \tag{2.62}$$

$$\partial_t \lambda_k = A_1(\lambda_k; d) + \eta_N(k) A_2(\lambda_k; d) \,, \tag{2.63}$$

with the *anomalous dimension*

$$\eta_N(k) = \frac{g_k B_1(\lambda_k; d)}{1 - g_k B_2(\lambda_k; d)} \,. \tag{2.64}$$

The functions A_1, A_2, B_1, B_2 are given explicitly in appendix C.1. The anomalous dimension is defined as $\eta := \partial_t G_k / G_k$ and receives its name because the factor $\sqrt{G_N/G_k}$ is found to multiply each graviton (canonically normalised) field $h_{\mu\nu}$ in the background-expanded EH action. It can be identified with the multiplicative, scale dependent field normalisation constant, denoted as $Z_k^h := G_N/G_k$. Hence $\eta = -\partial_t \ln Z_k^h$, the standard definition of the anomalous dimension of a field. Z_k^h equals unity at some reference scale, where the bare Newton's constant G_N equals the running one G_k.

2.2.5 Transverse-traceless decomposition of the metric

The case of general gauge fixing α requires some modifications to the above derivation. As mentioned in section 2.2.4, the term of Γ_k quadratic in $\bar{h}_{\mu\nu}$ does only take its form (2.48) for $\alpha = 1$. Otherwise, terms like $(\bar{D}\bar{h})^2$ appear. Since only scalar operators $-D^2$ allow the application of (2.59), the quadratic term has to be brought into such form by an adequate field decomposition, which differs from the previous one (2.51).

The decomposition of the metric fluctuations into transverse traceless, longitudinal and trace parts [106] used in [103] achieves this diagonalisation. The metric is decomposed as

$$h_{\mu\nu} = h_{\mu\nu}^T + \bar{D}_\mu \hat{\xi}_\nu + \bar{D}_\nu \hat{\xi}_\mu + \left(\bar{D}_\mu \bar{D}_\nu - \frac{1}{d} \bar{g}_{\mu\nu} \bar{D}^2 \right) \hat{\sigma} + \frac{1}{d} \bar{g}_{\mu\nu} \bar{D}^2 \phi \tag{2.65}$$

where the traceless transverse tensor $h_{\mu\nu}^T$, the transverse vector $\hat{\xi}_\mu$ and the scalars $\hat{\sigma}$ and ϕ are subject to the conditions

$$\bar{g}^{\mu\nu} h_{\mu\nu}^T = 0 \,, \quad \bar{D}^\mu h_{\mu\nu}^T = 0 \,, \quad \bar{D}^\mu \hat{\xi}_\mu = 0 \,, \quad \phi = \bar{g}^{\mu\nu} h_{\mu\nu} \,. \tag{2.66}$$

This decomposition is valid for complete, closed Riemann spaces and can be extended to open, asymptotically flat spaces if the fields fulfil certain asymptotic conditions [106]. In [103] the flow equation of the action functional in these fields is re-derived. Proper cutoffs are introduced, which bear the correct tensorial structure and differ accordingly from the cutoffs of type A (2.54). They are called *cutoffs of type B*. Due to the larger number of fields, the derivation of the flow equation and the application to the Einstein–Hilbert truncation is more involved than in the harmonic gauge case.

The main steps are conceptually identically to the case of cutoffs type A. The resulting β-functions for g_k and λ_k are structurally identical to (2.62). They are given explicitly in appendix C.2. The gauge fixing parameter α enters these flow equations. These flow equations will henceforth also be referred to as "type B", extending the naming of the tensorial structure of the cutoffs to the resulting β-functions.

2.3 Fixed Point of Gravity in four Dimensions

The flow equations for Newton's constant and the cosmological constant obtained with the ERG allow the discussion of the scale dependence of these quantities. A question of paramount interest is that of the existence of FPs in the present truncation. Such a FP would be a first indication of the asymptotic safety of gravity, i.e. its non-perturbative renormalisability, cf. section 1.4. The dimensionful couplings behave necessarily as $\bar{\lambda} = k^2 \lambda_*$, $G_k = k^{2-d} g_*$ at a FP of the dimensionless ones. Near a FP, Newton's constant decreases with energy, it shows anti-screening behaviour. Whereas the dimensionless gravitational coupling is asymptotically safe, the dimension*full* one is asymptotically *free*.

For harmonic gauge and cutoffs of type A, such a FP was found [107] for $2 < d \leq 4$ for an exponential cutoff. At dimensions near two, it reproduced the findings of Weinberg in the $2 + \epsilon$ expansion. This FP is seen to continue smoothly to four space-time dimensions (higher ones were not studied in [107]). For generic gauge fixings and a class of cutoff functions, the FP was found with cutoffs of type B in [103] and further discussed in [108]. They were detected with all used cutoff functions for up to six space-time dimensions. For higher dimensions, the FP shows strong cutoff dependence, disappearing for some of the used function. In [134], FPs have been studied analytically in general dimensions with the optimised cutoff function in one gauge.

By investigating the stability matrix at the FP, it is seen that both directions of the EH truncation are UV-stable. The numerical values of the stability matrix eigenvalues are rather independent of the cutoff function and the gauge fixing at and below four dimensions, but display increasingly varying results for dimensions higher than four.

For four or less dimensions, all results agreed remarkably well with each other at a quantitative level. The loss of reliability in higher dimensions was interpreted as indicating the non-adequacy of the Einstein–Hilbert truncation for dimensions higher than four. It is one of the main topics of thesis to clarify this point. It is shown in chapters 3 and 4 that the qualitative and quantitative cutoff and gauge fixing dependence of the higher dimensional results can be reduced to the percent level with cutoff optimisation.

Further results fuelling the hope for gravity's asymptotic safety are procured from extended truncations.

In [109], [110] and [111] the scalar R^2 term was included into the truncation. A FP is reported and discussed explicitly in $2 + \varepsilon$ and four dimensions. Its projection onto the Einstein–Hilbert truncation coincides with the previous, lower truncation results to high accuracy. All three directions are UV attractive in four dimensions. In $2 + \varepsilon$ dimensions, the third, new coupling-direction is repulsive, in accordance with perturbative expectations. This indicates explicitly that at least for dimensions close to two, the UV critical surface may be finite dimensional.

Phenomenologically very relevant is the inclusion of matter. This is investigated in [112], [113] and [114]. In [112] a scalar fields with non-minimal coupling to curvature was added to the Einstein–Hilbert action. The addition of a similar scalar with arbitrary potential was found in [114] to leave the UV FP of pure Einstein–Hilbert gravity nearly unchanged, whereas these couplings vanish at the FP. The case of minimally coupled general matter of different spin was investigated in [113] and [114]. The existence of the

non-Gaussian FP depends in that case on the number and type of fields added (similar to the case of asymptotic freedom for QCD). However, a wide range of these parameters (including those of the standard model) allow the existence of the FP.

Non-local truncations including functions of the volume of space-time, $V = \int d^d x \sqrt{g}$, were considered in [115], [116]. FP searches have not yet been fully conducted in these truncations, since they are mainly intended as large-scale effective models [117], [118].

Further signs for a non-Gaussian FP have been detected independently in a lattice approach to quantum gravity by Hamber et al. [119], [120], [121], [122] and in dimensionally reduced theories [123].

It can be concluded from the results described above that asymptotic safety is a viable scenario for gravity. The first one or two steps (=truncations) toward asymptotic safety have been made quite successfully. If the FP should continue to persist reliably in higher truncations, the non-perturbative renormalisability of gravity as a local field theory becomes more and more probable.

2.4 Applications

We conclude this recapitulation of quantum gravity in the framework of ERG with some of the phenomenological implications investigated so far.

The full effective action $\lim_{k \to 0} \Gamma_k$ contains the full physics of a theory. However, the effective action can also be used for non-zero cutoffs k. Including an external lowest momentum scale p^2 into the effective action of a theory, the flow generally stops at $k^2 \approx p^2$, providing a physical cutoff, $\lim_{k \to 0} \Gamma_k(p) \approx \Gamma_p(p)$ (p is short for $\sqrt{p^2}$). Using the effective action Γ_p to calculate processes with typical energies p, all quantum effects are contained at tree-level. Although no external scale has been included in Einstein–Hilbert gravity, previous experience makes the validity of the above mechanism very likely in this case, cf. [124]. For momenta in the scaling FP regime this cutoff-identification must be true, since only one scale remains in this regime.

As mentioned at the end of section 2.2.4, the quantity η (2.64) can be interpreted as the anomalous dimension of the gravitons, i.e. the metric perturbations around a (flat) background. Employing the cutoff-identification $k \to p$, the scalar part of the Fourier transformed graviton propagator in the FP regime is given by [103]

$$\tilde{G}_2(p)^{-1} \propto Z^h_{k \to p} p^2 \propto (p^2)^{1-\eta/2} \xrightarrow{FP} p^d \,. \tag{2.67}$$

This propagator is valid for calculations performed in the far UV-regime of gravity.

Whereas it is straightforward to identify an euclidean momentum scale k with another euclidean momentum p, the situation is less clear when trying to extract phenomenological implications of euclidean ERG results for our Riemannian universe. To do this, it is paramount to *define* a consistent, physically motivated cutoff-identification procedure connecting space-time quantities like conformal time, distance, or curvature to the renormalisation scale, i.e. to fix appropriate functions $\{x_\mu, t, R, \ldots\}(k)$ proper to a certain question.

In the far UV and in the presence of only one physical dimensionful quantity, cutoff identification is straightforward. Introducing a length l, $[l] = -1$, it can be identified with k as $l := c/k$, where c is, in natural units, some positive number of order one. Solving the effective Einstein equation (the e.o.m. $\delta\Gamma_k/\delta g_{\mu\nu}$) assuming maximal symmetry of space (2.47), one finds that $\bar{R} = 4\bar{\lambda}_k$. In the FP-regime and using the cutoff-identification $l = c/k$, the curvature radius is $r_c^{-2} \equiv \bar{R} = 4\lambda_* c^2 l^{-2}$ and, since both λ_* and c are of order one, $r_c \approx l$. Interpreting l as the spacial resolution with which space-time is looked upon, the resulting picture is that of space-time being stronger and stronger curved the closer one looks at it[2][111]. Once in the FP regime, the relation between r_c and l stays independent of further decrease in l. Space-time behaves in a self-similar, fractal way [111].

Another situation where "naive" cutoff-identification seems plausible is earliest time cosmology. Interpreting k as proportional to the inverse of the conformal time T, Robertson–Walker cosmology (with classical matter) was studied in [125]. The cosmological scale factor $a(T)$ is found to be $a(T) = T$ in the FP-regime and the cosmological particle horizon is absent, solving the causality problem otherwise requiring an additional inflationary phase. In a spatially flat universe, the (normalised) energy densities of matter and the cosmological constant are equal to each other and one half in the Planck era. Furthermore, the UV graviton propagator (2.67) is argued to give rise to the observed flat spectrum of primordial gravitational perturbations [103]. Similar results are obtained with more involved scale setting procedures [124], [126]. The evolution of cosmological perturbations in the present setting was studied in [127].

To deal with more general situations in the presence of other, external scales, a consistent cutoff identification procedure has to be defined. General prescriptions have been proposed in [124] and [126]. They partly confirm results obtained earlier with situation specific identifications, underlining the importance of choosing the "right" prescription.

Black holes have been examined in the present setting in [128], [129]. The intriguing picture which arises (for appropriate cutoff identification) is that for a certain critical black hole mass, which is of the order of the Planck mass, the event horizon vanishes. Accordingly, Hawking evaporation stops and leaves a cold remnant of order Planck mass.

Although the Einstein–Hilbert truncation seems to work surprisingly well in the FP-regime, it breaks down for large, $O(1)$, positive values of λ_k, cf. the discussion in [108] and sections 2.1.1, 5.1.1, 5.5.3 of this work in particular. As shown previously [108] and in chapter 5, all trajectories leading to positive cosmological (and gravitational) constant are affected by this breakdown at some large scale. From the ERG point of view such a breakdown signals that operators becoming important at these scales have been neglected. It can hence be expected that new effects not described by standard general relativity come into play at large scales. This is already witnessed in the present truncation by the onsetting of strong quantum effects before the actual breakdown. These observations become especially intriguing when estimating the present day size of λ_k. Identifying the cutoff with the largest available scale set by Hubble's constant

---

[2]Of course phrases like "looking on space-time" are rather meaningless and only serve to illustrate the intuitive picture.

and using the best experimental fit for $\bar{\lambda}_0$ one finds that $\lambda_0 \sim O(1)$ on cosmological scales. But for these values Einstein–Hilbert gravity is expected to be insufficient. These questions were studied in [130], where furthermore a connection between the extreme weakness of quantum effects over a wide range of scales to the smallness of the cosmological constant was observed. A slight running of Newton's constant at galactic scales may explain the observed anomalies in galactic rotation curves usually attributed to the presence of dark matter [131]. The cosmological consequences of the existence of a hypothetical IR FP were investigated in [132], [133]. Especially the equality of matter and dark energy density in a FP regime is very intriguing when compared to present data. In [115], [116], non-local truncations were constructed to further investigate the IR in particular. It was argued that they could, in principle, provide an explanation for the extreme smallness of the observed cosmological constant.

Chapter 3

Fixed Points in Higher Dimensions

The FP of Einstein–Hilbert quantum gravity found previously are stable in dimensions $2 + \varepsilon$ to 4 (cf. section 2.3). The conjecture that non-perturbative RG modified general relativity could provide a sufficient description of gravity even for energies beyond the Planck scale is supported by these results. Unfortunately, a direct experimental confirmation or falsification of the implications of these results seems not prospective, comparing the energies of this and next generations accelerators to the Planck mass.

On the other hand, one of the reasons why models with large extra dimensions have recently received considerable interest is the potential experimental accessibility of quantum gravity in the near future, cf. section 1.2. The application of ERG to quantum gravity in higher dimensions than four would allow to make predictions within this setting. Of decisive importance for the reliability of this description of quantum gravity for energies higher than the Planck mass (which could, in these models, be as low as a few TeV) is its renormalisability. In the asymptotic safety scenario this is equivalent to the existence of a FP.

In Einstein–Hilbert truncation, such FPs have been found also in higher dimensions. However, their existence and properties depended increasingly on the implementation of the cutoff, so that it remained unclear how far these findings could be trusted, see the recapitulation in section 2.3. From a perturbative point of view, it could be suspected that the Einstein–Hilbert truncation becomes less and less reliable for capturing the essential physics in an increasing number of dimensions: the higher the dimension, the more perturbatively relevant (with mass-dimension lower to the dimension of space-time) and marginal (with mass-dimension equal to that of space-time) operators exist for a given theory, cf. appendix 1.3. It is reasonable to assume that these perturbatively relevant and marginal operators will play a role non-perturbatively, too. Hence their truncation will endanger its validity, seemingly witnessed by the loss of reliability observed in [103], [108].

In this chapter, we demonstrate that Einstein–Hilbert ERG gravity possesses reliable FPs also in higher dimension. Indeed, FP in generic dimensions have been found analytically in [134] for the optimised cutoff function and a certain choice of gauge-fixing. Reliability is found to decrease with increasing dimension, but no qualitative breakdown is observed. This allows the interpretation that although an increasing number of operators comes into play with increasing number of dimensions, they do not induce a

qualitative change and Einstein–Hilbert truncation remains a valid approximation even in higher dimensions. Such a scenario of no qualitative change is also motivated by the fate of the fixed point in lower dimensions: it exists continuously and smoothly in dimension, starting from its trivial origin in two dimensions. In the sense of the mass dimension of Newton's constant, two dimensions can be considered "natural" for gravity, all others being equally "unnatural". In this light, it seems rather "natural" for the non-Gaussian FP to continue its existence into higher dimensions, as confirmed by the results below. This receives support from the fact that including the (perturbatively marginal) operator R^2 in four dimensions did not alter the situation with respect to the lower Einstein–Hilbert truncation.

3.1   Fixed Point Search and Cutoff Optimisation

In this section, we search for FPs of quantum gravity in four and more dimensions. We work in the Einstein-Hilbert truncation and harmonic gauge, using cutoffs of type A. The FP-values of the couplings, henceforth denoted as λ_*, g_*, are attained when their flow stops, i.e. $\beta_\lambda(\lambda_*, g_*) = 0$, $\beta_g(\lambda_*, g_*) = 0$. By dropping the suffix k we comply with the essential attribute of a FP, its scale independence.

We find them for generic space-time dimensions and cutoffs. This confirms and extends results presented in [101], [103], [108]. In the full, untruncated theory, universal quantities at the FP would be independent of the cutoff used. In turn, by truncation an artificial cutoff-dependence is induced. We study this cutoff-dependence. The λ-boundary marking the breakdown of the truncation [101], [108] is found for generic cutoffs and dimensions. The optimisation procedure laid out in section 2.1.1 is applied to the FP-values of λ with respect to this boundary.

As an example, we choose the modified exponential cutoff function (B.1). We calculate (g_*, λ_*) for a (sufficiently) dense set of values of the cutoff parameter b for space-time dimensions d 4 to 10. The resulting curves $\lambda_*^{(d)}(b)$ are displayed in fig. (3.1(a)) together with the stability boundary λ_{bound}, (2.15). FPs are found for all dimensions d for an interval in the cutoff parameter bound to the left by the intersection of $\lambda_*^{(d)}(b)$ with $\lambda_{\text{bound}}(b)$. The qualitative behaviour of $\lambda_*^{(d)}(b)$ is the same for all dimensions. The value of b where $\lambda_*^{(d)}(b)$ runs into the boundary increases with dimension. All values $\lambda_*^{(d)}(b)$ are positive, for all d and all (allowed) cutoffs. A local minimum of $\lambda_*^{(d)}(b)$ can be discerned in all dimensions. It is rather weak for $d > 5$. The curves $\lambda_*^{(d)}(b)$ move upward with increasing dimension. This trend decelerates, hinting at the existence of an asymptotic value $\lim_{d\to\infty} \lambda_*^{(d)}(b) < \infty$. The higher the dimension, the closer to the boundary $\lambda_*^{(d)}(b)$ is for each b. This behaviour is expected for the dimensional reasons given above. For large b, all curves approach each other. Whether they converge to a single value $\lambda_*(b \to \infty)$ independent of dimension remains to be investigated. On the other hand, there is an intermediate b-region of maximal distance to the boundary.

As argued in section 2.1.1, it is this distance which controls the stability of the solution. For the reasons given there, we choose the ratio of this difference over λ_{bound}, ξ, as the
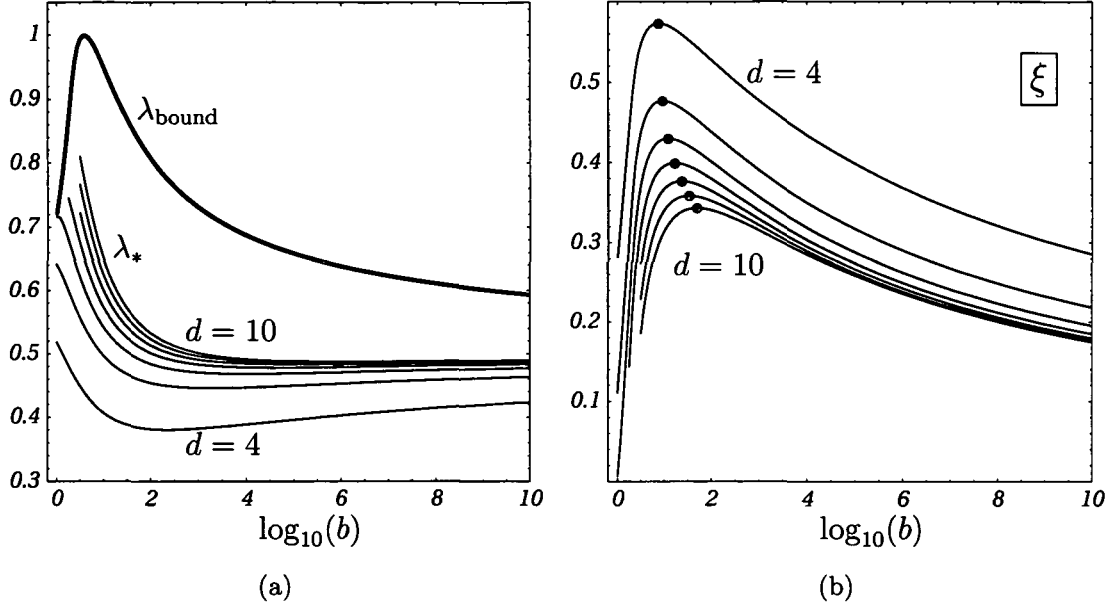
Figure 3.1: FP results for the modified exponential cutoff (a) FP values of the dimensionless cosmological constant, λ_*, for 4 to 10 dimensions. In red the stability boundary λ_{bound}. (b) Normalised stability control parameter $\xi := 1 - \lambda_*/\lambda_{\text{bound}}$. The maxima of $\xi(b)$ are highlighted as red dots.

control parameter. We expect to minimise the residual cutoff sensitivity of physical quantities by maximising ξ with respect to b. $\xi(b)$ is displayed for the present cutoff in fig. (3.1(b)). A local maximum is found for all dimensions, allowing the optimisation of the cutoff. The maxima of ξ are henceforth denoted as ξ_m, their loci as b_{NNLO}. They are given in table 3.1(a), together with those of the other two control parameters, λ_{bound} and $\lambda_{\text{bound}} - \lambda_*$, called b_{LO} and b_{NLO}, cf. section 2.1.1. The corresponding values of λ_{bound} in table 3.1(b) show how the difference between the three optimisation schemes increases with dimension: λ_{bound} at b_{NNLO} remains within 10% of the LO-optimal value 1 for dimensions up to 7. The values at b_{NLO}, albeit decreasing, stay within 10% of 1 up to dimension 10.

Since λ_{bound} depends only on the cutoff, b_{LO} is the same for all physical theories and, of course, dimensions. In contrast, b_{NLO} and b_{NNLO} contain information from the theory at hand.

This throws some light on the issue of the apparent non-existence of the FP beyond 6 dimensions for the modified exponential $b = 1$ cutoff discussed in [108]: using the same (low) value of b (e.g. 2, 10, ...) for all dimensions, one inevitably moves away from the optimised cutoff and eventually hits the stability boundary, beyond which no FP can be found. This quite severe qualitative change vanishes if we go to higher b and hence move away sufficiently from the boundary. Adapting the cutoff to the dimension provides a way out of this loss of FP for higher dimensions. Although the optimised

Table 3.1: (a) Loci of the maxima of λ_{bound}, $\lambda_{\text{bound}} - \lambda_*$ and ξ denoted as $b_{\text{LO}}, b_{\text{NLO}}$ and b_{NNLO}. (b) Values of λ_{bound} for cutoff-parameters $b_{\text{LO}}, b_{\text{NLO}}$ and b_{NNLO}.

	(a)				(b)		
d	b_{LO}	b_{NLO}	b_{NNLO}	λ_{bound}	LO	NLO	NNLO
4	3.922	4.964	7.629	$d=4$	1	0.995	0.970
5	3.922	5.632	9.244	5	1	0.989	0.957
6	3.922	6.588	12.270	6	1	0.980	0.935
7	3.922	7.890	16.901	7	1	0.968	0.912
8	3.922	9.676	23.842	8	1	0.953	0.888
9	3.922	12.169	34.288	9	1	0.936	0.864
10	3.922	15.729	50.130	10	1	0.917	0.842

quality measured by ξ_m decreases with increasing dimension, this loss is of an expected quantitative nature and does not introduce any new qualitative features. Optimised cutoffs permit the retrieval of FP in arbitrary extra dimensions.

We repeated the above analysis for the exponential (B.3), the generalised optimised (B.4) and the modified cutoff functions (B.6). The qualitative picture is identical to the one laid out above. Fixed points are found for all dimensions for a range of cutoff-parameters bound to the left by the intersection $\lambda_*^{(d)} \cap \lambda_{\text{bound}}$. The three control parameters $\lambda_{\text{bound}}, \lambda_{\text{bound}} - \lambda_*$ and ξ have local maxima in all cases.

For the generalised optimised cutoff function all three maxima coincide at the value of the cutoff parameter $b = 1$. Optimising the generalised optimised cutoff yields the optimised cutoff (2.19) for all three (LO, NLO, NNLO) criteria.

The quantitative comparison of the three cutoffs is postponed to section 3.3.

3.2 Universality

We now turn to universal quantities. In the full, untruncated theory they would be insensitive to the implementation of the cutoff. In turn, truncation introduces an artificial cutoff-dependence. The extent of this sensitivity can be used to estimate the reliability of the employed truncation. Subsets of cutoff space leading to minimal cutoff-dependence can be interpreted as being "best suited" to the truncation at hand. Our expectation is that these sets are found around the optimised cutoffs of the previous section.

To verify this claim we investigate the cutoff-dependence of two such quantities. The first are the eigenvalues of the stability matrix at the non-Gaussian FP. They determine the nature of the FP. All FPs are found to be UV-attractive in both directions. This is the case for all dimensions and admissible cutoffs investigated. This confirms the results of [101], [103] and [108] and extends them to higher dimensions. The findings of [134] are reproduced wih different cutoff functions and gauge-fixing.

The second quantity is the dimensionless combination of the couplings at the FP,

$\tau := \lambda_* \times g_*^{2/(d-2)}$. It is the extra dimensional generalisation of $\lambda_* \times g_*$, for which it has been argued already in [135] that it constitutes the essential coupling of pure gravity with cosmological constant. This product features certain scaling-invariances and was found to be very insensitive to the cutoff in four dimensions [103]. Likewise τ displays comparable stability in higher dimensions.

Our expectations concerning cutoff optimisation are confirmed. It indeed marks out a region of reduced cutoff dependence of the investigated universal quantities.

Again we restrict the detailed discussion of this section to the modified exponential cutoff. Similar results are obtained for the exponential (B.3), the modified (B.6) and the generalised optimised one (B.4). The quantitative comparison is postponed to section 3.3.

Remember that g_* and λ_* are not universal quantities themselves. Their values can be shifted by redefinitions of unphysical quantities. The action is invariant under rescaling the field degrees of freedom by some factor a. This results in a rescaling of g_* and λ_* by $a^{(1-d/2)}$ and a. Further, any redefinition of the – auxiliary – momentum scale k leads to a similar rescaling of the FP-solutions g_*, λ_*. Any quantity displaying universal attributes must be invariant under such reparametrisations, whereas g_*, λ_* are not.

This non-universality is reflected in the LO and NLO optimisation procedures: λ_{bound} scales like λ_* with respect to field- or k-rescalings. Comparing LO and NLO optimised stability across different types of cutoffs may turn out problematic since they could imply differently scaled k from the beginning. On the other hand, ξ remains rescaling-invariant. It can be considered as a universal measure for the stability of the flow. It provides an unambiguous measure for the quality of a FP. Thence comparison between different types of cutoffs are meaningful even without fixing the cutoff functions to the same normalisations. It will be undertaken in detail in section 3.3.

3.2.1 Eigenvalues of the stability matrix

The first universal quantity under investigation are the eigenvalues of the stability matrix at the FP. They are universal critical exponents of the theory and determine its behaviour near the fixed point, cf. section 1.4. Since there are two couplings in the present theory, there are two eigenvalues of the 2×2 stability matrix.

These eigenvalues are complex conjugated for all considered dimensions and generic cutoffs. The real part is referred to as θ' and the (absolute value of the) imaginary part as θ''. The sign of θ' determines UV-attraction (IR-repulsion) (+) or -repulsion (-attraction) (-). The imaginary part θ'' describes how the trajectories rotate around the FP as they approach or leave it. In this sense the UV-FP can be understood as a degenerate limit cycle.

θ', θ'' and the modulus $|\theta| = \sqrt{(\theta')^2 + (\theta'')^2}$ are displayed in fig. (3.2(a)), fig. (3.2(b)) and fig. (3.2(c)) for the modified exponential cutoff function.

θ' is positive for all dimensions. The FP remains UV attractive for $d \in [4, 10]$. This confirms and extends previous results [103], [110]. The red dots depict the values at b_{NNLO}. The fact that these values are very close to the local minima of θ' and $|\theta|$ is taken as a first example for the success of cutoff-optimisation. The outcome of

the optimisation of the quality-control parameter ξ nearly coincides with the result of applying a minimal sensitivity criterion to θ' alone.

θ'' looses its local minimum for dimension 7 and higher, but b_{NNLO} still lies in a region of minimal gradient. Cutoff-dependence over the whole interval increases with dimension. This accords with decreasing reliability measured by ξ.

The numerical values of θ', θ'' and $|\theta|$ at $b_{\text{LO}}, b_{\text{NLO}}$ and b_{NNLO} are given in tables 3.2(a), 3.2(b) and 3.2(c). The three control maxima lie to the left of b corresponding to minimal cutoff dependence of θ', θ'' and $|\theta|$ separately. The differences between these three values are much smaller than the overall variation over the whole b-interval. The relative difference lies in the few-percent range. The difference between the NLO and NNLO results is even smaller. b_{NLO} and b_{NNLO} are closer to the local b-minima of θ' and $|\theta|$ (inflection point of θ'') than b_{LO}. This confirms our conjecture that including information pertaining to the theory at hand improves the gain in reliability cutoff optimisation yields.

One could view this remaining variance in the optimised values as an estimate for the order of magnitude of the "error-bar". The bottom qualitative conclusion of this consideration is that θ' is safely positive in all dimensions, the FPs retain their UV-attractiveness.

Repeating these calculations for the exponential (B.3), the generalised optimised (B.4) and the modified cutoff (B.6) yields quantitatively similar results. Due to technical reasons we were able to push their cutoff parameters closer to the boundary. For these cutoffs one has $\xi \rightarrow 0$ and observes the breakdown of the truncation expected from our optimisation considerations. This is signalled by the divergence of θ', θ''. Another qualitative change occurs for very high values of the cutoff parameters. For some high $b_r \gg b_{\text{NNLO}}$ the complex conjugated eigenvalues pass to two real ones. The values of b_r decrease with increasing dimension. Again, for the quantitative results we refer to section 3.3.

3.2.2   Universal dimensionless combination of couplings

We turn now to the second universal quantity, $\tau = \lambda_* \times g_*^{2/(d-2)}$, the generalisation of the product $\lambda^* g^*$ from 4 to general dimensions. It has been argued already in [103] that this product constitutes an observable quantity in four dimensions, cf. also [135] for its interpretation as an essential coupling.

The argument presented in [103] readily applies to the generalised case: Since τ can also be written as the dimensionless combination of the dimensionfull couplings in the FP limit, $\tau = \lim_{k \to \infty} (\bar{\lambda}_k \times G_k^{2/(d-2)})$, it inherits their universality.

Alternatively, it is straightforward to check that τ is invariant under rescaling of g^* and λ^*, either due to field- or k-redefinitions [135].

If containing universal meaning, it should be robust to variations of the cutoff. Indeed we find it to be very stable in all dimensions and cutoffs investigated.

The curves $\tau^{(d)}(b)$ are displayed in fig. (3.2(d)) for the case of the modified exponential cutoff function. The strong cutoff-independence found in [103] is reproduced in higher dimensions. The corresponding plots for the other two cutoffs are similar, again
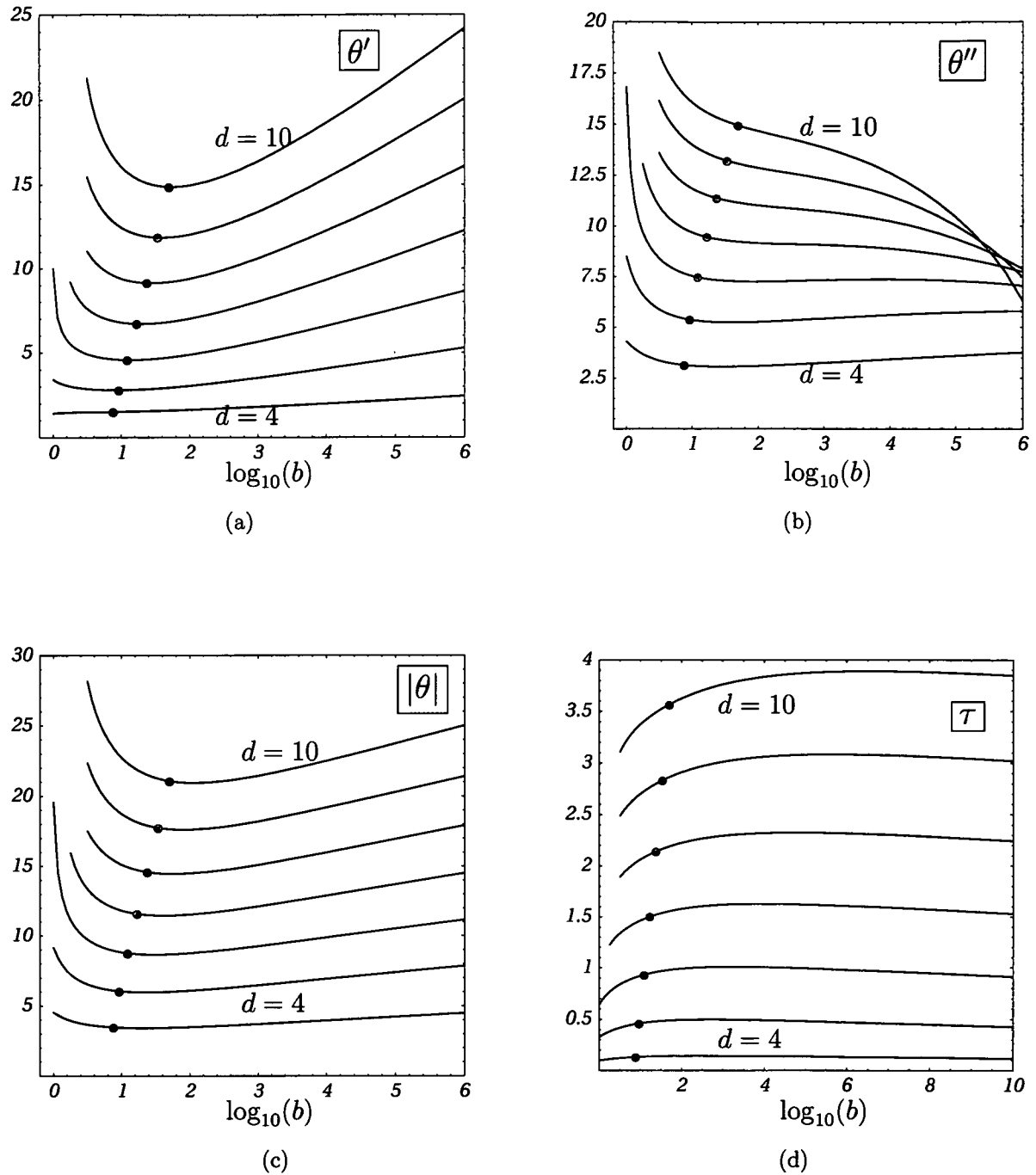
Figure 3.2: Universal quantities for the modified exponential cutoff. The red dots indicate the results of NNLO-optimised cutoffs. (a) θ', (b) θ'', (c) $|\theta|$, (d) τ.

Table 3.2: Values of the universal quantities (a) θ', (b) θ'', (c) $|\theta|$ and (d) τ for the modified exponential cutoff optimised to LO, NLO and NNLO in various dimensions.

<table>
<tr><td colspan="4" align="center">(a)</td><td colspan="4" align="center">(b)</td></tr>
<tr><th>θ'</th><th>LO</th><th>NLO</th><th>NNLO</th><th>θ''</th><th>LO</th><th>NLO</th><th>NNLO</th></tr>
<tr><td>d=4</td><td>1.494</td><td>1.499</td><td>1.510</td><td>d=4</td><td>3.291</td><td>3.226</td><td>3.144</td></tr>
<tr><td>5</td><td>2.842</td><td>2.812</td><td>2.802</td><td>5</td><td>5.718</td><td>5.528</td><td>5.369</td></tr>
<tr><td>6</td><td>4.812</td><td>4.647</td><td>4.583</td><td>6</td><td>8.143</td><td>7.727</td><td>7.461</td></tr>
<tr><td>7</td><td>7.346</td><td>6.867</td><td>6.712</td><td>7</td><td>10.595</td><td>9.842</td><td>9.456</td></tr>
<tr><td>8</td><td>10.500</td><td>9.419</td><td>9.143</td><td>8</td><td>13.070</td><td>11.875</td><td>11.370</td></tr>
<tr><td>9</td><td>14.445</td><td>12.279</td><td>11.861</td><td>9</td><td>15.521</td><td>13.816</td><td>13.203</td></tr>
<tr><td>10</td><td>19.424</td><td>15.435</td><td>14.869</td><td>10</td><td>17.817</td><td>15.645</td><td>14.943</td></tr>
<tr><td colspan="4" align="center">(c)</td><td colspan="4" align="center">(d)</td></tr>
<tr><th>$|\theta|$</th><th>LO</th><th>NLO</th><th>NNLO</th><th>τ</th><th>LO</th><th>NLO</th><th>NNLO</th></tr>
<tr><td>d=4</td><td>3.614</td><td>3.226</td><td>3.488</td><td>d=4</td><td>0.125</td><td>0.128</td><td>0.132</td></tr>
<tr><td>5</td><td>6.385</td><td>6.202</td><td>6.056</td><td>5</td><td>0.430</td><td>0.445</td><td>0.461</td></tr>
<tr><td>6</td><td>9.458</td><td>9.017</td><td>8.756</td><td>6</td><td>0.860</td><td>0.899</td><td>0.933</td></tr>
<tr><td>7</td><td>12.892</td><td>12.001</td><td>11.596</td><td>7</td><td>1.369</td><td>1.445</td><td>1.502</td></tr>
<tr><td>8</td><td>16.770</td><td>15.157</td><td>14.590</td><td>8</td><td>1.935</td><td>2.060</td><td>2.142</td></tr>
<tr><td>9</td><td>21.203</td><td>18.484</td><td>17.748</td><td>9</td><td>2.541</td><td>2.728</td><td>2.834</td></tr>
<tr><td>10</td><td>26.358</td><td>21.978</td><td>21.080</td><td>10</td><td>3.179</td><td>3.441</td><td>3.568</td></tr>
</table>

see section 3.3.

This time b_{NNLO} does not lie near a local extremum but rather on the onset of the plateau of minimal cutoff sensitivity. The relative variability of τ near this optimised cutoff is typically as small as that of θ', as can be seen by comparing $\tau^{(d)}(b_{\mathrm{LO}}), \tau^{(d)}(b_{\mathrm{NLO}})$ and $\tau^{(d)}(b_{\mathrm{NNLO}})$ in table 3.2(d).

The relative difference $\left[\tau^{(d)}(b_{\mathrm{NNLO}}) - \tau^{(d)}(b_{\mathrm{LO}})\right]/\tau^{(d)}(b_{\mathrm{NNLO}})$ increases slightly with dimension. One observes a clustering of $\tau(b_{\mathrm{NLO}})$ and $\tau(b_{\mathrm{NNLO}})$ opposed to $\tau(b_{\mathrm{LO}})$. This becomes more pronounced with increasing dimension. This is to be expected since b_{NNLO} and b_{NLO} lie further up the plateau than b_{LO}.

In table 3.3(a) the values of the UV-FP couplings for the ξ-optimised modified exponential cutoff are displayed together with the corresponding values of τ. Although g_* increases strongly with dimension, τ experiences only a relatively mild increase. This is due to the decreasing exponential $2/(d-2)$ with which g_* enters τ.

Modified exponential cutoff with alternative normalisation

By choosing a different normalisation of the cutoff function (i.e. different from $r(1) = 1$ for all values of b) one can alter the magnitude of the FP couplings. τ however remains unaffected by this. This can be seen in the example of a modified exponential cutoff with non-universal normalisation, see (B.2). It is normalised to $r^{alt}_{mexp}(1) = b/(e-1)$. This b-dependence of the normalisation does not allow for a LO or NLO optimisation procedure.

Table 3.3: UV FP couplings and respective values of τ at b_{NNLO} for two different normalisations of the modified exponential cutoff in various dimensions. (a) Canonical normalisation $r(1) = 1$ used throughout the rest of this work. (b) Alternative normalisation (B.2).

<table>
<tr><td colspan="4">(a)</td><td colspan="4">(b)</td></tr>
<tr><td>NNLO</td><td>λ_*</td><td>g_*</td><td>τ</td><td>NNLO</td><td>λ_*</td><td>g_*</td><td>τ</td></tr>
<tr><td>d=4</td><td>0.414</td><td>0.319</td><td>0.132</td><td>d=4</td><td>0.893</td><td>0.148</td><td>0.132</td></tr>
<tr><td>5</td><td>0.500</td><td>0.886</td><td>0.461</td><td>5</td><td>1.163</td><td>0.250</td><td>0.461</td></tr>
<tr><td>6</td><td>0.533</td><td>3.059</td><td>0.933</td><td>6</td><td>1.379</td><td>0.458</td><td>0.933</td></tr>
<tr><td>7</td><td>0.548</td><td>12.464</td><td>1.502</td><td>7</td><td>1.580</td><td>0.882</td><td>1.502</td></tr>
<tr><td>8</td><td>0.553</td><td>58.018</td><td>2.142</td><td>8</td><td>1.777</td><td>1.750</td><td>2.142</td></tr>
<tr><td>9</td><td>0.554</td><td>302.033</td><td>2.834</td><td>9</td><td>1.975</td><td>3.536</td><td>2.834</td></tr>
<tr><td>10</td><td>0.553</td><td>1730.650</td><td>3.568</td><td>10</td><td>2.176</td><td>7.223</td><td>3.568</td></tr>
</table>

The rescaling of the (auxiliary) momentum scale $k \to k \ln^{-\frac{1}{2}}(1 + b)$ transfers this cutoff to the canonically normalised r_{mexp}. The FP couplings and λ_{bound} obtained from r^{alt}_{mexp} are hence related to those from r_{mexp} by this factor, $\lambda^{alt}_{mexp} = \ln(1 + b) \lambda_{mexp}$, $g^{alt}_{mexp} = \ln^{(2-d)/2}(1 + b) g_{mexp}$. ξ-optimisation is accordingly unaffected by using this alternative normalisation instead of the canonical one. b_{NNLO} is the same for both cases. As discussed above, τ is invariant with respect to such rescalings and hence stays the same too.

These features are displayed in table 3.3(b): λ_*, g_* differ from those in table 3.3(a) precisely by the respective powers of $\ln(1 + b_{\text{NNLO}})$, whereas τ is the same for all normalisations.

3.3 Cutoff Independence

In the previous sections we have discussed the cutoff dependence of the UV FP properties within the family of modified exponential cutoff functions. As mentioned above, we repeated this procedure for other one-parameter families of cutoff functions. In addition to the modified exponential (B.1) we used the exponential (B.3), the modified (B.6) and the generalised optimised (B.4) (whose optimisation yields the optimised) cutoff as given in [84]. A synopsis of the respective cutoff functions appears in tab.3.4 together with the values of b_{LO} at which their respective λ_{bound}'s assume their maximal value of 1^1. This range of cutoff functions allows for a comparison of the ξ-optimised results obtained by the use of the various cutoff functions. This constitutes an important test for the optimisation procedure: it must yield the same physical results for all cutoffs. Any difference between optimised cutoffs can be ascribed as an minimal error to the results.

This extends the studies of [103], [108] to other cutoff functions and higher dimensions.

---

[1]In tab. 3.4 we also included an entry for the power-like cutoff which will be only needed in chapter 4.

Table 3.4: Cutoff functions and the parameter values b_{LO}.

Cutoff		b_{LO}
$r_{\mathrm{mexp}}(z)$	$\dfrac{b}{(b+1)^z - 1}$	3.9215
$r_{\mathrm{exp}}(z)$	$\dfrac{1}{2^{z^b}-1}$	1.4427
$r_{\mathrm{go}}(z)$	$b(\tfrac{1}{z}-1)\Theta(1-z)$	1
$r_{\mathrm{mod}}(z)$	$\left(2^{\frac{z+(b-1)z^b}{b}}-1\right)^{-1}$	1.92255
$r_{\mathrm{pow}}(z)$	z^{-b}	2

Table 3.5: Comparison of ξ_m for modified exponential, exponential, modified and optimised cutoff.

ξ_m	mexp	exp	mod	opt
d=4	0.573	0.572	0.582	0.614
5	0.477	0.479	0.490	0.525
6	0.430	0.435	0.445	0.482
7	0.399	0.408	0.416	0.454
8	0.377	0.388	0.396	0.433
9	0.359	0.373	0.379	0.416
10	0.343	0.359	0.365	0.401

The UV FPs are found in all investigated cases and share the same qualitative features. No signs of artificial dependence of the qualitative features on the cutoff functions could be discovered.

One of the advantages of using ξ is that it can straightforwardly be compared for different cutoffs irrespective of their normalisation. We take its maxima ξ_m as a basis to compare the optimised stability of the flows at the FP for the various cutoffs. The information gleaned thereby can be used as a bias in the interpretation of the reliability of the results obtained through the respective cutoff functions. The maximum values of ξ, ξ_m, for the different cutoff functions are shown in tab.3.5. These values are close to each other. Hence the three cutoffs can be considered as approximately equally trustworthy, although the optimised cutoff yields ξ_m about 7-10 % higher than the other two cutoffs in all dimensions. Thus it could be preferable. All cutoffs exhibit the same expected monotonous decrease with dimension.

In tab.3.6(a)–3.6(c) we compare θ', θ'' and $|\theta|$ at b_{NNLO} between the four cutoffs. To facilitate this comparison, we define *mean* values $\bar{\theta}'_A, \bar{\theta}''_A, |\bar{\theta}|_A$ as the halfsums of the largest and the lowest value of the respective quantities obtained from the four cutoff functions. An *error-bar* can be a assigned by taking the half-difference. The resulting *relative error* is in the 1–5 % range. It is of the same size as the relative difference

between the quantities at b_{NLO} and b_{NNLO} within each cutoff function, cf. tab.3.2(a)–3.2(c). However, generally it is far smaller then the relative difference between values at b_{LO} and b_{NNLO}, especially for higher dimensions.

The choice of the stability optimisation procedure – LO, NLO or NNLO – influences the results for the optimised universal quantities at least as strongly as the choice of the cutoff function subjected to this optimisation. This underlines the importance of the choice of the optimisation procedure.

So far, we have studied the universal behaviour of τ with the modified exponential cutoff function. Proceeding to other functions provides new insights into the extent of τ's universality.

The exponential, modified and optimised cutoff reproduce the universal behaviour found for the case of the modified exponential to a high degree. The curves $\tau^{(d)}(b)$ of all three cutoffs are similar. They share the high stability found for the case of the modified cutoff function. Though, the exponential, modified and generalised optimised cutoff functions have weak maxima on top of the plateaus. It can be safely excluded that τ's stability is a mere artifact of the choice of the cutoff function.

The four sets of $\tau^{(d)}(b_{NNLO})$ coincide with higher precision than the full $\tau^{(d)}(b)$, see tab. 3.6(d). This means that changing the cutoff parameter b within one cutoff function induces a larger change in $\tau^{(d)}$ than switching between different cutoff functions with optimised parameter values b_{NNLO}.

The mean value and its error is defined as for θ as half the sum and half the difference of the largest and the smallest of the four optimised values. The typical spread across the schemes is of the same width as the one between values at b_{NNLO} and b_{NLO} of one cutoff function separately. By making use of cutoff-optimisation, cutoff sensitivity has been reduced to the one per cent level.

In this chapter, we have searched for FPs in the Einstein–Hilbert truncation of gravity in higher dimensions (4 to 10). This was done with four different one-parameter sets of cutoff functions. For each set NNLO cutoff optimisation singled out one optimised cutoff. Universal quantities at the FP coincided with good accuracy for all four optimised cutoffs. This evidences the non-artificiality of the FPs.

The cutoff independence of the four-dimensional FP is shared by its higher-dimensional extensions. This confirms the expectation that the FP-structure is universal in all dimensions higher than two. It may hence be surmised that the robustness of the Einstein–Hilbert FP under extension of the truncation established in four dimensions transfers to higher ones too. If this holds true, the Einstein–Hilbert truncation may provide a quantitatively reliable description of quantum gravity also in higher dimensions.

The results of this chapter were obtained with cutoffs of type A, implying harmonic gauge-fixing, $\alpha = 1$. The extension of these investigations to general gauges is the topic of the next chapter.

Table 3.6: Comparison of the NNLO optimised values of the observables (a) θ', (b) θ'', (c) $|\theta|$ and (d) τ for the four cutoff functions and their mean values (barred) and errors (cf. main text).

(a)

θ'	mexp	exp	mod	opt	$\bar{\theta}'_A$
d=4	1.510	1.534	1.506	1.475	1.505 ± 0.029
5	2.802	2.833	2.770	2.687	2.760 ± 0.073
6	4.583	4.597	4.496	4.332	4.465 ± 0.133
7	6.712	6.679	6.540	6.271	6.492 ± 0.220
8	9.143	9.029	8.855	8.459	8.801 ± 0.342
9	11.861	11.632	11.424	10.881	11.371 ± 0.490
10	14.869	14.485	14.240	13.534	14.202 ± 0.667

(b)

θ''	mexp	exp	mod	opt	$\bar{\theta}''_A$
d=4	3.144	3.133	3.095	3.043	3.094 ± 0.050
5	5.369	5.325	5.269	5.154	5.262 ± 0.107
6	7.461	7.370	7.313	7.142	7.301 ± 0.159
7	9.456	9.315	9.259	9.054	9.255 ± 0.201
8	11.370	11.185	11.143	10.916	11.143± 0.227
9	13.203	12.987	12.965	12.737	12.970± 0.233
10	14.943	14.718	14.716	14.516	14.730± 0.214

(c)

$|\theta|$	mexp	exp	mod	opt	$\overline{|\theta|}_A$
d=4	3.488	3.488	3.442	3.382	3.435 ± 0.053
5	6.056	6.032	5.953	5.813	5.934 ± 0.122
6	8.756	8.686	8.584	8.353	8.554 ± 0.201
7	11.596	11.462	11.336	11.014	11.305± 0.291
8	14.590	14.375	14.233	13.811	14.200± 0.390
9	17.748	17.435	17.280	16.752	17.250± 0.498
10	21.080	20.651	20.477	19.847	20.464± 0.617

(d)

τ	mexp	exp	mod	opt	$\bar{\tau}_A$
d=4	0.132	0.134	0.135	0.137	0.135 ± 0.002
5	0.461	0.468	0.469	0.478	0.469 ± 0.008
6	0.933	0.946	0.946	0.963	0.948 ± 0.015
7	1.502	1.521	1.521	1.544	1.523 ± 0.021
8	2.142	2.165	2.162	2.192	2.167 ± 0.025
9	2.834	2.858	2.853	2.888	2.861 ± 0.027
10	3.568	3.591	3.585	3.623	3.596 ± 0.028

Chapter 4

Gauge Independence of Fixed Points in Higher Dimensions

In the previous chapter cutoff independent UV FP results in higher dimensions were obtained from the most stable flows identified by a stability optimisation procedure.

But spurious cutoff dependence is not the only artifact potentially induced by truncation: the modified Ward identities are violated by this approximation, cf. section 2.2.2. This induces a dependence of physical quantities on the gauge fixing parameter. To establish the physicality of the results obtained in chapter 3, it is important to study this dependence, which must be small and under control for reliable ones. This constitutes a non-trivial test for the reliability of the used truncation: the artificial gauge fixing dependence manifests in the truncated flow in a structurally different way than the artificial cutoff dependence. Low gauge fixing dependence of the most stable flows is hence strong evidence for the physical relevance of the used truncation. Furthermore, deeper insights into the structure of the theory, notably potential deficits of the used approximations, may be gleaned from such investigations.

This issue is studied for Einstein–Hilbert gravity in extra dimensions in this chapter. FP are found for all choices of gauge fixing. Cutoff optimisation is performed for 4 to 10 dimensions, different gauge fixings for the harmonic gauge condition and four sets of cutoff functions. The stability matrix eigenvalues show small dependences on gauge fixing. Large gauge fixing dependence of the FP couplings for $\alpha > 1$ is interpreted as a signal for the need of an extension of the truncation into the gauge fixing sector. Einstein–Hilbert truncation is argued to be quantitatively most reliable for $0 \leq \alpha \leq 1$. In this regime, all observables display excellent gauge independence.

The good quantitative gauge fixing independence of cutoff optimised results demonstrated in this chapter further strengthens confidence in the physical significance in more than four dimensions of FPs obtained in the Einstein–Hilbert truncation of ERG.

4.1 Fixed Points

In this section we repeat the FP search and optimisation procedure introduced in section 2.1.1 and applied to the case of harmonic gauge in section 3.1 for general gauges,

using cutoffs of type B. We find non-Gaussian UV FPs in all investigated space-time dimensions for generic cutoffs and all choices of gauge fixing. This confirms and extends results presented in [101], [103], [108].

The λ-boundary, marking the loss of stability of the flow, is encountered for generic cutoffs and dimensions. The optimisation procedure laid out in section 2.1.1 is applied to the FP values of λ with respect to this boundary.

Concerning the artificial gauge fixing dependence, we argue on technical grounds and find explicitly that for large α both λ_* and g_* become inversely proportional to α.

For $\alpha > 1$ we have to redefine the stability boundary with respect to type A (i.e. $\alpha = 1$). This follows from the construction of the optimisation procedures in section 2.1.1 and can be seen explicitly in the definition of the threshold functions (C.1) and their arguments in the flow equations, cf. appendix C.2: for $\alpha < 1$ the terms $\Phi(-2\lambda)$ encounter the zero in the denominator for smaller values of λ than $\Phi(-2\alpha\lambda)$, whereas for $\alpha > 1$ the situation is reversed. Hence we re-define

$$\alpha \leq 1 : \qquad \lambda_{\text{bound}} := \frac{1}{2}\left(\min_{z>0} z(1 + r(z))\right) \quad ,$$

$$\alpha > 1 : \qquad \lambda_{\text{bound}} := \frac{1}{2\alpha}\left(\min_{z>0} z(1 + r(z))\right) . \tag{4.1}$$

As an explicit example we consider the one parameter family of modified exponential cutoff functions (B.1). The same analysis has been repeated for three other families, the exponential (B.3), power-like (B.5) and modified (B.6) cutoff functions. The comparison of their results together with those of the optimised cutoff (B.4) and those of chapter 3 is performed in section 4.4.

FPs were searched for in integer dimensions 4 to 10 and a set of values of the gauge fixing constant $\alpha \in \{0, \frac{1}{2}, 1, \frac{3}{2}, 2, 10, 100, 1000\}$ for a (sufficiently) dense set of members of the four cutoff function families, parametrised by b.

The results of this search confirm and extend those of [103] and are very similar to those of cutoff type A: FPs below the stability boundary $\lambda_* < \lambda_{\text{bound}}$ are found in all dimensions and all choices of gauge fixing for a left bound interval of b. For low dimensions – 4 to 5 or 6, depending on the gauge fixing – no constraint on the cutoff arises from λ_{bound}. The value of b where λ_* runs into the boundary increases with the number of dimensions.

The FP values λ_* are displayed in fig. 4.1 for 4 and in fig. 4.2 for 10 dimensions as functions of the cutoff parameter b and gauge fixing α. A short look at fig. 4.1 and 4.2 discloses a basic difference between the intervals $\alpha \leq 1$ and > 1: in the first interval, λ_* is rather independent of α for both dimensions (and the non-displayed ones 5 – 9 too). A difference of less than 4% for 4 dimensions, which monotonously decreases with dimension to less than 2% for $d = 10$, is found for fixed cutoff parameter b. On the other hand, taking a closer look at a constant b section in fig. 4.3(a) we read off $\lambda_* = \text{const.} \times \alpha^{-1}$ for large α in the second interval. The transition between these two behaviours is fast, the $1/\alpha$ scaling is quite accurate for $\alpha \geq 2$. The FP value of the dimensionless Newton's constant, g_*, shows the same behaviour, see fig. 4.3(b).
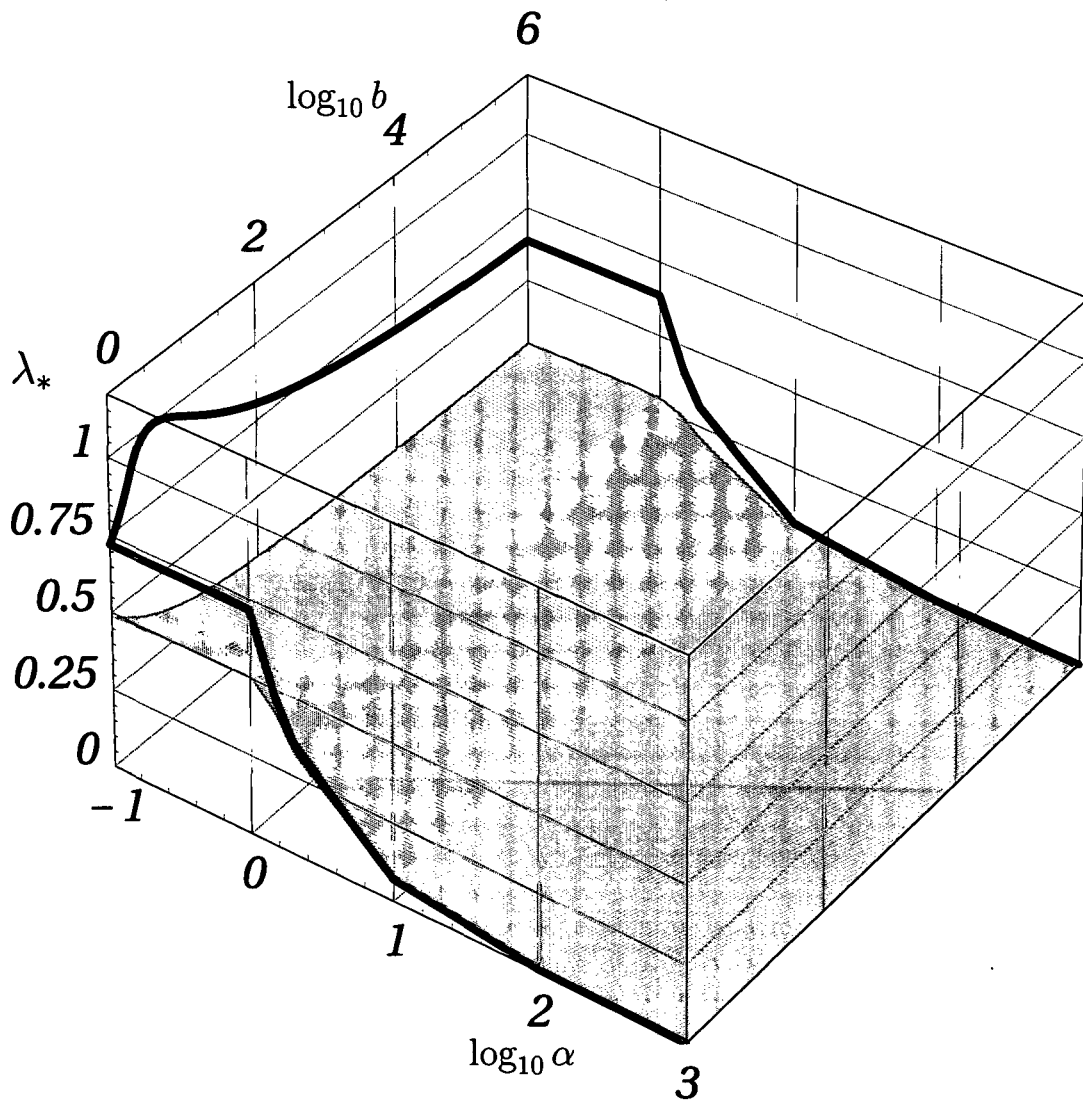
Figure 4.1: FP values of the dimensionless cosmological constant, λ_*, for the modified exponential cutoff in 4 dimensions. The red curve denotes the intersection of the $\lambda_{\text{bound}}(\alpha, b)$-plane with the confining box of the plot.
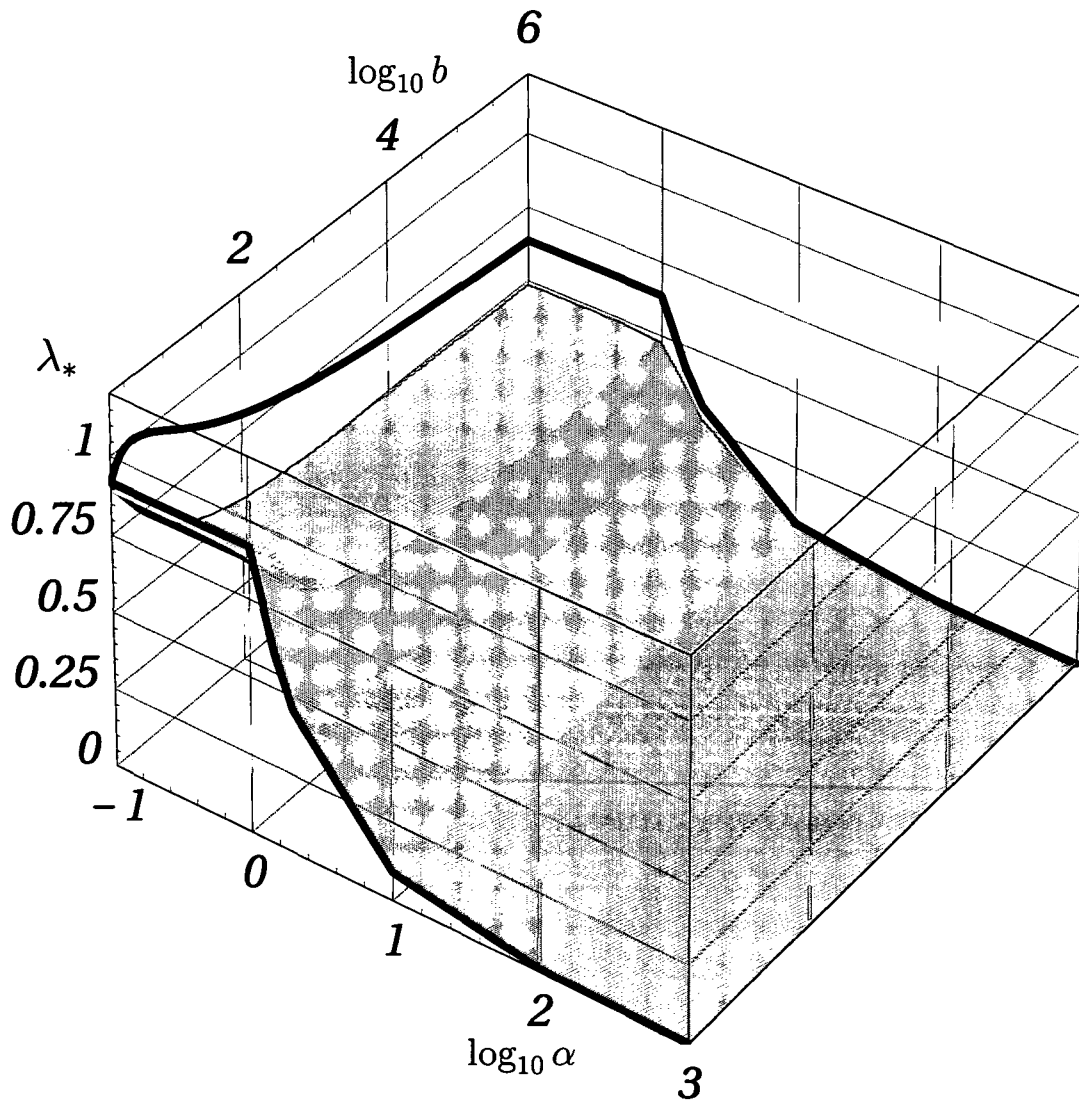
Figure 4.2: FP values of the dimensionless cosmological constant, λ_*, for the modified exponential cutoff in 10 dimensions. The red curve denotes the intersection of the $\lambda_{\text{bound}}(\alpha, b)$-plane with the confining box of the plot.
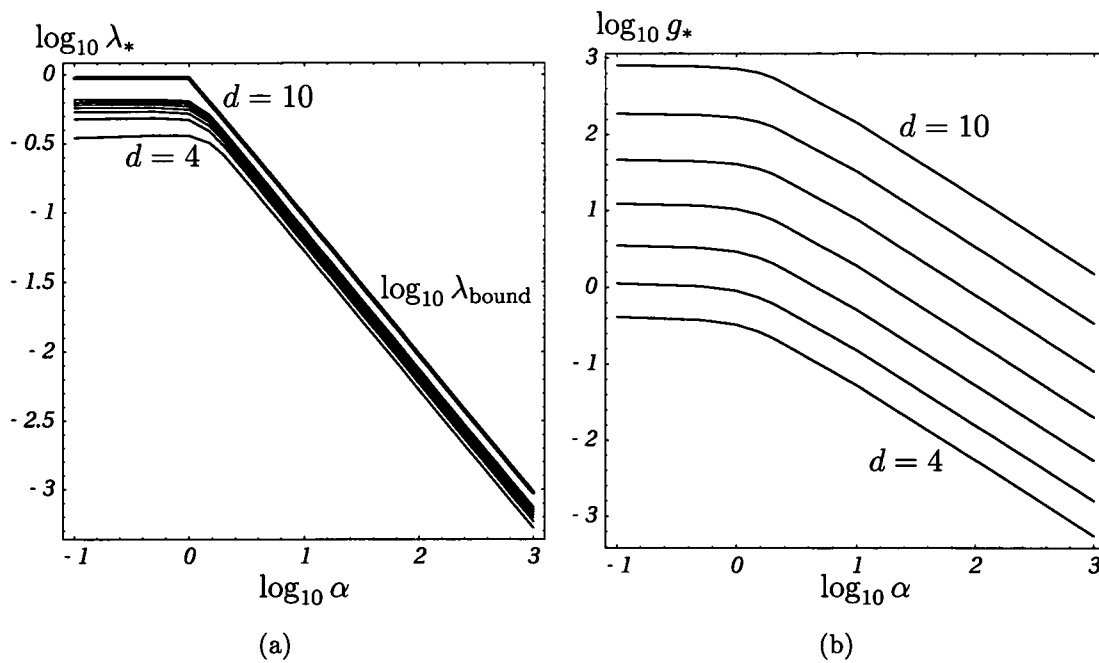
Figure 4.3: Double logarithmic plots of the couplings at the FP, (a) λ_* and (b) g_*, as functions of the gauge fixing parameter α for the modified exponential cutoff with $b = 10$ in dimensions 4 to 10.

This behaviour can be understood from the flow equations in appendix C.2. Since all solutions lie below the stability boundary for $\alpha > 1$: $\lambda_* < \lambda_{\text{bound}}(b, \alpha) = C(b)\,\alpha$ holds, where $C(b)$ depends only on the cutoff (and dimension) but not on α. Threshold functions with two different arguments, (-2λ) and $(-2\alpha\lambda)$ occur in the flow equations. For λ_* below the boundary, the first one goes to zero for sufficiently large values of α, the respective functions become asymptotically independent of λ. The precise meaning of "sufficiently large" is best read off from the exact solutions: $\alpha \geq 2$. The first FP condition, $\eta = 2 - d$, hence reads $\phi^2_{d/2}(-2\alpha\lambda_*) = \text{const}_d\,\tilde{\phi}^2_{d/2}(-2\alpha\lambda_*)$. In this case, all solutions behave like $\lambda_*^{(d,\alpha)} = \text{const}_d\,\alpha^{-1}$. Inserting this solution into the second FP condition, $\beta_\lambda = 0$, one reads off the solutions $g_* = \text{const}_d\,\lambda_* = \text{const}_d\,\alpha^{-1}$.

In [103] it is argued that $\alpha = 0$ is a FP of the gauge fixing and thus constitutes the "physical" gauge, cf. [93], [94] for Yang–Mills theory. According to this argument, the first-order gauge fixing dependence of the FP couplings could be viewed as irrelevant. It is furthermore quite reassuring that the technically advantageous case of $\alpha = 1$ does not suffer from this effect and reproduces the FP of $\alpha = 0$ accurately. In hindsight, this confirms the physical relevance of the historically prior cutoffs of type A.

On the other hand, the exact theory would show no gauge fixing dependence at all. Note that the strong dependence of λ_* and g_* on α does not necessarily imply that the Einstein–Hilbert truncation is unreliable for $\alpha > 1$. Remember that λ_* and g_* are not universal quantities themselves. They can be changed arbitrarily by redefining the auxiliary cutoff scale k or by rescaling the fields. Universal quantities, like eigenvalues of the stability matrix, or S-matrices, are invariant under such transformations.

To reach a definite conclusion on the potential artificiality of gauges $\alpha > 1$, we have to study the gauge dependence of observables or universal quantities, foremost the stability matrix eigenvalues. We also expect that ξ will yield a measure of the reliability of solutions in the interval $\alpha > 1$.

4.2 Cutoff Optimisation

We turn now to the stability control parameter ξ, cf. (2.18). As argued in section 2.1.1, it provides a measure for the stability and reliability of the FP solution. This has been confirmed by our findings for type A in chapter 3, where the maximisation of ξ lead to a reduction in the cutoff dependence of universal quantities. For the present case of general gauge fixing, we expect furthermore that the cutoff optimisation leads to reduced gauge fixing dependence of the universal quantities.

The first question to be posed for the present case of general gauge fixing is, whether extremization of ξ is possible for all values of the gauge fixing parameter. The answer is affirmative. A maximum in b is found for all dimensions and gauge fixings, see fig. 4.4 and fig. 4.5 for 4 and 10 dimensions.

Concerning the dependence on α, two qualitative features are noted: first, for fixed cutoff parameter b and sufficiently large α, ξ becomes independent of α. This follows from the definition of λ_{bound}, (4.1), and the α^{-1} behaviour of λ_* discussed above.

Second, ξ decreases systematically from the low-α to the high-α interval, while it stays independent of α within each interval separately. This is true for all dimensions
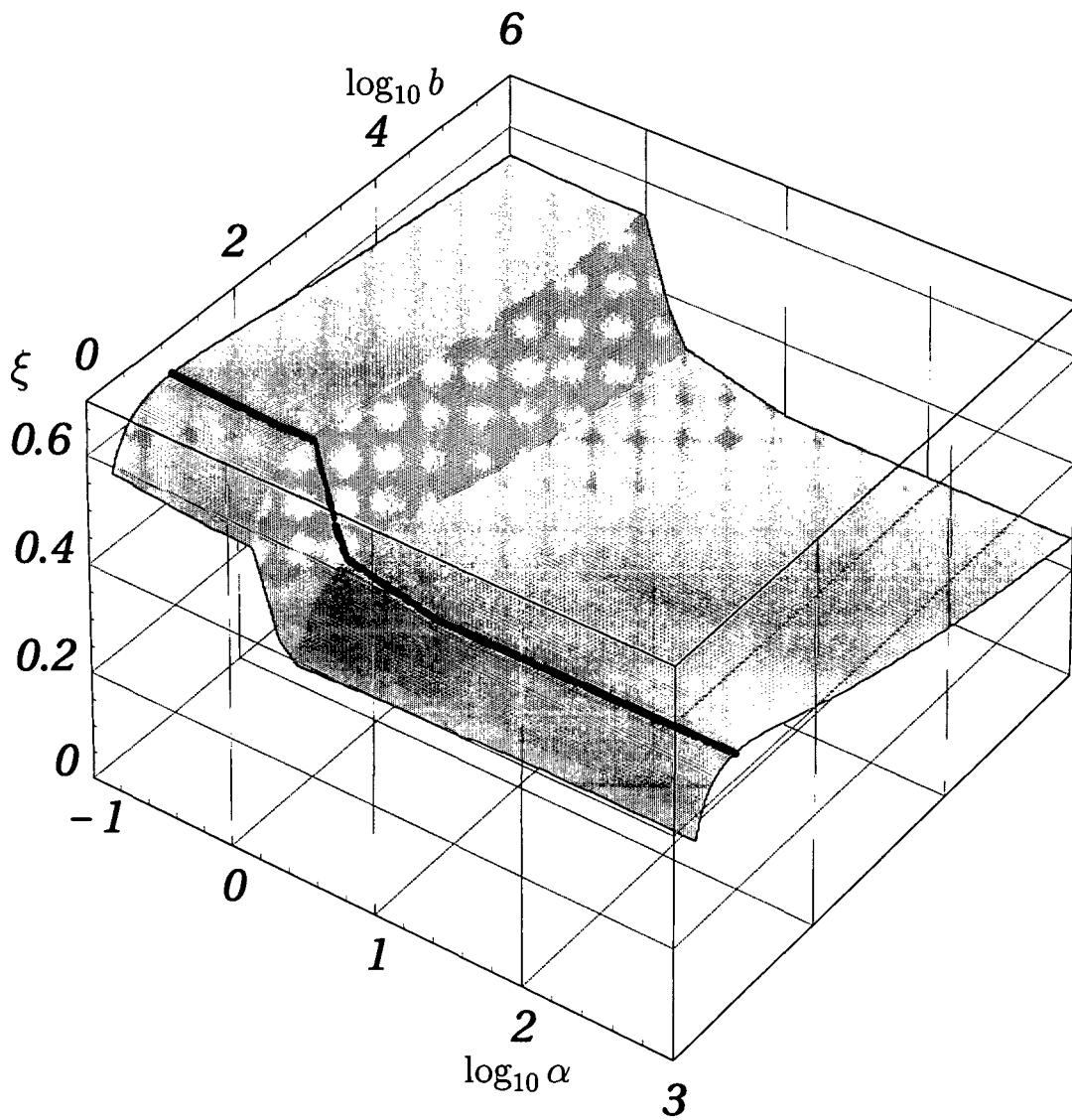
Figure 4.4: Stability control quantity ξ in 4 dimensions. The maxima of ξ in b for fixed α are displayed as a red curve.
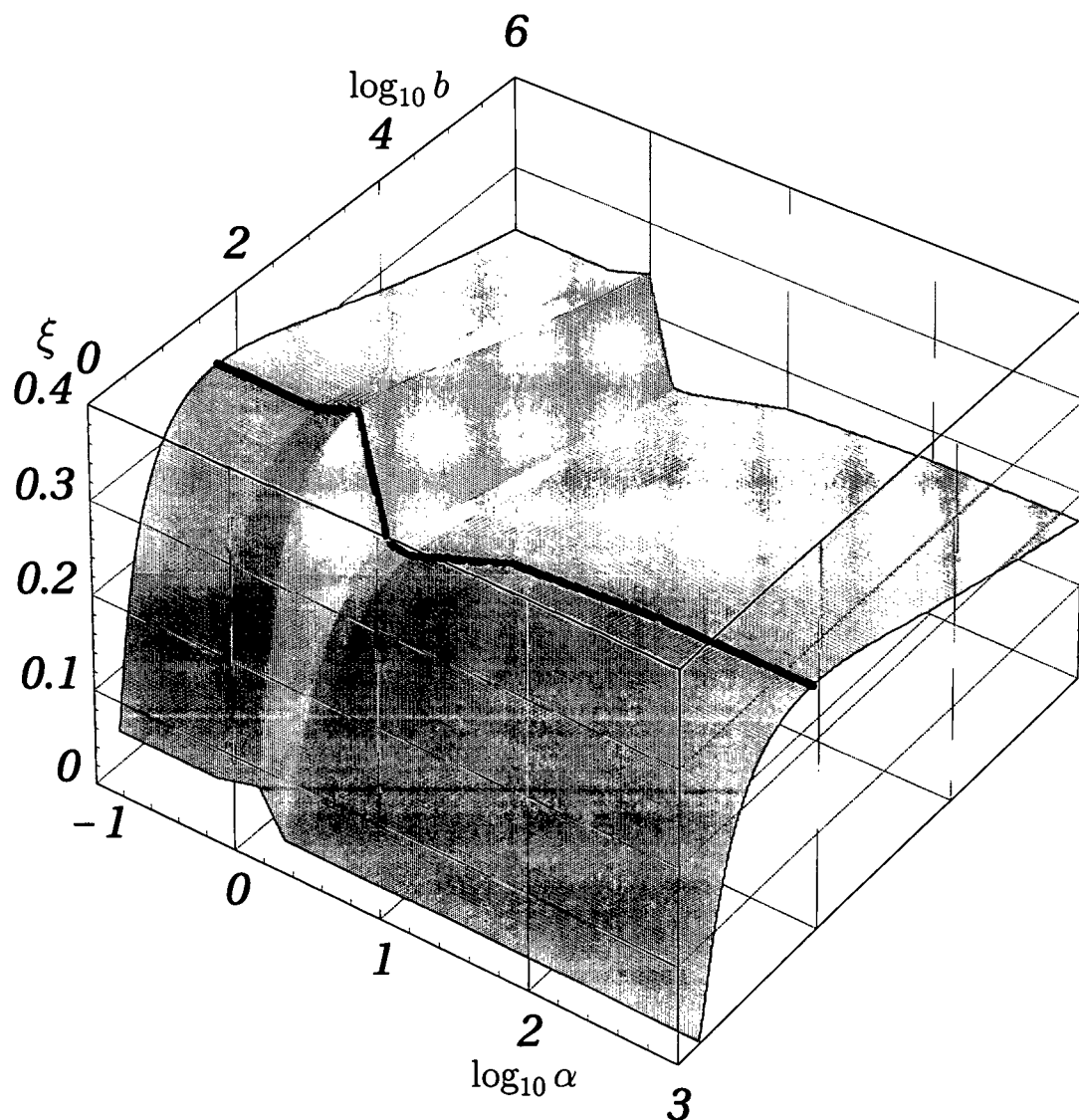
Figure 4.5: Stability control quantity ξ in 10 dimensions. The maxima of ξ in b for fixed α are as a red curve. ξ goes to zero where λ_* runs into the stability boundary.
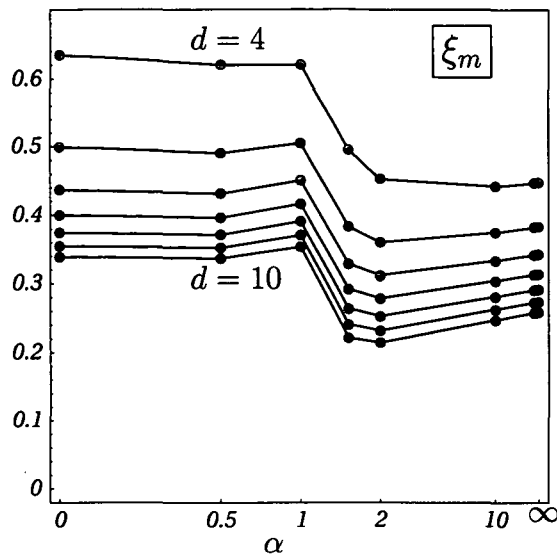
Figure 4.6: Maxima of ξ for different gauge fixings α and the modified exponential cutoff function.

and all fixed values of b.

In fig. 4.6 we display the values of the maxima of ξ and ξ_m for all dimensions and gauge fixings under consideration. ξ_m decreases by about 30% from $\alpha \leq 1$ to $\alpha > 1$ too. Otherwise, ξ_m remains quite constant within each interval separately. Interpreting ξ as a measure for stability of the flow and reliability of the cutoff, one concludes that they are higher for the interval $\alpha \leq 1$ than for its complement. This agrees with the interpretation of $\alpha = 0$ as the physical gauge, although an indistinct maximum is reached in the vicinity of $\alpha = 1$ for all dimensions except 4, where it is attained at $\alpha = 0$. This elevation is, however, too small to warrant any clear preference of $\alpha = 1$ over $\alpha = 0$ for $d > 4$.

ξ is universal in the sense that every redefinition of λ rescales λ_{bound} in the same way and ξ hence stays invariant. It is worthwhile to note that the qualitative leading order difference in the non-universal FP couplings between the low- and the high-α interval corresponds only to a quantitative 30% effect in this universal stability control parameter. This outcome is not obvious from the onset nor from the qualitative difference found for λ_* and g_* for low and high α in particular. Following our understanding of ξ as a measure for the reliability of the results, those from large α should be considered less reliable than those from small gauge fixings. This observation is further substantiated by the results for universal quantities discussed below.

The loci of ξ_m, b_{NNLO}, are given in table 4.1 for some values of α and various dimensions. As long as α remains low or high, b_{NNLO} is insensitive to it. The difference in b_{NNLO} between $\alpha \leq 1$ and $\alpha > 1$ depends on the dimension: while for dimensions 4 and 5 b_{NNLO} is higher for low gauge fixings than for high ones, this relation is reversed for dimensions 6 and above.

Table 4.1: Loci of ξ_m, b_{NNLO}, for the modified exponential cutoff function.

b_{NNLO}	$\alpha = 0$	1	2	10	1000
$d = 4$	13.429	14.207	10.440	7.518	7.165
5	11.343	11.373	10.892	10.191	10.002
6	13.975	13.942	14.324	14.620	14.801
7	18.681	18.544	19.998	21.567	22.156
8	25.918	25.621	28.833	32.415	33.755
9	36.860	36.310	42.547	49.558	52.306
10	53.458	52.509	63.979	76.899	82.414

4.3 Universality

In the full theory, the universal quantities are insensitive to the choice of the cutoff function and the gauge fixing. Truncation introduces an artificial cutoff and gauge fixing dependence. By optimising the cutoff with respect to stability of the flow, regions in cutoff space were identified which exhibit reduced cutoff dependence.

If cutoff optimisation corresponds to choosing the most reliable projection of the full theory (infinite dimensional in theory space) onto the (finite dimensional) truncation subspace, it would be expected that the optimised universal quantities show reduced gauge dependence too. To verify this claim, we investigate again the cutoff-dependence of the eigenvalues of the stability matrix at the FPs and the potential universal quantity τ.

As for type A, θ' is positive in all cases, all FPs are UV-attractive for both couplings. This is the case for all dimensions, gauge fixings and admissible cutoffs investigated, and confirms previous results [101], [103], [108] as well as those presented in chapter 3, extending them to higher dimensions and a wider range of gauge fixings.

Our expectations concerning cutoff optimisation are confirmed: it leads indeed to reduced gauge dependence of the stability matrix eigenvalues.

Concerning τ, a more complicated picture arises. Although τ is remarkably insensitive to the choice of the cutoff and the gauge fixing for $\alpha \leq 1$, it acquires a strong α dependence in dimensions higher then 4.

Again, we restrict the detailed discussion of this section to the modified exponential cutoff function. Similar results are obtained for the exponential, power-like, modified and optimised one. The quantitative comparison is performed in section 4.4.

4.3.1 Gauge dependence of stability matrix eigenvalues

To furnish a concrete example we now discuss the full α and b dependence of the stability matrix eigenvalues for one specific space-time dimension, $d = 10$.

θ' and θ'', as well as the modulus $|\theta| = \sqrt{(\theta')^2 + (\theta'')^2}$, in 10 dimensions are displayed in fig. (4.7), fig. (4.8) and fig. (4.9) for 10 space-time dimensions and the modified

exponential cutoff function. The values for the optimised cutoffs at fixed α are displayed by the red lines. The qualitative features displayed for 10 dimensions are also present in the other dimensions, but they are less pronounced. The planes in fig. (4.7) to fig. (4.9) become monotonously flatter with decreasing number of dimensions: cutoff and gauge fixing dependence increase with the number of with dimensions. In this sense, $d = 10$ constitutes the "worst example" investigated.

First, one notes a step in all three quantities along the line $\alpha = 1$. This happens in all dimensions and accords with the differences in λ_*, g_* and ξ for low and high gauge fixing. For the stability matrix, the typical height of the step (for fixed b) is of the same order as for ξ, amounting to a relative difference of about 30%.

Within each of the two intervals $\alpha \leq 1$ and $\alpha > 1$, the cutoff dependence is mild over a wide range of b-values, although it is higher for the $\alpha > 1$ interval than its complement in all dimensions. Cutoff optimisation picked out a sequence of values of θ' and $|\theta|$ which lie very close to the bottom of the valley of minimal cutoff dependence. For θ'', which is monotonously falling in b, the optimised results lie near to those of minimal, though non-extremal, cutoff dependence. The same happens in the other dimensions, although it depends on dimension and gauge fixing whether a clear extremum exists – as in $d = 10$ and all α for θ', $|\theta|$ – or not (cf. θ''). See chapter 3 for the analogous discussion for type A.

This is a success of cutoff-optimisation: the b-minima of these universal quantities were identified without referring to these quantities themselves. Furthermore, the step between the $\alpha \leq 1$ and $\alpha > 1$ intervals is of reduced height for the optimised cutoffs compared to generic cutoffs.

A (semi-) qualitative changes occurs for small values of b close to the stability boundary and for very large ones: θ'' vanishes and the eigenvalues become real. They are both positive, both directions in the $\lambda - g$ plane remain UV-attractive. The difference between this case and the generic one is that trajectories approach the fixed point straight on without spiralling. The FP is UV-attractive for both directions in all studied cases.

Again, this phenomenon extends to some of the other dimensions. The lower of the two values of b, where this transition happens, decreases rapidly with dimension toward the minimally allowed one, where ξ goes to zero. The available data-point density is insufficient to resolve this effect for dimensions lower than 9. Whether the transition actually takes place for $d \leq 8$ hence remains unclear. One should remark that also in 9 and 10 space-time dimensions these β-values lie so close to the stability boundary that the reliability (as measured by ξ) of this finding is very low. This is also illustrated by the very large b-dependence of θ' and $|\theta|$ very close to the stability boundary.

Also the high b-value, above which θ'' vanishes, increases with dimension and decreases with gauge fixing. Since the maximal cutoff parameter investigated is 10^{10} and we did not investigate the sharp cutoff, which is the $b \to \infty$ limit of the modified exponential one, we cannot comment whether the transition from complex to real eigenvalues holds for all dimensions and gauge fixings. Since complex eigenvalues are reported for the sharp cutoff of type A in 4 dimensions [108], we suspect that this is not the case.

We conclude that even for these non-generic cases of poor reliability (i.e. low ξ) the FP remains UV-attractive, a feature which proves to be very resilient. All of the above

Figure 4.7: $\log b$-$\log \alpha$ plot of θ' in 10 dimensions for the modified exponential cutoff, in red the values for the NNLO optimised cutoff.

Figure 4.8: $\log b$-$\log \alpha$ plot of θ'' in 10 dimensions for the modified exponential cutoff, in red the values for the NNLO optimised cutoff.
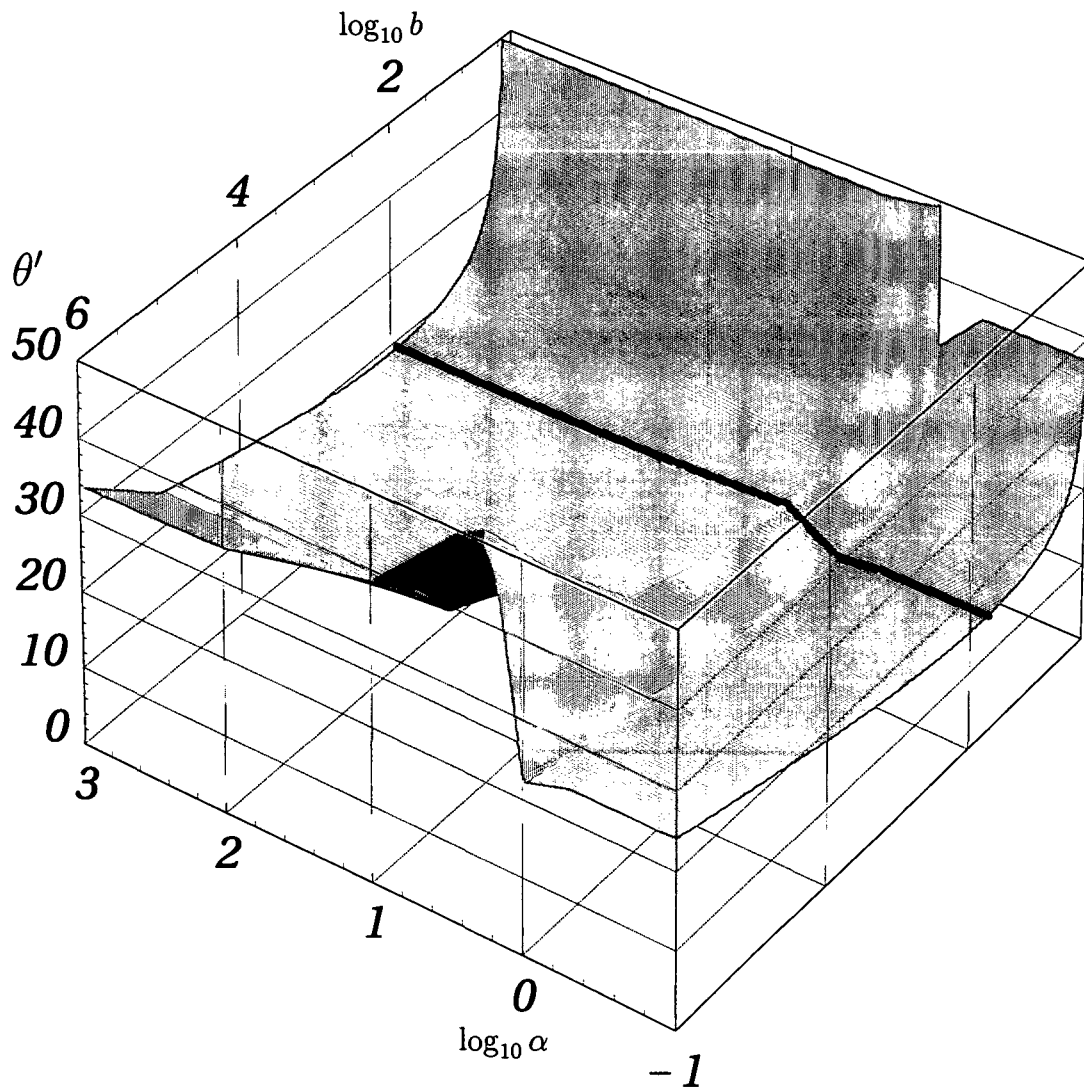
Figure 4.9: $\log b$-$\log \alpha$ plot of $|\theta|$ in 10 dimensions for the modified exponential cutoff, in red the values for the NNLO optimised cutoff.

Table 4.2: (a) Mean values $\bar{\theta}', \bar{\theta}''$ over $\alpha \in \{0,,\frac{1}{2},1,\frac{3}{2},2,10,100,1000\}$ and (b) reduced mean values $\hat{\theta}', \hat{\theta}''$ over the reduced set $\alpha \in \{0,,\frac{1}{2},1\}$ for optimised modified exponential cutoffs.

	(a)				(b)	
d	$\bar{\theta}'$	$\bar{\theta}''$	d	$\hat{\theta}'$	$\hat{\theta}''$
4	1.769 ± 0.280	3.443 ± 1.031	4	1.882 ± 0.167	2.507 ± 0.094
5	3.191 ± 0.399	5.712 ± 1.044	5	2.944 ± 0.152	4.829 ± 0.161
6	5.216 ± 0.785	7.831 ± 1.067	6	4.607 ± 0.176	6.995 ± 0.231
7	7.624 ± 1.189	9.842 ± 1.070	7	6.664 ± 0.230	9.053 ± 0.281
8	10.370 ± 1.623	11.752 ± 1.038	8	9.046 ± 0.299	11.022 ± 0.308
9	13.486 ± 2.133	13.555 ± 0.969	9	11.729 ± 0.376	12.903 ± 0.317
10	16.930 ± 2.677	15.260 ± 0.881	10	14.710 ± 0.457	14.686 ± 0.307

confirms and extends previous results [103], [108], [134].

4.3.2 Optimised cutoff values of stability matrix eigenvalues

After having discussed the entire accessible $b - \alpha$ plane, we focus now on the results for optimised cutoffs. They are shown in fig. 4.10(a) to fig. 4.10(c).

The difference between low ($\alpha \leq 1$) and high gauge fixing parameters is clearly visible. The gauge fixing dependence of the cutoff optimised results is very low within each interval and mild in between (in the 25 - 30 % range). Except for θ' in $d = 4$, the minima in α lie in the vicinity of $\alpha = 1$. This accords perfectly with the picture gained from the analysis of ξ, see section 4.2.

Note also that for each α the difference $\theta'_{NNLO}(\alpha, d+1) - \theta'_{NNLO}(\alpha, d)$ increases with d whereas $\theta''_{NNLO}(\alpha, d+1) - \theta''_{NNLO}(\alpha, d)$ decreases. The value of $|\theta|_{NNLO}(\alpha, d+1) - |\theta|_{NNLO}(\alpha, d)$ approximately stays constant. This rotation of the complex eigenvalues toward the real axis extends the findings for type A to general gauge fixings. It fits to the fact that the size of the b-interval for which complex eigenvalues are found decreases with dimension.

To facilitate the comparison of the NNLO optimised results for the modified cutoff to others, we use again *mean values* and corresponding *errors*. This should be viewed as a rough estimate for the "error-bar" of the results.

The mean values of the cutoff optimised quantities $\bar{\theta}'$ and $\bar{\theta}''$ are defined as half the sums between the respective biggest and the smallest value over α. The error-bar is introduced as half the difference between them. The resulting numbers are given in table 4.2(a). The relative error of θ' stays approximately constant for all dimensions, whereas the absolute error of θ'' even decreases slightly. The major contribution to these error bars comes from the difference between low- and high-α results.

One could take the point of view that results for $\alpha > 1$ should be excluded from these condensed results. This could be argued both on the ground that $\alpha = 0$ is the "correct" gauge fixing and that the (albeit non-universal) FP couplings are qualitatively
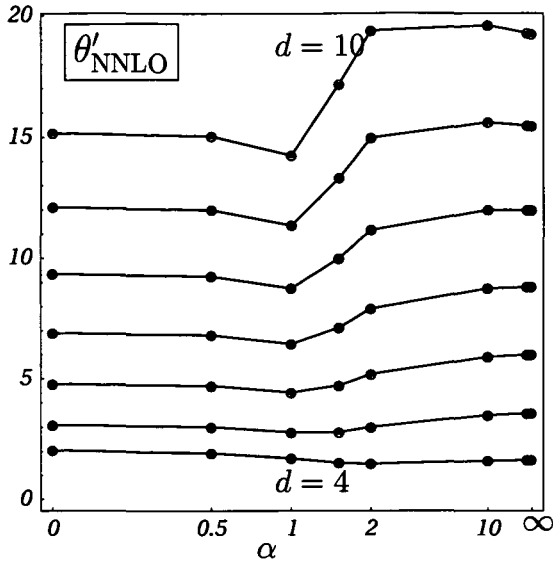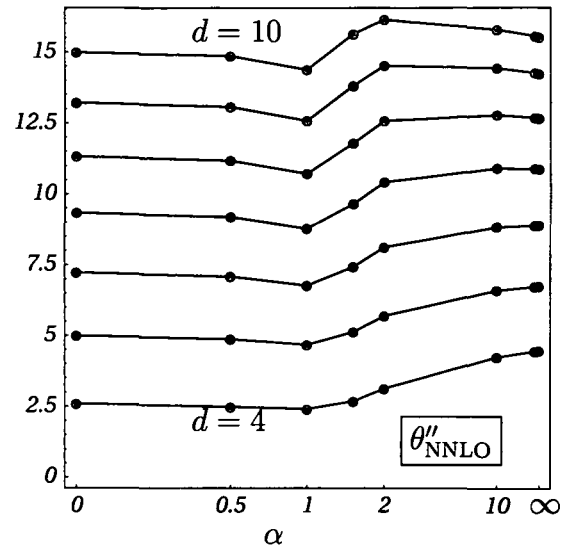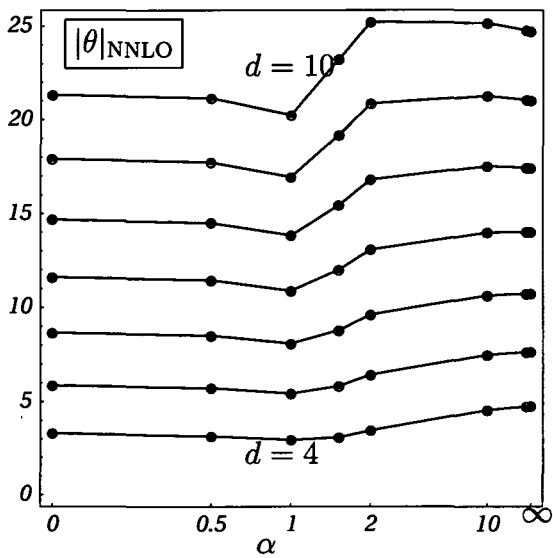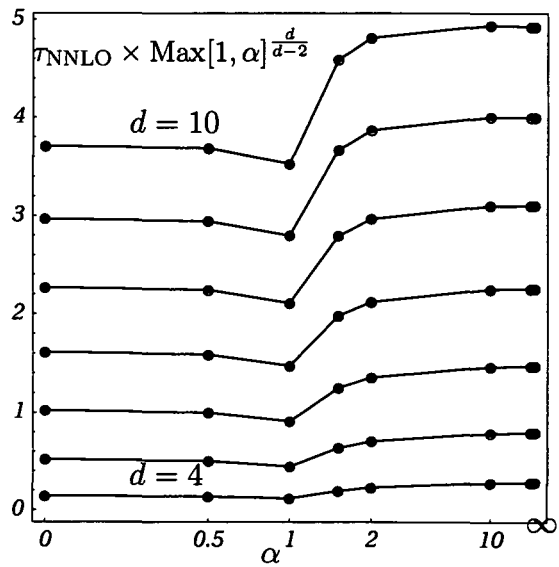
Figure 4.10: Universal quantities (a) θ', (b) θ'', (c) $|\theta|$ and (d) $\tau(b_{\text{ratio}}) \times \text{Max}[1, \alpha]^{\frac{d}{d-2}}$ (cf.main text) for NNLO-optimised modified exponential cutoff and different dimensions and gauge fixings.
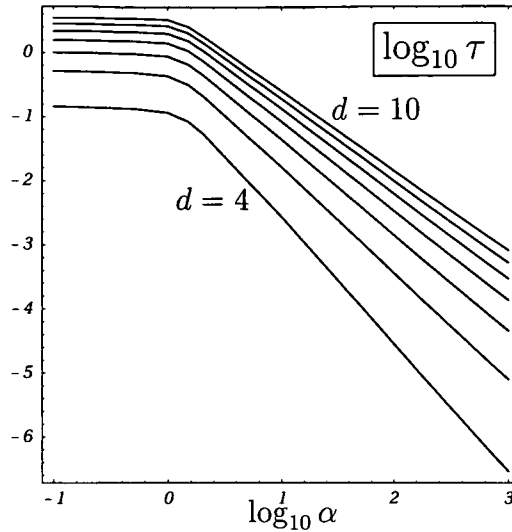
Figure 4.11: Double logarithmic plot of τ for dimensions 4 to 10 and the modified exponential cutoff function with parameter $b = 10$.

different for $\alpha > 1$ from those at $\alpha = 0$. Furthermore, the maximal quality achievable for fixed α, as measured by ξ_m, is systematically lower for the high-α interval than for the low-α one. On this ground, we define the reduced mean values $\hat{\theta}'$, $\hat{\theta}''$ as the half-sum of θ'_{NNLO}, θ''_{NNLO} for $\alpha = 0$ and $\alpha = 1$. These modified mean values are given in table 4.2(b). They are systematically lower than the full mean values, except for $\hat{\theta}'$ in 4 dimensions. The corresponding errors are lower by a factor of 2 to 6. The relative error is now reduced down to the few percent range.

4.3.3 Gauge dependence of dimensionless combination of couplings

We turn now to the second quantity, $\tau = \lambda_* \times g_*^{2/(d-2)}$, introduced in section 3.2 as the generalisation of the product $\lambda_* g_*$ from 4 to general dimensions.

If permitting for an interpretation as a universal quantity, it should be robust to variations of the cutoff. Indeed it was found to be very stable under variations of b in 4 to 10 dimensions and for all investigated cutoffs. For fixed gauge fixing α, τ shows cutoff sensitivity similar to that of cutoffs of type A. We will not repeat the discussion of the cutoff dependence performed in section 3.2.2 for $\alpha = 0$.

Presently, we concentrate on the gauge fixing dependence of τ. To constitute a physical quantity in the present theory, it should be independent of the choice of gauge fixing. For $\alpha \le 1$, the gauge fixing independence of λ_* and g_* carries through to τ. But, as can be surmised immediately from the behaviour of λ_* and g_*, this fails to be the case for $\alpha > 1$: asymptotic α^{-1} scaling of the fixed point couplings leads to

$$\alpha > 1 : \tau \sim \alpha^{-\frac{d}{d-2}} . \tag{4.2}$$

This is displayed explicitly in the double-logarithmic plot in fig. 4.11. This result can

be interpreted in three different ways.

(i) One possible interpretation is to discard τ as a candidate for a universal quantity, since it exhibits strong gauge fixing dependence. Against this speaks the excellent degree of gauge fixing independence in the low-α interval.

(ii) With a look to both the understanding of $\alpha = 0$ as the physical choice and inferior quality (cf. section 4.2) for $\alpha > 1$, one could regard the interval of high values of the gauge fixing as plagued by artificial α dependence and hence disregard any results obtained from it. The first-order α dependence of τ lies then outside the applicability of the truncation. Only an extended truncation could open $\alpha > 1$ for reliable calculations.

(iii) An intermediate stance would be to grant τ physical status for $\alpha \leq 1$ only. Consequently, one would have to view Einstein–Hilbert gravity with $\alpha > 1$ as a theory distinct from the same truncation for $\alpha \leq 1$. Whether it possesses a physical interpretation or simply indicates the need to extend the truncation remains open. An argument for this point of view is that the difference in optimised quality ξ_m and universal θ for low and high α is only quantitative. Furthermore, after taking out the asymptotic α behaviour, $\tau \times \mathrm{Max}[1, \alpha]^{\frac{d}{d-2}}$ shows very little residual gauge fixing dependence, see fig. 4.10(d) for the values for optimised cutoff. Values of cutoff optimised τ rescaled in this way within the intervals $\alpha \leq 1$ or > 1 are strongly correlated: relative internal differences are between 5 to 20 % and decrease with dimension. But even between the two intervals the difference of rescaled values of τ is only a factor of two for $d = 4$, decreasing with dimension to 50% in 10 dimensions.

4.4   Cutoff Independence

In the previous sections we have discussed cutoff and gauge fixing dependence of the UV FP properties obtained via the modified exponential cutoff function. Cutoff optimisation was repeated with the exponential (B.3), power-like (B.5) and modified (B.6) cutoff functions. In this section we compare the optimised results from these three, the modified exponential and the optimised cutoff (2.19) with each other and the results of chapter 3.

The respective cutoff functions are listed in table 3.4 together with the values of the cutoff parameter b_{LO} at which the respective λ_{bound}'s are maximal.

This broad range of cutoff functions allows for a twofold analysis: first, we compare the NNLO-optimised results obtained by the use of the various cutoff functions within either type A or B. This constitutes an important test for the optimisation procedure: it must yield the same physical results for all cutoffs. Any difference between optimised cutoffs can be ascribed as a minimal error to the results.

Second, comparing results found for cutoffs of type A with those of type B gives a quantitative measure of the impact of the different decompositions of field space underlying the two types. In the full, untruncated theory this would make no difference. But in the present, truncated case, this distinction serves as a profound test for the reliability of the cutoff optimised truncation. These investigations extend those of [103], [108] to other cutoff functions and higher dimensions.

Table 4.3: Legend for fig. (4.12) – fig. (4.13(d)).

cutoff	colour	symbol
power-like	green	filled circle
modified exp.	black	circle
exponential	red	square
modified	blue	triangle
optimised	rosé	diamond

The results displayed below exhibit stability to all of the above variations in all investigated space-time dimensions. The UV FP arise in all investigated cases and share the same qualitative features. No signs of significant, qualitatively relevant artificiality could be discovered. Einstein–Hilbert truncation, enhanced by cutoff optimisation, passes these tests very well.

4.4.1 Comparison of optimised qualities

One of the advantages of using the universal quality control quantity ξ is that it can be straightforwardly compared for different cutoffs and gauge fixings. We take its maxima ξ_m as a basis to compare the optimised qualities of the various cutoffs. The information gleaned thereby can be used as a bias in the interpretation of the reliability of the results obtained through the respective cutoff functions.

We repeated the cutoff optimisation for the four plus one cutoff functions of type B for general gauge fixings. The first observation is that optimisation of the stability was possible for all four cutoffs, for all considered dimensions and values of α. The resulting values ξ_m together with those for the optimised cutoff are displayed exemplary for dimensions 4 and 10 in table 4.12. Those of dimensions 5 to 9 interpolate between them like those of the modified exponential cutoff in fig. 4.6. The colour-symbolic legend for this and the following figures of the present section is given in table 4.3.

The characteristic features discovered for type A and the modified exponential type B cutoff (black circles) are reproduced for the other cutoffs. Especially the pertinence of the difference between low (≤ 1) and high (> 1) gauge fixing parameters supports its interpretation of stemming directly from the structure of the flow. For all five cutoffs ξ_m stays rather constant for low and high α's separately, but decreases from the first to the latter interval. It decreases monotonously with dimension for all gauge fixings. As observed already for type A, the optimised cutoff leads by a 3-10% margin. Exponential, modified exponential and modified cutoffs are of equal quality.

The monomial power-like cutoff function displays lower values of ξ_m than the other four ones for $\alpha > 1$ or higher dimensions. We are lead to expect lessened reliability of results obtained with the power-like cutoff. This furnishes a "bad example" to check the relevance of the biases based on ξ_m. One expects an increased spread in physical results calculated with this cutoff and those obtained via the other cutoff functions.

Comparing ξ_m's from type A with those of type B, we note the accordance of the
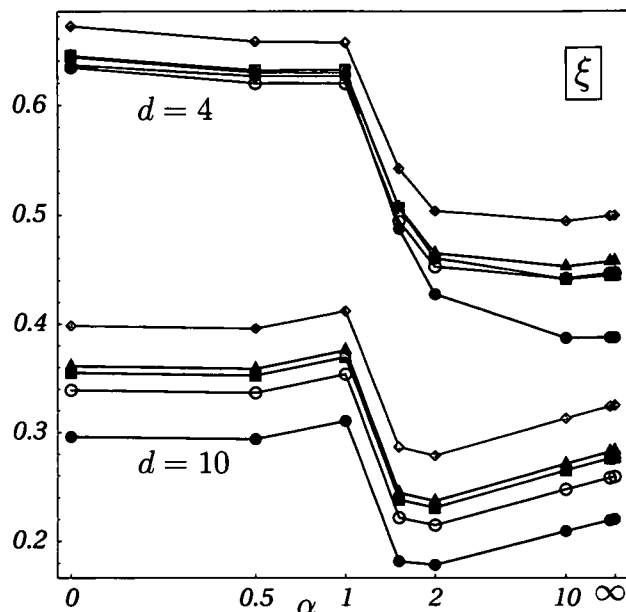
Figure 4.12: ξ_m for 4 and 10 dimensions and five different cutoff functions. The full legend is given in tab.4.3.

former with $\alpha \leq 1$ of the latter. Although the quality appears to be consistently better for all cutoffs of low α type B than for type A at dimension 4, this difference vanishes when going to higher dimensions. For $d = 10$ it becomes indiscernible. Judging from ξ_m alone, we find type A and low-α type B cutoffs to be equally trustworthy, whereas type B for $\alpha > 1$ appears inferior in quality. Equipped with these biases, we turn now to θ and τ.

4.4.2 Comparison of cutoff optimised θ–values

NNLO-optimised θ', θ'' and $|\theta|$ are displayed in fig. 4.13(a) to fig. 4.13(c). Dimensions 4, 6 and 10 were chosen as examples. The results for dimensions 5, 7, 8, and 9 obtained for the four new cutoff functions interpolate between the displayed ones. Qualitatively, they behave as those yielded by the modified exponential cutoff, cf. fig. 4.10(a) to fig. 4.10(c).

The accordance of the four new sets of curves with the already discussed ones belonging to the modified exponential cutoff is striking. All features discovered with that cutoff function are reproduced by the other four functions. Furthermore, our identification via ξ_m of the monomial power-like cutoff as the rotten apple receives confirmation: whereas the results of the other 4 optimised cutoffs coincide accurately, those obtained with the power-like cutoff function (represented by the green curve with the filled circles) are outliers for practically all dimensions and gauge fixings that were studied. Conse-

quently, the power-like cutoff is excluded from the determination of the mean values and according errors.

But if we trust our stability considerations so far as to apply this cut, another exclusion is inevitable. Following the arguments presented in section 4.3.2, we restrict the averaging to gauge fixings $\alpha = 0, \frac{1}{2}, 1$. One further argument for this restriction is that the type A results belong to the low α interval and should be compared to those from B belonging to the same set. Consequently, we define the mean values $\bar{\theta}'_B, \bar{\theta}''_B$ and $|\bar{\theta}|_B$ as half the sums of the suprema and infima of the respective quantities on the product space $\mathfrak{A} \times \mathfrak{R}$ with $\mathfrak{A} := \{\alpha : 0, \frac{1}{2}, 1\}$ and $\mathfrak{R} := \{r : r^{\text{exp}}, r^{\text{mexp}}, r^{\text{opt}}, r^{\text{mod}}\}$. The error-bars are given by half the differences. These values are presented in table 4.4(a) to 4.4(c) together with a repetition of those of type A.

The error-bars of quantities for general gauge fixings are bigger than those obtained for harmonic gauge only. This is because of varying α in addition to varying the cutoff functions. Relavtive to the mean values, they range from 11% for $\bar{\theta}'_B(d = 4)$ to 3.6 % for $\bar{\theta}''_B(d = 10)$. Generally, they decrease with dimension. The relative errors of $\bar{\theta}''_B$ are smaller than those of $\bar{\theta}'_B$.

The accordance of type A mean values with type B ones increases with dimension. $\bar{\theta}'_A$ lies within one error bar of $\bar{\theta}'_B$ from 5 dimensions onward, with a less than two error-bars difference at $d = 4$. The error-bars of $\bar{\theta}''$ and $|\bar{\theta}|$ overlap for $d \geq 6$ [1] and $d \geq 4$. It seems justified to speak of identical results from type A and B, within the given errors.

Cutoff optimisation has suppressed the differences in the universal eigenvalues obtained in a wide set of calculational schemes to the few percent level. For different field decompositions (type A and B), gauge fixings and cutoff functions it consistently leads to coinciding results within this level of accuracy.

4.4.3 Comparison of cutoff optimised τ–values

In section 4.3.3 we studied τ using the modified exponential cutoff function. Utilizing the other functions confirms the degree of its cutoff independence.

The rescaled values of τ are displayed for the five optimised cutoffs of type B in fig. 4.13(d) for $d = 4, 6, 10$. The results for the other dimensions interpolate between them. With the exception of the power-like cutoff, the data points coincide to the degree of graphical indistinguishableness. The relative outlier status of the power-like cutoff values of τ confirms the previous observations.

Therefore, we exclude it from the determination of the mean value. Also only $\alpha \leq 1$ is taken into consideration since τ is not a meaningful quantity in the complement, at least not in the present truncation. Consequently, the mean values $\bar{\tau}_B$ are defined over the same set $\mathfrak{A} \times \mathfrak{R}$ as those of the θ's.

The main contribution to its error-bar comes from the residual α-dependence which exceeds the spread induced by the different cutoff functions. The relative error decreases from 12% in 4 dimensions to 3 % in 10. It is displayed together with the one mean values of type A, $\bar{\tau}_A$, in table 4.4(d). This error exceeds that of $\bar{\tau}_A$, which is around 1%, by half a magnitude. Nevertheless, the two means lie within one error bar (of $\bar{\tau}_B$) of each

---

[1] With less than 3 error-bars difference for $d = 4$ and less than 2 for $d = 5$.
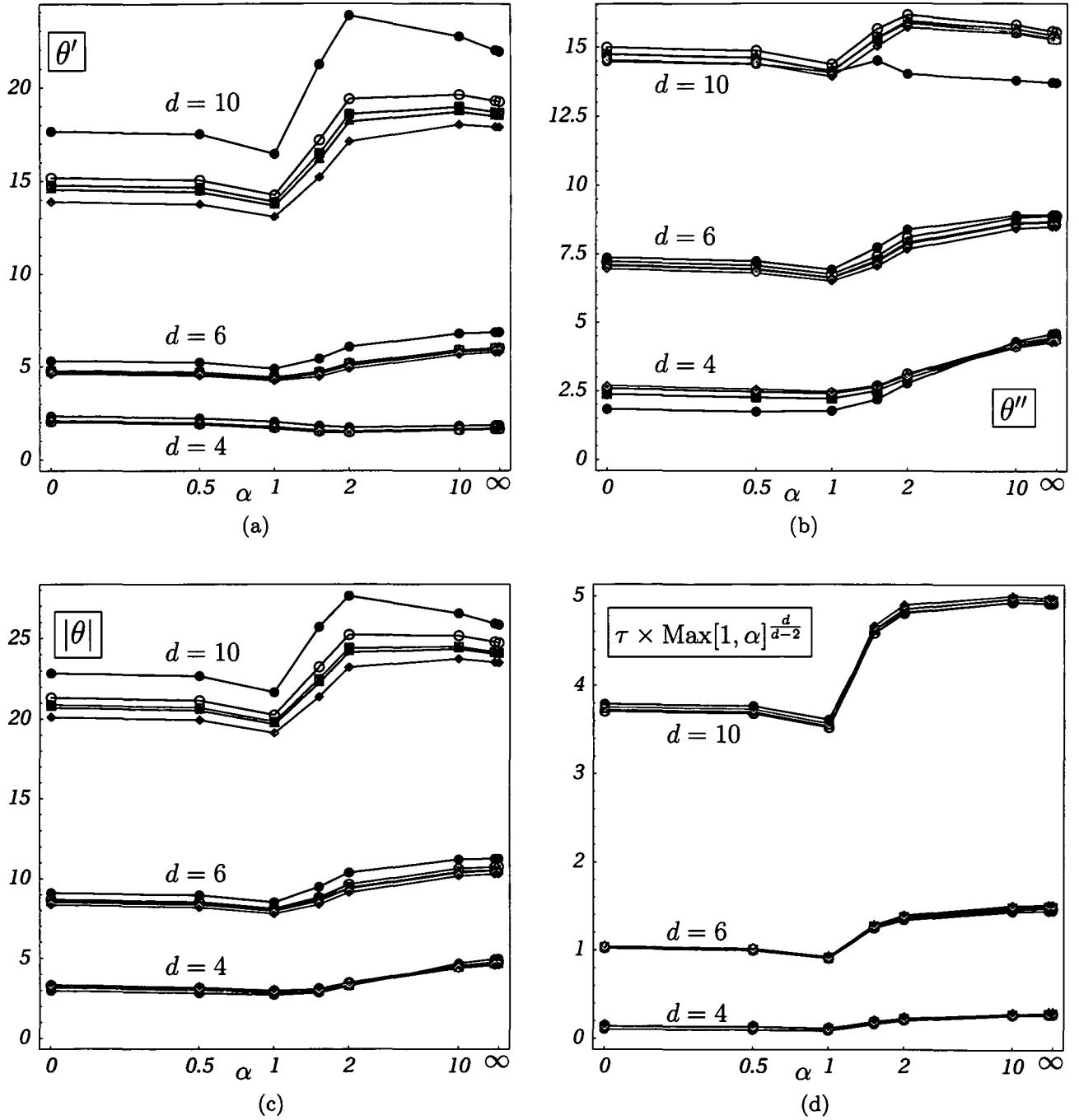
Figure 4.13: Universal quantities (a) θ', (b) θ'', (c) $|\theta|$ and (d) $\tau \times \text{Max}[1, \alpha]^{\frac{d}{d-2}}$ in 4, 6 and 10 dimensions and gauge fixings $\alpha \in \{0, \frac{1}{2}, 1, \frac{3}{2}, 2, 10, 100, 1000\}$ for five NNLO optimized cutoffs. The full legend is given in tab.4.3.

Table 4.4: Comparison of the mean values and errors of the universal quantities (a) θ', (b) θ'', (c) $|\theta|$ and (d) τ of type A and type B (suffixes A and B). See the main text for the defenition of these mean values.

(a)

d	$\overline{\theta'_A}$	$\overline{\theta'_B}$
4	1.505 ± 0.029	1.899 ± 0.210
5	2.760 ± 0.073	2.923 ± 0.184
6	4.465 ± 0.133	4.523 ± 0.260
7	6.492 ± 0.220	6.496 ± 0.398
8	8.801 ± 0.342	8.768 ± 0.577
9	11.371± 0.490	11.314 ± 0.791
10	14.202± 0.667	14.129 ± 1.039

(b)

d	$\overline{\theta''_A}$	$\overline{\theta''_B}$
4	3.094 ± 0.050	2.461 ± 0.230
5	5.262 ± 0.107	4.767 ± 0.223
6	7.301 ± 0.159	6.871 ± 0.355
7	9.255 ± 0.201	8.880 ± 0.453
8	11.143± 0.227	10.815± 0.515
9	12.970± 0.233	12.680± 0.539
10	14.730± 0.214	14.471± 0.522

(c)

d	$\overline{|\theta|_A}$	$\overline{|\theta|_B}$
4	3.435 ± 0.053	3.114 ± 0.260
5	5.934 ± 0.122	5.589 ± 0.283
6	8.554 ± 0.201	8.226 ± 0.440
7	11.305± 0.291	11.003± 0.601
8	14.200± 0.390	13.923± 0.763
9	17.250± 0.498	16.995± 0.929
10	20.464± 0.617	20.229± 1.099

(d)

d	$\overline{\tau_A}$	$\overline{\tau_B}$
4	0.135 ± 0.002	0.131 ± 0.016
5	0.469 ± 0.008	0.487 ± 0.042
6	0.948 ± 0.015	0.978 ± 0.068
7	1.523 ± 0.021	1.560 ± 0.087
8	2.167 ± 0.025	2.208 ± 0.101
9	2.861 ± 0.028	2.905 ± 0.1103
10	3.596 ± 0.028	3.641 ± 0.115

other for all dimensions. This concordance exceeds that found for the eigenvalues of the stability matrix.

Restricted to $\alpha \leq 1$, the quantity τ exhibits cutoff and gauge fixing independence at an even higher level than the eigenvalues of the stability matrix.

Concerning τ for $\alpha > 1$, one sees from fig. 4.13(d) that cutoff independence is as good as for the low α case. This may be taken as a sign for the not entire artificiality of this case. What kind of information could be encoded in this "partially universal behavior", i.e. with respect to the cutoff only, remains open for investigation. Perhaps it provides hints for the direction into which the truncation has to be extended to gain full gauge fixing independence.

In this chapter the gauge independence of FPs in higher dimensions was demonstrated for five different cutoff functions. NNLO-optimisation was applied to these cutoffs. The observable quantities calculated for these different, optimised cutoffs agreed with each other to within a few percent for each gauge fixing. For all cutoffs and dimensions, a difference for all results obtained with gauge fixing smaller than unity and larger than unity was observed. This difference did not change the qualitative properties of the FP. Based on the maxima of the NNLO-parameter, it was argued that the smaller values of the gauge fixing parameters lead to more reliable results. This argument was counter-checked by noting that it lead consistently to lower expected reliability for a certain cutoff already known to be of lower stability than the other cutoff functions that were employed. By applying these cuts to the available data, a narrow band of most reliable numerical results could be identified.

As an additional result, we note that ξ_m, the maximum of the NNLO-parameter, is highest for the optimised cutoff function in all dimensions and gauge fixings. Since this maximum corresponds to the most stable flows, as demonstrated in the two previous chapters, it follows that this cutoff functions yields the most reliable results. This confirmes previous results and arguments [86], [88], [53], and will be employed in the next chapter.

Chapter 5

Flows of Quantum Gravity

In the previous chapters, FPs of the ERG of gravity in the Einstein–Hilbert truncation were studied. Physically this means the study of the far UV-regime, where all intermediate scales have decoupled. The only remaining dimensionful quantity is the renormalisation scale. Furthermore, all renormalisable theories, which lie on the same UV-critical surface (cf. section 1.4), have their common bare limit in the FP, sharing its universal properties. At asymptotically high energies they are oblivious to their fate at low energies, in the IR, where they can and will describe different physical systems.

To investigate quantum effects of gravity at energies below the high UV, e.g. near the Planck scale where they are expected to set in, the full solution of the RG equations have to be considered. Furthermore, in order to establish the renormalisability of a theory describing specific low-energy physics, its flow-evolution (RG trajectory) into the UV has to be followed. Doing this for a dense set of starting points in the space of couplings yields a complete phase space portrait. *Phase* space, because various qualitatively different types of RG behaviour do occur, one already mentioned being renormalisability or its lack. Such a complete portrait further allows to classify theories according to their qualitatively different IR behaviour, allowing to investigate quantum gravitational effects at finite energies in a systematic way.

In the present chapter, we turn to such investigations of entire coupling phase space within the Einstein–Hilbert truncation. To make an analytic analysis possible, we employ the optimised cutoff (2.19), which yields explicit flow equations. It was noted in chapters 3 and 4 that the optimised cutoff exhibits consistently superior stability properties. These favourable properties motivate its choice for the present task. We discuss general properties of the system of flow equations in an analytic way before turning to explicit full phase space portraits in four dimensions and two different gauge fixings. These analytic equations have been used in [134] for an analytic FP-study in general dimensions for one choice of gauge fixing.

We provide a detailed classification of trajectories in the *entire* phase space. A similar study has been performed with the *sharp* cutoff function [108] for parts of phase space. The three-way comparison of the portrait and classification given there and our results provides a first handle on the cutoff and gauge independence of features of the entire flow, in the same spirit as the FP analysis of chapters 3 and 4.

A crucial question in the four-dimensional context is whether the one trajectory

realised in Nature lies on the UV-critical surface belonging to the found FP, i.e. whether this FP of quantum gravity discovered in the present setting bears any relevance to our physical world. The answer is affirmative [108], [130], [131] in the Einstein–Hilbert truncation (projection) and further strengthened by the results presented in this chapter. It is also shown that the physical trajectory lies in a part of phase space described in the present approximation with good stability, allowing to draw reliable conclusions to the quantum evolution of gravity.

5.1 Analytic Flow Equations

In the present chapter we use an alternative definition of the dimensionless coupling g, whereas λ remains the same:

$$\lambda := \bar{\lambda}_k / k^2, \tag{5.1}$$

$$g := \frac{k^{d-2} G_k}{\left((4\pi)^{\frac{d}{2}-1} \Gamma[\frac{d}{2}+2]\right)} \equiv \frac{\tilde{g}_k (4\pi)^{1-\frac{d}{2}}}{\Gamma[2+\frac{d}{2}]}. \tag{5.2}$$

Here $\bar{\lambda}_k$, G_k are the dimensionful cosmological constant and Newton's constant and $\tilde{g}_k$ coincides with the usual definition used in the other chapters. Including the factor of $(4\pi)^{\frac{d}{2}-1} \Gamma[2+\frac{d}{2}]$ in the definition of g eliminates it from the flow equations, de-cluttering our analytic expressions considerably (see for comparison appendix C.2 for the full flow equations for the usual dimensionless couplings). For the same reason the index k has been suppressed too.

Using the optimised cutoff (2.19), [86], the β-functions for these dimensionless couplings are

$$\partial_t \lambda := \beta_\lambda = (-2+\eta)\lambda + (a_1 - \eta a_2)g, \tag{5.3}$$

$$\partial_t g := \beta_g = (d-2+\eta)g, \tag{5.4}$$

where the anomalous dimension η is given by

$$\eta = \frac{g\, b_1(\lambda)}{1 + g\, b_2(\lambda)}, \tag{5.5}$$

and the coefficient functions read

$$a_1(\lambda) = \frac{d(d-1)(d+2)}{2(1-2\lambda)} + \frac{d(d+2)}{1-2\alpha\lambda} - 2d(d+2),$$

$$a_2(\lambda) = \frac{d(d-1)}{2(1-2\lambda)} + \frac{d}{1-2\alpha\lambda},$$

$$b_1(\lambda) = -\frac{(d+2)(d^3 - 4d^2 + 7d - 8)}{(d-1)(1-2\lambda)^2} + \frac{d(d+2)(d^3 - 2d^2 - 11d - 12)}{12(d-1)(1-2\lambda)}$$
$$-\frac{2(d+2)(\alpha d^2 - 2\alpha d - d - 1)}{d(1-2\alpha\lambda)^2} + \frac{(d+2)(d^2 - 6)}{6(1-2\alpha\lambda)} - \frac{1}{3}(1 + \frac{2}{d})(d^3 + 6d + 12),$$

$$b_2(\lambda) = -\frac{d^3 - 4d^2 + 7d - 8}{(d-1)(1-2\lambda)^2} + \frac{(d+2)(d^3 - 2d^2 - 11d - 12)}{12(d-1)(1-2\lambda)}$$
$$-\frac{2(\alpha d^2 - 2\alpha d - d - 1)}{d(1-2\alpha\lambda)^2} + \frac{(d+2)(d^2 - 6)}{6d(1-2\alpha\lambda)}. \tag{5.6}$$

These explicit results, which have been used in [134], were obtained by inserting the optimised cutoff (2.19) into the threshold functions, yielding

$$\Phi_n^p(w) = \frac{1}{\Gamma[n+1](1+w)^p}, \tag{5.7}$$

$$\tilde{\Phi}_n^p(w) = \frac{1}{\Gamma[n+2](1+w)^p}. \tag{5.8}$$

In the limit $\alpha \to \infty$ and appropriate redefinitions of the couplings, the analytic flow equations have already been given and discussed in [134]. The ones presented here hold for general α.

A fundamental property of the flow equations of Einstein-Hilbert gravity, which is independent of the choice of cutoff is the vanishing of β_g for $g = 0$. This has the consequence that the two halves of phase space $g \gtrless 0$ are disjunct for solutions of the RG-equations, the trajectories, which can never cross from one half to the other one.

5.1.1 Boundaries

A typical truncation artifact is the presence of poles in the threshold functions. For certain values of the couplings, denominators of the integrands are zero. This can be understood as a breakdown of stability of the truncation: the terms from the operators considered in the truncation cancel each other. In the full theory the (infinitely many) terms not present in the truncation would now determine the value of the threshold functions. Without extending the truncation it is not possible to estimate the correct value of the threshold function at and near the stability boundary. Even if the contribution of these neglected terms is otherwise perturbatively small, they will dominate the flow at the stability boundary in an uncontrolled manner, rendering it unstable. See section 2.1.1 for more detailed discussion.

In the present case, the stability boundaries are located at $\lambda_{\text{bound}} = 1/2, 1/2\alpha$, cf. (5.6). An interesting feature of the flow equations for the optimised cutoff is that

they remain well defined on the stability boundaries. All diverging contributions to the anomalous dimensions and the β-functions cancel:

$$\lim_{\lambda \to \frac{1}{2}} \eta = \lim_{\lambda \to \frac{1}{2\alpha}} \eta = 2 + d \tag{5.9}$$

This result holds for all values of d and α. The β-functions at the stability boundaries are given by:

$$\lim_{\lambda \to \frac{1}{2}} \beta_g = \lim_{\lambda \to \frac{1}{2\alpha}} \beta_g = 2\,d\,g\,, \tag{5.10}$$

$$\lim_{\lambda \to \frac{1}{2}} \beta_\lambda = \frac{d}{2} + \frac{g\,d}{12} \frac{(d^5 - 23d^4 + 63d^3 + 43d^2 - 154d + 360)}{d^3 - 4d^2 + 7d - 8}\,, \tag{5.11}$$

$$\lim_{\lambda \to \frac{1}{2\alpha}} \beta_\lambda = \frac{d}{2\alpha} + \frac{g\,d}{6} \frac{36 + 42d + 38\alpha d + 10d^2 - d^3 - 12\alpha d^3}{\alpha d^2 - 2\alpha d - d - 1}\,. \tag{5.12}$$

(5.11) diverges for 2.478 real dimensions and (5.12) for $d = 1 + \frac{1}{2\alpha} \pm \sqrt{1 + \frac{2}{\alpha} + \frac{1}{4\alpha}}$.

In the case of the sharp cutoff function [108], the stability boundaries are the same. However, in that case the divergences do not cancel and lead to the breakdown of the flow at the boundaries. On the other hand, the solutions of the RG equations for the optimised cutoff etend across the boundaries. However, the question remains whether the flow can be trusted at all near the boundary, since the vanishing of the denominator in the threshold functions still signals the missing of terms relevant at least close to the boundary. For the rest of this work, we assume as a working hypothesis that, as long as the flow equations remain finite, they can be taken at face value.

In addition to the stability boundary, which is generic in truncated ERG, a second potential source of breakdown of the flow is present in the the β functions in the Einstein-Hilbert truncation: the non-perturbative expression for the anomalous dimension, (5.5), contains the possibility of a real first order pole at $\tilde{g}^\eta(\lambda) = 1/D_2(\lambda)$ for general cutoffs and $g^\eta(\lambda) = -1/b_2(\lambda)$ for the optimised cutoff. This non-perturbative form of the anomalous dimension arises from taking into account the running of the coupling on the r.h.s. of the flow equation. This would not be the case in a perturbative treatment. However, it is this non-perturbative denominator which leads to the mutual cancellations of the stability boundary poles discussed in the previous paragraph.

Turning to the general properties of $g^\eta(\lambda)$, we note that it is zero at and only at a stability boundary, i.e. $g^\eta(1/2) = g^\eta(1/2\alpha) = 0$. Since η vanishes identically for $g = 0$, it is discontinuous at these points. We will return to this issue in section 5.3.8. The number of real poles of $g^\eta(\lambda)$ depends on the dimension and the gauge fixing as displayed for 4, 6 and 10 dimensions in fig. 5.1(a).

Beside marking the (potential) breakdown of the flow, g^η determines the global properties of the flow: as η has a first-order pole at $g^\eta(\lambda)$, it changes sign across this line. The other sign changes of η occur at $g = 0$ and $b_1(\lambda) = 0$. The solutions of the second condition depend on the dimension and the gauge fixing, cf. fig.5.1(b). Since $\eta = 2 + d$ at the stability boundary, any curve between the two branches of the boundary in phase space has to cross an even number of divergence or zero lines of η.
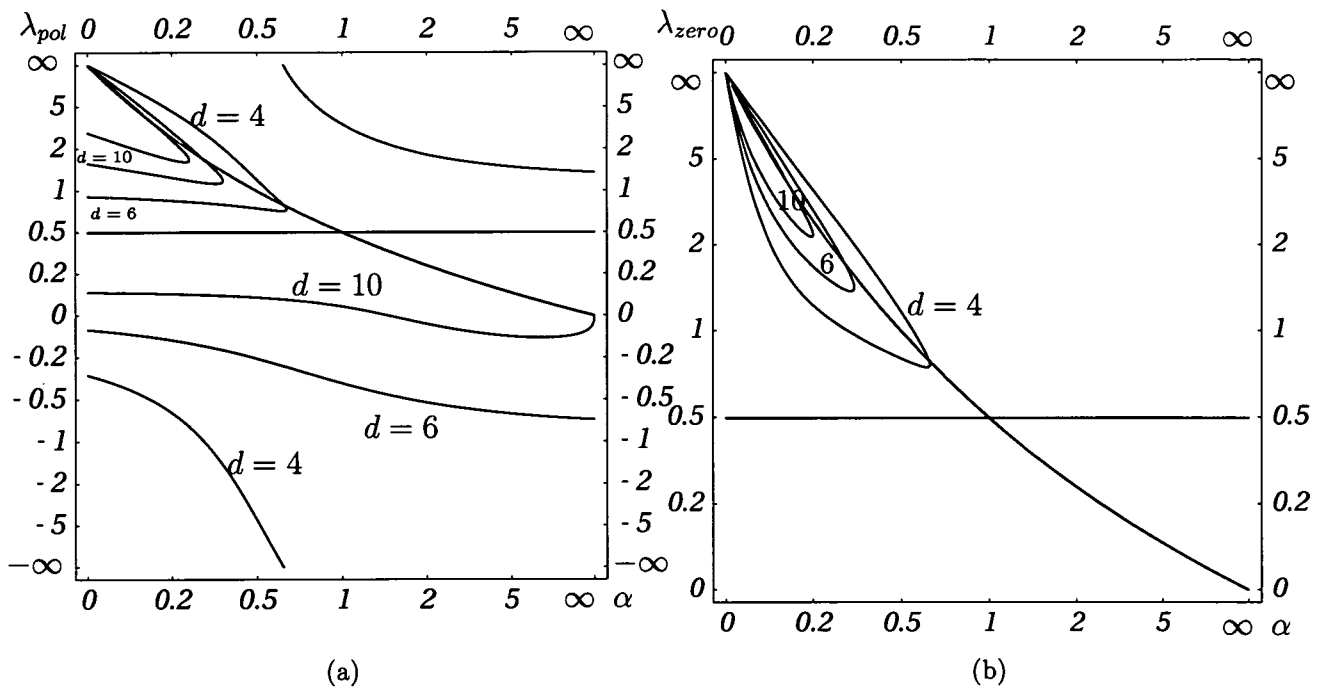
Figure 5.1: Loci of the (a) poles of $g^\eta(\lambda)$ and (b) zeros of η for 4, 6 and 10 dimensions and all gauge fixings. In red the stability boundary.

We illustrate these general considerations in detail in section 5.3 with the explicit example $d = 4$, $\alpha = 0$. In that case we can read off the global properties of η from figs.5.1(a), 5.1(a): there is only one finite stability boundary at $\lambda = 1/2$, no zero of η except on the λ-axis and g^η has two poles at $\frac{9 \pm 4\sqrt{21}}{30}$. Knowing $\eta(1/2, g) = 6$ one can determine the sign of η in the whole phase space.

Again, in the case of the sharp cutoff discussed in [108], the situation is somewhat different: the lines of diverging η are situated at a constant negative value of $\tilde{g}$ and at $\lambda = \frac{1}{2}$. However, only the divergence at $\tilde{g}^\eta < 0$ stems from the vanishing of the non-perturbative denominator of η. At the stability boundary the anomalous dimension suffers from the breakdown of the flow, as do the other terms.

For one modified exponential cutoff, which was also discussed in [108], a positive g branch of $\tilde{g}^\eta$ exists for $\lambda < \lambda_{\text{bound}}$, similar to the present case.

As suggested by the discussion of the stability boundary we have to ask whether the divergence of η really constitutes a breakdown of the flow in the case of the optimised cutoff. This time the answer is affirmative: both β_λ and β_g are linear in η. They too have a first-order pole at $g^\eta(\lambda)$. The only possible exception to this is for β_λ the zero measure set of intersection points between g^η and the solution of $\lambda = a_2(\lambda)g$ where it remains finite.

The RG-trajectories terminate at $g^\eta(\lambda)$. This marks a non-perturbative breakdown of the Einstein-Hilbert truncation.

5.1.2 Association across boundaries

The fact that both β-functions depend linearly on η gives rise to an interesting feature of the RG trajectories. The slope of the trajectories $g(t(\lambda))$ at $g^\eta(\lambda)$ is given by the ratio

$$\frac{\beta_g}{\beta_\lambda} = \frac{g^\eta}{\lambda - a_2 g^\eta} . \tag{5.13}$$

It is finite and continuous across g^η. Trajectories terminating at the same point $(\lambda, g^\eta(\lambda))$ but approaching it from opposite sides appear as one continuous and differentiable curve $g(\lambda)$, see for example fig. 5.5. We call two such trajectories *associates*. They are related to each other by terminating in the same point of g^η. This relation is called *association* and is associative. A set of associates is called a *society*. If a trajectory has no associates (if *both* its UV and IR limit exist), it is called *complete*. A society consisting of complete trajectories is also called complete.

Two different points of view concerning the interpretation of this procedure seem possible:

(i) Since Einstein-Hilbert truncation breaks down at g^η, the inclusion of new operators is inevitable to capture the essence of quantum gravity correctly. These new operators start to dominate the flow as one approaches g^η and may continue to do so beyond it. Nothing can be known about the general qualitative behaviour of the flow near or beyond g^η within the present truncation. The association of trajectories is irrelevant since the one on the wrong side of g^η does not pertain to the full theory at all.

(ii) Alternatively it may be the case that the terms necessary to remedy η's divergence are relevant only in the vicinity of g^η. They might alter the flows only locally but leave them qualitatively unchanged in the phase space regions where Einstein-Hilbert truncation works. Qualitative statements, especially about the IR asymptotic behaviour, made in this truncation may reflect properties of the full theory. Continuing flows across g^η by associating them allows us to discuss UV and IR complete phase portraits which capture the qualitative global features of the full theory.

An open issue in (i) is how to identify the "correct" side of g^η: except for the stability boundary, which could be used to argue that $\lambda \geq \text{Min}[\frac{1}{2}, \frac{1}{2\alpha}]$ is not correctly described in the present truncation, there is no evidence as to which is the "right" or the "wrong" side of g^η from the point of view of the flow equations. Both sides are equally well described.

Only the second point of view allows further discussion within the present truncation. It will be used as a working hypothesis at some points of the further discussion.

Associating two flows is not the same as continuing one flow across g^η in a very important respect: like η, both β-functions change sign at this line. A trajectory terminating into g^η from one side with decreasing logarithmic RG scale t is associated to one doing the same from the other side. The two trajectories cannot define one comprehensive trajectory piecewise, since the couplings would not be unique functions of t anymore. This reversal of the direction of the flow at g^η prohibits the interpretation of associated trajectories as pieces of full, IR and UV complete ones.

5.2 Non-Gaussian Fixed Points

Before turning to concrete examples of the whole phase space, we study the properties of the FP solutions of the system of analytic flow equations. In contrast to the other cutoffs used in chapters 3 and 4, the analytic form of the optimised cutoff flow equations permits a rigorous counting and qualification of solutions. For the case $\alpha \to \infty$, even the FP solutions are analytic [134]. Such explicit information is important to verify that one has not missed out on a solution of potential physical interest in numerical studies, such as those performed in chapter 3 and 4. Except for cutoff independence (which is per definition not studied in the present chapter), such a physical FP solution has to fulfil several conditions: (i) it must yield positive g_*, since g cannot change sign (since b_g vanishes for $g = 0$) and Newton's constant is measured to be positive, (ii) the solution must be real, and (iii) fulfilment of (i) and (ii) must not depend on gauge fixing, as should the stability properties at the FP. These conditions will suffice to single out exactly one solution as physical. It is precisely the FP studied in chapters 3 and 4 with the optimised cutoff and four other cutoff functions. In this sense, the present section serves as an a posteriori reason for the physicality of the subject of chapters 3 and 4.

The two-by-two system $\beta_g(\lambda_*, g_*) = 0 \cap \beta_\lambda(\lambda_*, g_*) = 0$ is easily reduced to a (generically) fifth-order polynomial equation in λ by solving $b_g = 0$ for g, which is linear in g. For the special choices $\alpha = 0, 1, \infty$, this reduces to a third order polynomial which admits explicit analytic solutions for all dimensions. Hence the number of solutions is reduced from five to three in these cases. Since we discuss the phase space of the

special cases $\alpha = 0, 1$ in 4 dimensions below, we must ascertain that these choices do not exclude FPs of potential physical relevance.

For general α and d, the fifth-order polynomial, whose roots are the FP solutions λ_*, is given by

$$\left\{ d(d-2)(d^2 - d - 4) \right\}$$

$$+ \lambda \left\{ -4\alpha d(d-2)(d^2 - d - 4) + \frac{8}{d-1} + 4 - 34d - \frac{7}{3}d^2 + \frac{55}{6}d^3 - 4d^4 + \frac{1}{6}d^4 \right\}$$

$$+ \lambda^2 \left\{ 4\alpha^2 d(d-4)(d-2)(d+1) + 16 + 64d - 2d^2 + \frac{19}{3}d^3 - \frac{1}{3}d^5 \right.$$

$$\left. - \alpha \left[\frac{32}{d-1} + 8 - 148d - 20d^2 + 36d^3 - \frac{50}{3}d^4 + \frac{2}{3}d^5 \right] \right\}$$

$$+ \lambda^3 \left\{ 2\alpha^2 \left[\frac{16}{d-1} - 72d - \frac{118}{3}d^2 + \frac{101}{3}d^3 - \frac{26}{3}d^4 + \frac{1}{3}d^5 \right] \right.$$

$$\left. - \frac{4}{3}\alpha \left[72 + 228d + 26d^2 + 21d^3 + 2d^4 - d^5 \right] - 16 - 24d - \frac{8}{3}d^2 - \frac{4}{3}d^3 \right\}$$

$$+ \lambda^4 \left\{ 4\alpha^2 \left[12 + 18d + \frac{20}{3}d^2 + d^3 + \frac{1}{3}d^4 \right] + 8\alpha \left[32 + 72d + \frac{58}{3}d^2 - \frac{1}{3}d^3 + \frac{4}{3}d^4 - \frac{1}{3}d^5 \right] \right\}$$

$$+ \lambda^5 \left\{ -\frac{16}{3}\alpha^2(d+2)(d^3 + 6d + 12) \right\} = 0 . \quad (5.14)$$

The coefficients of the polynom in λ are real for real values of α and d. Hence the five roots λ_*^i, $i = 1, \ldots 5$, are either real or complex conjugated. Constructing the continuous functions, $\lambda_*^i(\alpha, d)$, we can discuss the roots as entities with fixed labels over their entires domains $\alpha \in \mathbb{R}_+ \times (d \geq 2)$.

Only one root, λ_*^1, is real in its entirety. It is positive, as is the corresponding value g_*^i, over its domain. As a function of α it is rather constant over $0 \leq \alpha \leq 1$ and behaves as $1/\alpha$ for $\alpha > 1$. This behaviour is found for generic cutoff functions for the FP discussed in chapter 4 and was discussed in section 4.1. The corresponding stability matrix eigenvalues are positive or complex conjugated with a positive real part. They show only quantitative dependence on α. We identify this UV FP as physical. It is the one discussed with different cutoffs in chapters 3 and 4. The roots λ_*^2 and λ_*^3 are complex conjugated for $d < 8$[1]. For $8 \leq d$ they develop two real negative branches for an interval $0 \leq \alpha \leq \alpha_0$. α_0 grows monotonously with dimension and goes to ∞ for $14 \leq d$.

λ_*^4 and λ_*^5 do not exist for $\alpha = 0, 1$. For $\alpha \to 0$ they tend to $+\infty$. In all dimensions they are real positive for some interval $0 < \alpha \leq \alpha_1$. For $d = 4$ one finds $\alpha_1 = 0.654523$. They are complex conjugated for $\alpha_1 < \alpha$ in this dimension. In all other dimensions they re-enter the real plane at some $\alpha_2 > 1$. The general structure of FP solutions is illustrated by the two examples $d = 4$ and 10 in fig. 5.2(a) and 5.2(b).

The corresponding stability matrix eigenvalues of $\lambda_*^2, \ldots, \lambda_*^5$, show strong gauge fixing dependence even on the qualitative level, i.e. transitions from one to two attractive directions.

---

[1]For this discussion we consider integer dimensions only.
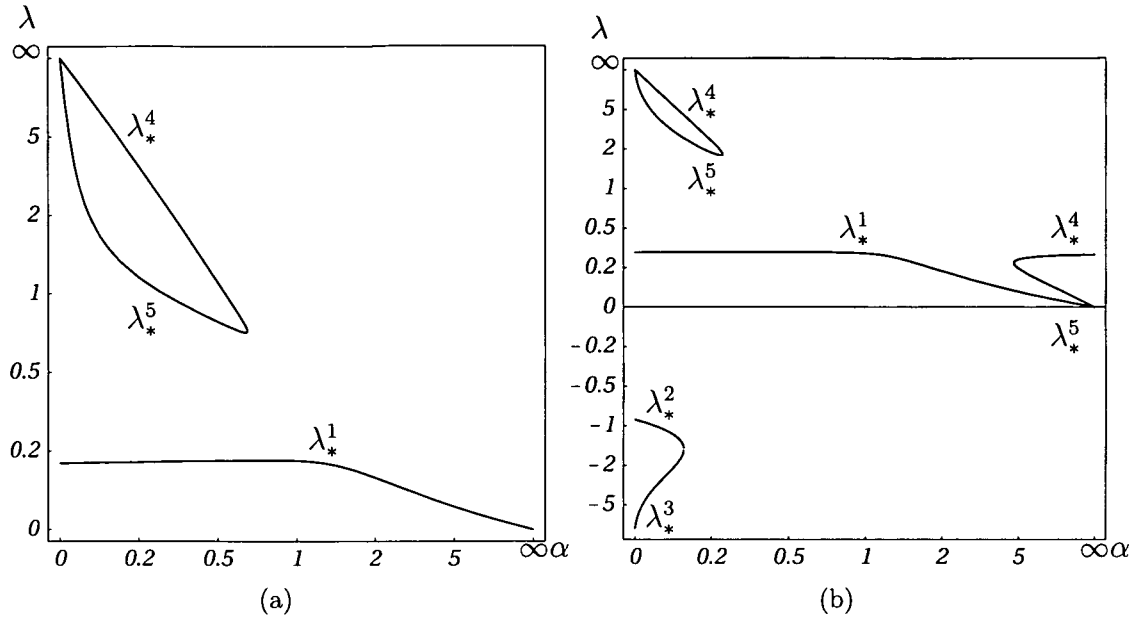
Figure 5.2: Real branches 1–5 of FP solutions λ_* in (a) 4 and (b) 10 dimensions.

We conclude that all but the first root display strong signs of being artifacts. It seems not only forgivable but rather recommendable to use such gauge fixings where they do not enter the real plane or are absent. This is the case for the two examples $\alpha = 0, 1$ explicitly studied in sections 5.3 and 5.4. Furthermore, these considerations serve as an a posteriori justification for studying only one FP solution in chapters 3 and 4, which is shown here to be the only physical one.

5.3 Flow Analysis for Four Dimensions and $\alpha = 0$

It is illuminating to illustrate the general discussion above with a concrete example. Its choice is dictated by several considerations: four dimensions are the choice corresponding to the real world, at least at large distances. $\alpha = 0$ was argued to be a FP for the gauge fixing parameter [103]. This was demonstrated in explicit examples [94] Furthermore, as argued in section 5.2, for this choice of gauge fixing only one non-trivial real FP solution exists, while the other, artificial ones, do not influence the real flow system.

The explicit expressions for the anomalous dimension and the β functions of the two dimensionless couplings are in this case:

$$\eta = -g\frac{100\lambda^2 - 132\lambda + 81}{(1 - 2\lambda)^2 + g(20\lambda^2 - 12\lambda - 17/3)}, \tag{5.15}$$

$$\beta_g = 2g\frac{(1 - 2\lambda)^2 - g(30\lambda^2 - 54\lambda + \frac{277}{6})}{(1 - 2\lambda)^2 + g(20\lambda^2 - 12\lambda - 17/3)}, \tag{5.16}$$

$$\beta_\lambda = -2\frac{\lambda(1 - 2\lambda)^2 + g^2(40\lambda^2 + 450\lambda - 371) + g(70\lambda^3 - 30\lambda^2 + \frac{137}{6}\lambda - 6)}{(1 - 2\lambda)^2 + g(20\lambda^2 - 12\lambda - 17/3)} \tag{5.17}$$

In the rest of this section we investigate the properties of the numerical solutions of this system of flow equations, the RG trajectories. We exploit their relatively simple analytic form for our analysis.

5.3.1 Fixed points

FP dominate the behaviour of the RG trajectories in their basin of attraction and determinate their UV or IR limit. For $d = 4$ and $\alpha = 0$ the FP condition $\beta_g(\lambda_*, g_*) = 0 \cap \beta_\lambda(\lambda_*, g_*) = 0$ has two real solutions, corresponding to a trivial Gaussian (G) and a non-Gaussian (NG) FP:

$$\lambda_*^G = 0 \quad , \quad g_*^G = 0; \tag{5.18}$$

$$\lambda_*^{NG} = 0.164 \quad , \quad g_*^{NG} = 0.0118 \,\hat{=}\, \tilde{g}_*^{NG} = 0.893 \tag{5.19}$$

The eigenvalues θ of the stability matrix $\theta_{ij} = -\partial\beta_i/\partial j|_{i_*,j_*}$; $i,j = \lambda, g$ determine the stability properties of the FP:

$$\theta^G = (-2, 2) \tag{5.20}$$

$$\theta^{NG} = 2.034 \pm i\, 2.691. \tag{5.21}$$

The Gaussian FP is IR-attractive for g and repulsive for λ (this can be seen from the directions of the eigenvectors of the stability matrix) and the non-Gaussian one is UV-attractive for both couplings.

5.3.2 Anomalous dimension

Before presenting the full phase portrait we turn to the properties of η in this concrete case. As mentioned in section 5.1.1, the anomalous dimension vanishes only for $g = 0$. It diverges with a pole of first order on the line

$$g_\eta(\lambda) = \frac{4\lambda^2 - 4\lambda + 1}{\frac{17}{3} + 12\lambda - 20\lambda^2}. \tag{5.22}$$

This curve has a double zero at $\lambda = 1/2$, a minimum at $1/2$, a maximum $13/6$ and two first order poles at $1/30(9 \pm 4\sqrt{21})$. Its asymptotes are $\lim_{\lambda \to \pm\infty} g^\eta = -4/20$.

The phase space is split into six trajectory-disjunct sectors by g^η and $g = 0$. They are labelled a to f, as shown in fig. 5.3. The sign of η can be determined in each of them by starting from the known positive value $\eta(1/2, g) = 6$, cf. (5.9). Since $\lambda = 1/2$ lies in sectors b and e and η changes sign across g^η and $g = 0$, it has negative sign in the other four sectors. The results of these considerations are visualised in fig.5.3.

5.3.3 Phase Portrait

After having set the necessary stage we display the solutions to the flow equations in fig. 5.4 and 5.5. Fig. 5.4 shows the whole of phase space with compactified coordinates $x/(1 + |x|)$, whereas fig. 5.5 provides a close-up of the region around the two FPs.
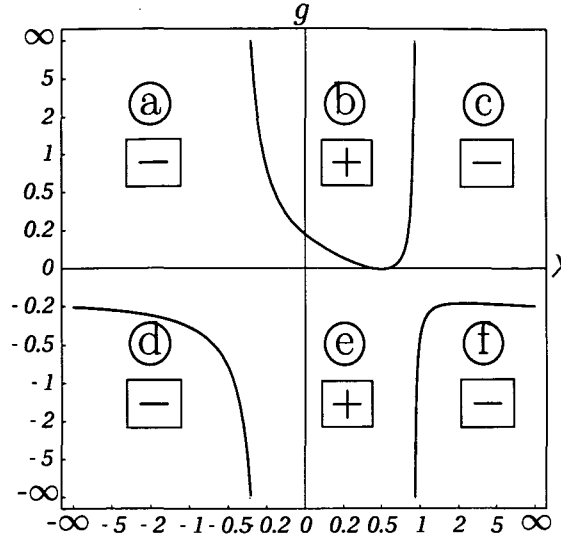
Figure 5.3: The six disjunct parts of phase space $a - f$ and the respective sign of η in them. η vanishes on the λ-axis and diverges on g^η (in red). The axis are rescaled as $x/(1 + |x|)$.

The plotted trajectories have been chosen to illustrate their association across the pole of η. The arrows indicate the IR-direction of the flow, they point into the direction of decreasing RG scale t. g^η is displayed in red. The separatrix, which connects the Gaussian and the non-Gaussian FP (red dots) is displayed in green, as is its continuation for negative g, which runs into the Gaussian FP only.

5.3.4 Global and local classifications

Because of the explicit form of the flow equations, an analytic understanding of the properties of the phase portrait and a comprehensive classification of trajectories according to their UV and IR behaviour is possible. This is the aim of the next two sections before presenting and discussing the classified phase portrait in section 5.3.7. In the present section, however, we discuss the *global* classification scheme, which is made possible by the association of trajectories, extending a *local* scheme enforced otherwise by the termination of the trajectories at g^η.

Local classification is performed in each of the six sectors separately. Possible endpoints of trajectories are FPs and asymptotic values for which the limit $t \to \pm\infty$ exists, and termination points on g^η. well as g^η.

To extend local to global classification, we make use of association. A society of trajectories ends per constructionem either at a FP or at an asymptotic value. Global classes (of societies) are defined by their distinct limits. Note that this does not necessarily imply the existence of both limits $t \to +\infty$ and $t \to -\infty$ for a society, since it may consist of an even number of associates, in which case there are two UV or IR limits. This illustrates again the impossibility to interpret a society as a piecewise defined trajectory.

A straightforward refinement of global classification is to label each associate with its
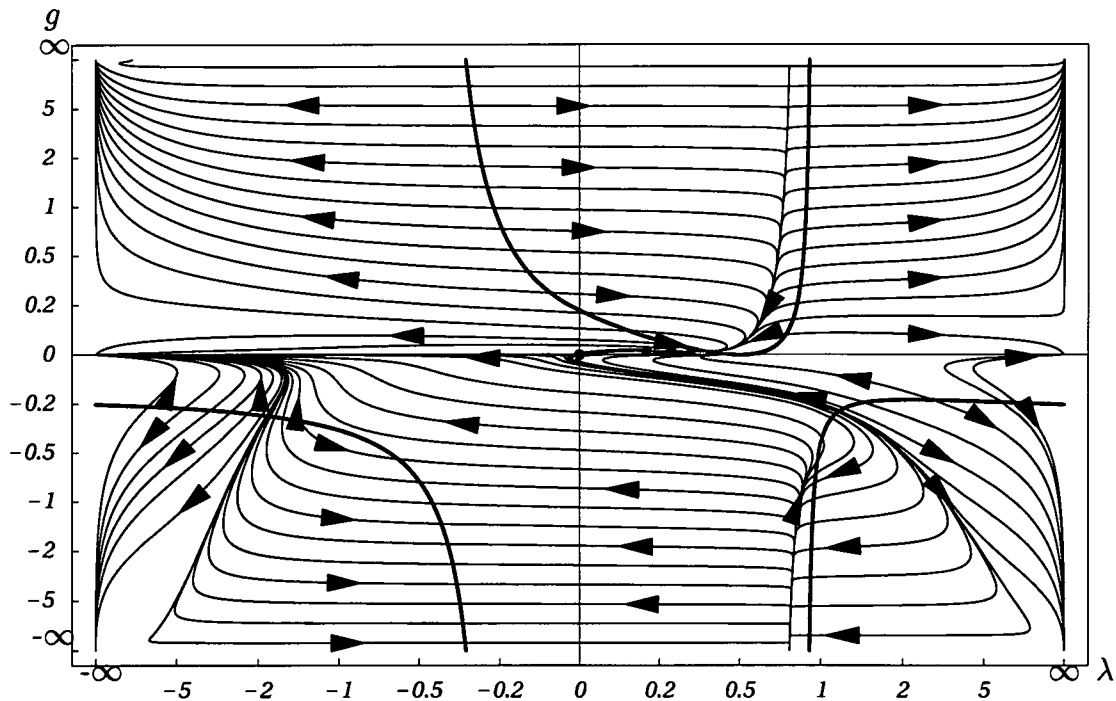
Figure 5.4: Phase portrait of RG trajectories for $d = 4$, $\alpha = 0$. The thick red line is the η divergence line g^{η}, in green the separatrix which connects the Gaussian and non-Gaussian FP (red dots) and the trajectory which approaches the Gaussian FP from the lower half-plane. The arrows point along the IR direction of the flow. Note that the axes are rescaled as $x/(1 + |x|)$.
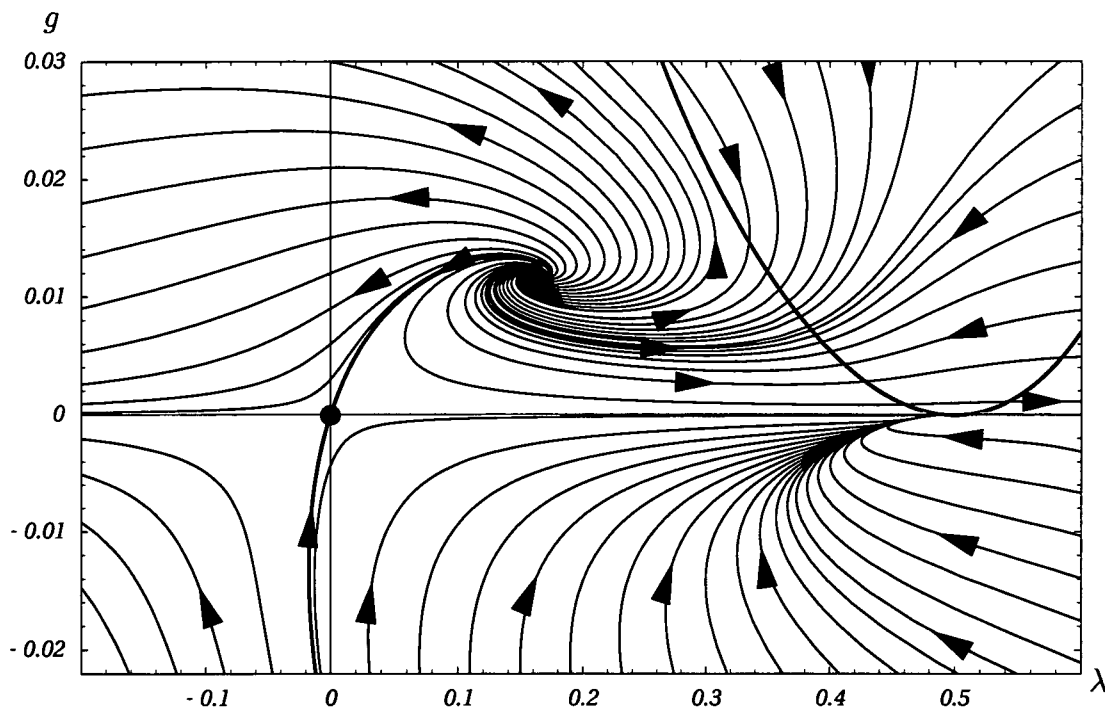
Figure 5.5: Close up of phase space around the FPs (red dots). In green the separatrix which connects the Gaussian and non-Gaussian FP and the trajectory which approaches the Gaussian FP from the lower half-plane. The arrows point along the IR direction of the flow.

supporting sector in addition to its society name. We call this scheme *global classification of trajectories*, the corresponding classes *global classes of trajectories*. The set of global trajectory classes contains the set of local classes as a subset. Since global classification of trajectories provides the most detailed ordering scheme. The phase portrait is classified according to it below.

5.3.5 Asymptotes

In this section an analytic understanding of the nine asymptotes approached by the trajectories is obtained from an analysis of the analytic flow equations (5.16), (5.17).

The asymptotic values of the couplings can be either finite or infinite. Thus there can be three qualitatively different cases:

(i) Both couplings are finite on a FP. The Gaussian FP and the non-Gaussian one have already been discussed in section 5.3.1.

(ii) One coupling assumes a finite value and the other one goes to infinity. This can only be the case on a fixed line where one of the two β-functions vanishes. The FPs are intersections of such fixed lines. For $d = 4$, $\alpha = 0$ the fixed lines are given by the curves

$$\beta_g = 0: \qquad g = 0, \tag{5.23}$$

$$g^g(\lambda) = \frac{6(4\lambda^2 - 4\lambda + 1)}{180\lambda^2 - 324\lambda - 277}. \tag{5.24}$$

$$\beta_\lambda = 0: \qquad g^\lambda_\pm(\lambda) = \frac{p_1 + \pm\sqrt{p_2}}{p_3}, \tag{5.25}$$

$$p_1 = 36 - 137\lambda + 180\lambda^2 - 420\lambda^3,$$

$$p_2 = 1296 + 43560\lambda - 246767\lambda^2 + 387576\lambda^3$$
$$\qquad -88680\lambda^4 - 174240\lambda^5 + 176600\lambda^6,$$

$$p_3 = -4452 + 5400\lambda + 480\lambda^2.$$

The non-trivial fixed line of β_g has a double zero at $\lambda = 1/2$, a minimum at $1/2$ and a maximum at $49/18$. Its asymptotes are $\lim_{\lambda \to \pm\infty} g^g(\lambda) = 2/15$.

The structure of the fixed line g^λ is more complicated: p_2 is negative on the open interval $(-1.32455, -0.025821)$, no real solutions exist there. Although p_3 has two real zeros at $\lambda^{(0)}_{1,2} = -\frac{225 \pm \sqrt{65465}}{40}$ so have the nominators of the two branches, g^λ_+ at $\lambda^{(0)}_2$ and g^λ_- at $\lambda^{(0)}_1$. Hence only one of the two branches has a pole at each zero of the denominator.

The special lines g^λ, g^g and g^η are displayed in fig .5.6(a) and 5.6(b) with the graphical representation given in table 5.1.

The asymptotes and poles of the fixed lines are candidates for asymptotic attractors of trajectories. Eight such candidates, $(\infty, 0)$, $(-\infty, 0)$, $(\infty, \frac{2}{5})$, $(-\infty, \frac{2}{5})$ for $\beta_g = 0$ and $(\lambda^{(0)}_1, +\infty)$, $(\lambda^{(0)}_1, -\infty)$, $(\lambda^{(0)}_2, +\infty)$, $(\lambda^{(0)}_2, -\infty)$ for $\beta_\lambda = 0$, have been found above. Whether they are candidates for UV or IR-limits is determined by the sign of the non-vanishing β-function: if that sign is equal to the that of the diverging coupling, it is a possible UV attractor, if opposite, an IR one. Accordingly, $(\infty, 0)$, $(-\infty, 0)$, $(\infty, \frac{2}{5})$, $(-\infty, \frac{2}{5})$, $(\lambda^{(0)}_1, +\infty)$ and $(\lambda^{(0)}_1, -\infty)$ are candidates for IR asymptotes, $(\lambda^{(0)}_2, +\infty)$ and

name	properties	graphics
g^η	$|\eta| \to \infty$	——
g^λ	$\beta_\lambda = 0$	······
g^g	$\beta_g = 0$	— ·· —

Table 5.1: Names, definition and graphical representation of special lines.

$(\lambda_2^{(0)}, -\infty)$ for UV ones. As a last step, we have to analyse the stability of these fixed limits. It is given by the signs of the derivatives of the vanishing β-functions after their couplings in the respective fixed limits:

$$\lim_{\lambda \to \pm\infty} \frac{\partial \beta_g}{\partial g}\Big|_{g=0} > 0 \quad , \quad \lim_{\lambda \to \pm\infty} \frac{\partial \beta_g}{\partial g}\Big|_{g=\frac{2}{15}} < 0 ,$$

$$\lim_{g \to +\infty} \frac{\partial \beta_\lambda}{\partial \lambda}\Big|_{\lambda=\lambda_1^{(0)}} > 0 \quad , \quad \lim_{g \to -\infty} \frac{\partial \beta_\lambda}{\partial \lambda}\Big|_{\lambda=\lambda_1^{(0)}} < 0 ,$$

$$\lim_{g \to +\infty} \frac{\partial \beta_\lambda}{\partial \lambda}\Big|_{\lambda=\lambda_2^{(0)}} > 0 \quad , \quad \lim_{g \to -\infty} \frac{\partial \beta_\lambda}{\partial \lambda}\Big|_{\lambda=\lambda_2^{(0)}} < 0 . \tag{5.26}$$

Positive sign implies IR (UV) stability (instability), negative sign the opposite. For a candidate to be an actual attractor, it must be UV or IR-stable for both β-functions. This is the case for three of the candidates: $(\pm\infty, 0)$ and $(\lambda_1^{(0)}, +\infty)$ are IR-stable fixed limits, and $(\lambda_2^{(0)}, -\infty)$ is a UV-stable one.

(iii) If both couplings diverge, we have to ask whether this is stable limits for both couplings either in the IR or the UV. This is determined by the sign of the β-functions for the limits $\lambda \to \pm\infty \cap g \to \pm\infty$. If the signs of the β-functions are equal (opposite) of that of the limit of the respective coupling, the coupling approaches this limit in the UV (IR). An inconsistency would mean that no trajectory is attracted toward this limit, it is not attractive. The two limits (∞, ∞) and $(-\infty, -\infty)$ are consistently IR-attractive. For the other two cases, the limits $\lambda \to \pm\infty \cap g \to \mp\infty$ do not commute. The resolution to this problem is provided by the fixed line g^λ: it diverges asymptotically as $g^\lambda \sim -\frac{7}{4}\lambda$. Since β_λ vanishes on its fixed line, the value of its limit in both couplings depends on whether g diverges stronger or weaker than g^λ. If $|g| \lesssim \frac{7}{4}|\lambda|$, the limits $(\pm\infty, \mp\infty)$ are IR-attractive, for $|g| \gtrsim \frac{7}{4}|\lambda|$ they are IR-repulsive. All stable asymptotic values are summarised in table 5.2.

5.3.6 Special trajectories and global classification

The six unstable limits $(\pm\infty, \frac{2}{15})$, $(\lambda_2^{(0)}, \infty)$, $(\lambda_1^{(0)}, -\infty)$ and $\lim_{\lambda \to \pm\infty}(\lambda, \mp\frac{7}{4}\lambda)$ are each approached by one and only one trajectory. These special trajectories act as *asymptotic separatrices*, they separate flows converging to the two attractive limits lying next to each repulsive one. We use the asymptotic separatrices for the classification of the flows according to their asymptotic behaviour. Since their asymptotic values were determined analytically, this classification is analytical and comprehensive.

The notion of the separatrix is extended to include its associates for $g < 0$. It

asymptotic	attractive
$NG - FP$	UV
$(\lambda_2^{(0)}, -\infty)$	UV
$(+\infty, +\infty)$	IR
$\lim_{\lambda \to \infty}(\lambda, g \gtrsim -\frac{7}{4}\lambda)$	IR
$\lim_{\lambda \to -\infty}(\lambda, g \lesssim -\frac{7}{4}\lambda)$	IR
$(-\infty, -\infty)$	IR
$(+\infty, 0)$	IR
$(-\infty, 0)$	IR
$(\lambda_1^{(0)}, +\infty)$	IR

Table 5.2: Attractive fixed limits and FP for $d = 4, \alpha = 0$.

seperates the trajectories with positive and negative cosmological constant weak coupling limits, see [108].

The discontinuous point $(\frac{1}{2}, 0)$ (see the discussion in section 5.3.8) gives rise to another special trajectory, the *quasi-separatrix*. It runs into the discontinuity in the IR-limit.

The line of divergent anomalous dimension, g^η, gives rise to another type of special trajectories. Trajectories tangent to g^η go through the points which are solutions of the equation

$$\frac{\partial g^\eta(\lambda)}{\partial \lambda} = \frac{\beta_g(\lambda, g^\eta(\lambda))}{\beta_\lambda(\lambda, g^\eta(\lambda))}. \tag{5.27}$$

Each of the three real solutions to this equations is a tangent of one of the three branches of g^λ. The three special trajectories defined by these points are UV and IR-complete. They delimit classes of complete trajectories from incomplete ones, which terminate at g^η. Hence we call them *marginally asymptotic* trajectories.

The special trajectories define special societies via association across g^η. The societies of special trajectories classify phase space globally. For local classification, only the original special trajectories are relevant.

All together, there are six special trajectories (societies) in the $g \geq 0$ half-plane and six in the $g \leq 0$ one. How many global classes of trajectories are there in total? To answer this topological question, we have to know "both ends" of the special societies, i.e. the two existing parametric limits of each society containing a special trajectory. To this end, the numerical solutions for all trajectories of the special societies have to be used. They lead to the conclusion that all special trajectories for $g \geq 0$ are associated to trajectories running into the non-Gaussian FP (or do so themselves in the case of the separatrix and the marginal asymptotic). To determine the number of global classes between the special societies, we use Euler's formula,

$$2 - 2g - b = V - E + F, \tag{5.28}$$

where g, b, V, E, F are the genus (number of holes) and the number of boundaries, vertexes, edges and faces on the considered manifold. In the case of the half-plane without

name	properties	classes	graphics
sep.$g > 0$	IR: GFP; UV: NG	1 - 2	———
sep.$g < 0$	IR: GFP	8 - 10	———
q-sep.	IR: $(\frac{1}{2}, -0)$	8 - 9	———
marg.as.1	tangent g_{ab}^{η}	2 - 3	— · — ·
marg.as.2	tangent g_{de}^{η}	12 - 13	— · — ·
marg.as.3	tangent g_{ef}^{η}	11 - 12	— · — ·
as.sep.$g1$	IR: $g \to \frac{2}{15}, \lambda \to \infty$	1 - 6	- - - -
as.sep.$g2$	IR: $g \to \frac{2}{15}, \lambda \to -\infty$	3 - 4	- - - -
as.sep $\lambda1$	IR: $\lim_{\lambda \to +\infty}(\lambda, -\frac{7}{4}\lambda)$	10 - 11	— · · —
as.sep $\lambda2$	IR: $\lim_{\lambda \to -\infty}(\lambda, -\frac{7}{4}\lambda)$	4 - 5	— · · —
as.sep $\lambda3$	IR: $(\lambda_1^{(0)}, -\infty)$	7 - 13	— · · —
as.sep $\lambda4$	UV: $(\lambda_2^{(0)}, +\infty)$	5 - 6	— · · —

Table 5.3: The abbreviated names, defining properties and graphical representation of the special trajectories and societies for $d = 4, \alpha = 0$. In the third column, the two global classes separated by the respective special society are given.

defects, $g = 0, b = 1$. The non-Gaussian FP is a vertex for the six edges, given by the special societies. Hence the number of faces is 6, which is the number of global classes of societies for $g \geq 0$. For the lower half-plane, all special societies end either at the λ-axis (the boundary) or diverge. In this case there is no vertex and the number of faces (global classes of societies) is 7.

In order to complete the global classification, the special societies and hence the classes delimited by them have to be labelled according to some scheme. This is conveniently done by, e.g., going around each half-plane in a clockwise direction and ordering the societies according to the sequence in which their endpoints are encountered. Special care has to be given to degenerate limits of trajectories, but a definite order exists due the definiteness of the flow in the whole plane, except for the discontinuity $(1/2, 0)$.

The global classes of societies are labelled 1-6 in the upper and 7-13 in the lower half-plane. How they are delimited by the special societies is presented in the third column of table 5.3. The legend for the graphical representation of the special societies together with the defining analytic properties of the name-giving special trajectory is also given in table 5.3 .

5.3.7 Full classification

To complete the global classification of the trajectories, we have to know the supporting sectors of the special societies. To answer this question, the full numerical solutions of the special trajectories and their associates have to be determined. In fact, this knowledge has already been used in the previous section. The global classification of all trajectories follows from that of their delimiting special trajectories.

The resulting global classes are listed in table 5.4. The labels of the global trajectory

classes in the first column consist of the arabic numerals of the global society class the trajectory belongs to, as introduced in the previous section, and the lower case latin letter of the supporting sector of the individual trajectories. In the second column, the line type used for the graphical representation of the class in the phase space portraits fig. 5.6(a) and fig. 5.6(b) is displayed. The columns labelled UV and IR give the endpoints of the trajectories for its highest and lowest value of t. In the cases where $t \rightarrow \pm\infty$ exists, these are either the non-Gaussian FP ($NGFP$) or one of the asymptotic values discussed in section 5.3.5. If the trajectories of this class terminate at g^η the branch of this boundary is further specified by labelling it according to the sectors it separates.

Fig. 5.6(a) and fig. 5.6(b) are the fully classified versions of the phase portraits fig. 5.4 and fig. 5.5. The legend for the different types of lines can be found in table 5.1 for the (red) special lines, table 5.3 for the (green) special societies and table 5.4 for the various classes of trajectories. The FPs are denoted as red points. The arrows point into the direction of decreasing RG parameter t. The full phase space portrait fig. 5.6(a) uses compactified coordinates $\frac{\lambda}{1+|\lambda|}, \frac{g}{1+|g|}$.

In section 5.3.4 it was argued that global classification of trajectories is yields more categories than local classification. Table 5.5 contains the local classes of trajectories. They are labelled by the lower case letter of the respective sector followed by a roman numeral counting classes for each sector independently. The column labelled "global" lists the global classes contained in the local one. Many local classes consist of several global ones. For local classification they are indiscernible, inheriting their distinctions from associates in other sectors. The third and fourth column give again the endpoints of the local trajectories.

5.3.8 Discontinuity

The point ($\frac{1}{2}$, 0) necessitates a separate discussion. All special lines ($g = 0$), g^g, g^η, g^λ intersect in it. The values of β_λ, β_g at it depend on how they approach it. This is obvious for the special lines themselves, on which the respective β-functions take on their defining values.

From the point of view of the trajectories, this discontinuity is only problematic for class 8e, which is focused into it, cf. fig. (5.6(b)). All other classes are repelled from it. This can be seen from the sign of the β-functions around ($\frac{1}{2}$, 0): for all parts of phase space, except the wedge filled by class 8e, at least one direction of the flow points away from the discontinuity. The numerical solutions confirm this argument.

However, the ultimate fate of 8e trajectories still remains an open issue. Does the discontinuity represent a FP for the direction of approach of trajectories 8e, i.e. do β_λ, β_g approach zero along such a trajectory or not? The alternative to FP-behaviour would be that ($\frac{1}{2}$, 0) is a focal point for trajectories 8e: all of them run into it and are merged into one trajectory. Such a trajectory would run trivially along the λ-axis, $g = 0, \lambda = \text{const.}/k^2$.

We have to stress that even if the discontinuity represents an IR FP for class 8e it is not a phenomenologically relevant candidate for the hypothetical IR FP discussed in the literature: the physical trajectory, see section 5.5.3, does not belong to class 8e since

traj.	graphics	UV	IR
$1a$	$-\,-\,-$	$NGFP$	g_{ab}^η
$1b$	$-\!-\!-$	g_{bc}^η	g_{ab}^η
$1c$	$-\,-\,-$	g_{bc}^η	$(+\infty,+0)$
$2a$	$-\!-\!-$	$NGFP$	$(-\infty,+0)$
$3a_1$	$\cdots$	$NGFP$	g_{ab}^η
$3b$	$\cdots\cdots$	g_{ab}^η	g_{ab}^η
$3a_2$	$\cdots$	g_{ab}^η	$(-\infty,+0)$
$4a_1$	$-\cdot-\cdot-$	$NGFP$	g_{ab}^η
$4b$	$-\cdot\cdot-\cdot\cdot$	g_{ab}^η	g_{ab}^η
$4a_2$	$-\cdot-\cdot-$	g_{ab}^η	$(-\infty,+\infty)$
$5a_1$	$-\,-\,-$	$NGFP$	g_{ab}^η
$5b$	$-\!-\!-$	g_{ab}^η	g_{ab}^η
$5a_2$	$-\,-\,-$	g_{ab}^η	$(\lambda_1^{(0)},+\infty)$
$6a$	$\cdots$	$NGFP$	g_{ab}^η
$6b$	$\cdots\cdots$	g_{bc}^η	g_{ab}^η
$6c$	$\cdots$	g_{bc}^η	$(+\infty,+\infty)$
$7d$	$-\,-\,-$	g_{de}^η	$(-\infty,-\infty)$
$7e$	$-\cdot-\cdot-$	g_{de}^η	$(-\infty,-0)$
$8f$	$-\,-\,-$	g_{ef}^η	$(+\infty,-\infty)$
$8e$	$-\cdot-\cdot-$	g_{ef}^η	$?(\frac{1}{2},-0)?$
$9f$	$-\!-\!-$	g_{ef}^η	$(+\infty,-\infty)$
$9e$	$\cdots\cdots$	g_{ef}^η	$(+\infty,-0)$
$10f$	$-\!-\!-$	g_{ef}^η	$(+\infty,-\infty)$
$10e$	$\cdots\cdots$	g_{ef}^η	$(-\infty,-0)$
$11e_1$	$-\,-\,-$	g_{ef}^η	$(-\infty,-0)$
$11f$	$-\cdot\cdot-\cdot\cdot$	g_{ef}^η	g_{ef}^η
$11e_2$	$\cdots\cdots$	$(\lambda_2^{(0)},-\infty)$	g_{ef}^η
$12e$	$-\cdot-\cdot-$	$(\lambda_2^{(0)},-\infty)$	$(-\infty,-0)$
$13e_1$	$\cdots\cdots$	g_{de}^η	$(-\infty,-0)$
$13d$	$\cdots$	g_{de}^η	g_{de}^η
$13e_2$	$-\!-\!-$	$(\lambda_2^{(0)},-\infty)$	g_{de}^η

Table 5.4: Global classes of trajectories. The classification is discussed in the main text.
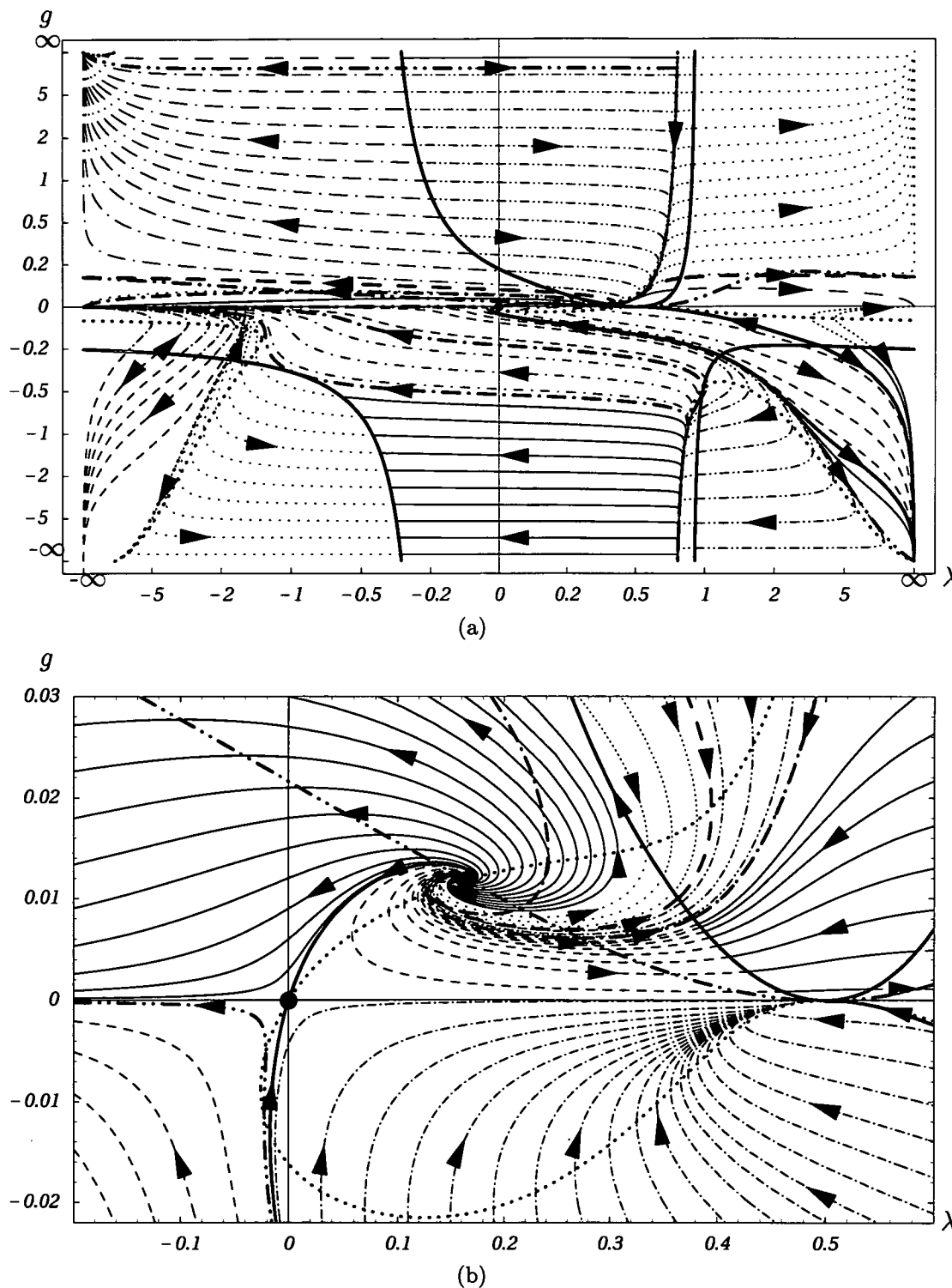
Figure 5.6: Phase space portrait of the globally classified trajectories for $d = 4, \alpha = 0$. (a) Entire phase space with rescaled axis $x \to \frac{x}{1+|x|}$. (b) Close up around the FPs.

local.	global	UV	IR
aI	$2a$	$NGFP$	$(-\infty, +0)$
aII	$3a_2$	g_{ab}^η	$(-\infty, +0)$
$aIII$	$4a_2$	g_{ab}^η	$(-\infty, +\infty)$
aIV	$5a_2$	g_{ab}^η	$(\lambda_1^{(0)}, -\infty)$
aV	$1a, 3a_1, 4a_1, 5a_1, 6a$	$NGFP$	g_{ab}^η
bI	$1b, 6b$	g_{bc}^η	g_{ab}^η
bII	$3b, 4b, 5b$	g_{ab}^η	g_{ab}^η
cI	$1c$	g_{bc}^η	$(+\infty, +0)$
cII	$6c$	g_{bc}^η	$(+\infty, +\infty)$
dI	$7d$	g_{de}^η	$(-\infty, -\infty)$
dII	$13d$	g_{de}^η	g_{de}^η
eI	$13e_2$	$(\lambda_2^{(0)}, -\infty)$	g_{de}^η
eII	$11e_2$	$(\lambda_2^{(0)}, -\infty)$	g_{ef}^η
$eIII$	$12e$	$(\lambda_2^{(0)}, -\infty)$	$(-\infty, -0)$
eIV	$7e, 13e_1$	g_{de}^η	$(-\infty, -0)$
eV	$10e, 11e_1$	g_{ef}^η	$(-\infty, -0)$
eVI	$9e$	g_{ef}^η	$(+\infty, -0)$
$eVII$	$8e$	g_{ef}^η	$?(\frac{1}{2}, -0)?$
fI	$8f, 9f, 10f$	g_{ef}^η	$(+\infty, -\infty)$
fII	$11f$	g_{ef}^η	g_{ef}^η

Table 5.5: Dictionary between local and global classification of trajectories for $d = 4, \alpha = 0$.

Newton's constant is positive. Furthermore, since the present truncation breaks down at g^η, the discontinuity lies outside the present approximation.

5.4 Phase Portrait for Four Dimensions and Harmonic Gauge

The dependence of the flow equations on the gauge fixing parameter α and on the employed cutoff is an artifact of the truncation. Before we can turn to a physical interpretation of the phase space portrait, we have to determine to what degree it depends on the cutoff and on the gauge fixing. The comparison to portraits from other cutoffs given in [108] is performed in section 5.5. In the present section we provide the classified portraits for the optimised cutoff type B in four dimensions and $\alpha = 1$. This allows for an estimate of the gauge fixing dependence of the whole phase space. In section 5.5 we extract features of the flow which hold true for general values of the gauge fixing parameter.

5.4.1 Fixed points and special lines

For $d = 4$ and $\alpha = 1$ the β-functions and the anomalous dimension are given by

$$
\begin{aligned}
\beta_\lambda &= -(2 + 50g)\lambda - 45g + \frac{75}{2}g^2 \\
&\quad + g\frac{57 + \frac{923}{2}g + \frac{725}{2}g^2 - 163\lambda - \left(\frac{4027}{3} + \frac{225}{2}g\right)g\lambda}{(1 - 2\lambda)^2 + g(-\frac{29}{3} + 3\lambda)},
\end{aligned}
\tag{5.29}
$$

$$
\beta_g = 2g - g^2\frac{105 - 212\lambda + 200\lambda^2}{(1 - 2\lambda)^2 + g(-\frac{29}{3} + 3\lambda)},
\tag{5.30}
$$

$$
\eta = -g\frac{105 - 212\lambda + 200\lambda^2}{(1 - 2\lambda)^2 + g(-\frac{29}{3} + 3\lambda)}.
\tag{5.31}
$$

The anomalous dimension diverges on the line

$$
\frac{1}{\eta} = 0 : g^\eta(\lambda) = \frac{(1 - 2\lambda)^2}{\frac{29}{3} - 3\lambda}.
\tag{5.32}
$$

It has a double zero at $\lambda = 1/2$ and a first order pole at $\frac{29}{9}$, cf. fig. 5.1(a). It behaves asymptotically like $-\frac{4}{3}\lambda$. This constitutes a first global difference to the $\alpha = 0$ case of the previous sections, where g^η displayed two poles and approached finite values asymptotically. This time we identify only five disjunct sectors. To facilitate later comparison, we omit sector d as the "missing sector".

The FP condition $\beta_\lambda = 0 \cap \beta_g = 0$ has one real, non-trivial solution corresponding to a non-Gaussian UV FP in addition to the Gaussian one:

$$
\lambda_* = 0.171503 \quad , \quad g_* = 0.00929975 \,\hat{=}\, \tilde{g}_* = 0.701185
\tag{5.33}
$$

$$
\theta = 1.68911 \pm i\,2.48567.
\tag{5.34}
$$
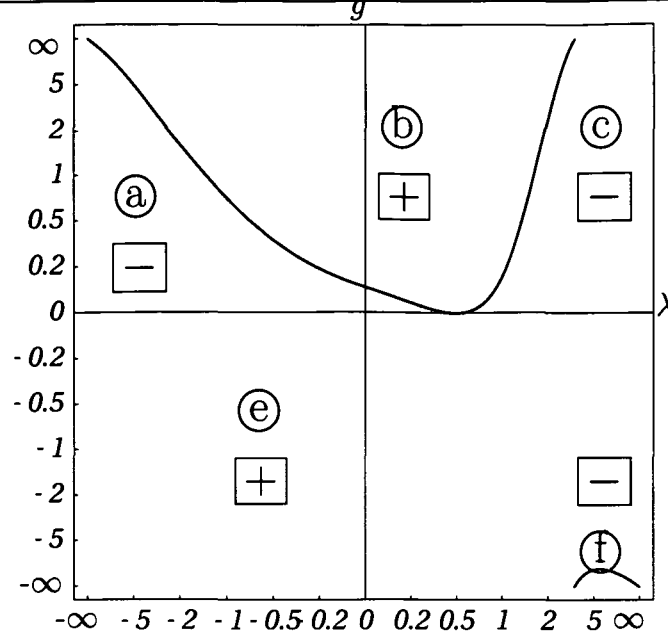
Figure 5.7: The five disjunct parts of phase space a, b, c, e, f and the respective sign of η in them. η vanishes on the λ-axis and diverges on g^η (in red). The axis are rescaled to $x/(1 + |x|)$.

The fixed lines, at which only one β-function vanishes, are given by

$$\beta_\lambda = 0: \quad g_\pm^\lambda(\lambda) = \frac{q_1 \pm \sqrt{q_2}}{q_3}, \tag{5.35}$$

$$q_1 = 3 - \frac{41}{12}\lambda + \frac{7}{2}\lambda^2 - 50\lambda^3,$$

$$q_2 = 1296 + 64296\lambda - 346655\lambda^2 + 551820\lambda^3,$$
$$-278508\lambda^4 - 50400\lambda^5 + 360000\lambda^6,$$

$$q_3 = -467 + 572\lambda,$$

$$\beta_g = 0: \quad g^g(\lambda) = \frac{(1 - 2\lambda)^2}{\frac{373}{6} - 109\lambda + 100\lambda^2}. \tag{5.36}$$

$g^g(\lambda)$ has a double zero and a minimum at $\lambda = \frac{1}{2}$ and one saddle point at $\lambda = 0$. Its asymptotic values for $\lambda \to \pm\infty$ are $1/25$. $g_+^\lambda(\lambda)$ vanishes at $\lambda = 1/2$ and $g_-^\lambda(\lambda)$ at $\lambda = 0$. For $g^\lambda(\lambda)_+$ a further zero of the nominator cancels the zero of the denominator at $\lambda^{(0)} = \frac{467}{572}$ so that only the branch $g^\lambda(\lambda)_-$ has a first order pole there. In the interval $(-1.459, -0.0183)$, q_2 is negative and both branches are complex. Whereas $\lim_{\lambda \to \pm\infty} g^\lambda(\lambda)_+ = -\frac{1}{25}$, the other branch diverges asymptotically like $-\frac{25}{143}\lambda^2$.

5.4.2   Asymptotic behaviour

The possible asymptotic behaviour of trajectories is determined by the properties of the ten potential limits (∞, ∞), $(\infty, -\infty)$, $(-\infty, \infty)$, $(-\infty, -\infty)$, $(\infty, 0)$, $(-\infty, 0)$, $(\infty, \frac{1}{25})$, $(-\infty, \frac{1}{25})$, $(\lambda^{(0)}, \infty)$, $(\lambda^{(0)}, -\infty)$ and the two FPs.

asymptotic	attractive
$NGFP$	UV
$(\lambda^{(0)}, -\infty)$	UV
$\lim_{\lambda \to -\infty}(\lambda, g \gtrsim -\frac{25}{143}\lambda^2)$	UV
$(+\infty, +\infty)$	IR
$\lim_{\lambda \to \infty}(\lambda, -\frac{25}{143}\lambda^2 \lesssim g \gtrsim -\frac{4}{3}\lambda)$	IR
$\lim_{\lambda \to -\infty}(\lambda, g \gtrsim -\frac{4}{3}\lambda)$	IR
$(+\infty, 0)$	IR
$(-\infty, 0)$	IR
$(0, 0)$	repulsive
$(\infty, \frac{1}{25})$	repulsive
$(-\infty, \frac{1}{25})$	repulsive
$\lim_{\lambda \to \infty}(\lambda, g \lesssim -\frac{25}{143}\lambda^2)$	repulsive
$\lim_{\lambda \to -\infty}(\lambda, g \lesssim -\frac{25}{143}\lambda^2)$	repulsive
$(\lambda^{(0)}, \infty)$	repulsive

Table 5.6: Stability properties of the FP and fixed limits for $d = 4$, $\alpha = 1$.

The lines of vanishing β_λ and diverging η lead to a differentiation of the double asymptotic limits $(+\infty, -\infty)$, $(-\infty, +\infty)$, $(-\infty, -\infty)$ into seven cases. The properties of these limits depend on whether they are approached from above or from below these lines. In the case of g^λ the distinction is between attractive and repulsive behaviour with an asymptotic separatrix delimiting the two possibilities. Because of g^η we encounter a novel situation for $(-\infty, +\infty)$ and $(+\infty, -\infty)$: if the limit is per se attractive (which is the case for both limits), g^η separates asymptotically UV and IR-attractive behaviour. This is due to the simultaneous change of sign in both β-functions across g^η. No separating trajectory can be defined in this case since it would have to approach g^η asymptotically. Accordingly, all trajectories in this limit's basin of attraction must approach it either in the UV or IR. To determine which case is realised, one has to compare the slope of the trajectories at g^η, which is given by $\lim_{g \to g^\eta} \beta_g/\beta_\lambda$, cf. section 5.1.1, to that of g^η itself. The result of these considerations is that all trajectories in the basin eventually cross g^η toward the IR-attractive side of g^η.

The respective UV side is, strictly speaking, an "empty attractor". Since it does not generate any influence on the flows in addition to that of g^η itself, we have excluded it from table 5.6 where all the asymptotes and their properties are given. The other results in table 5.6 were obtained by repeating the analysis detailed in section 5.3.5 for the present case. The stable limits show up in the phase space portraits as attractors of certain global classes of trajectories.

On the other hand, the unstable limits are approached by one and only one special trajectory each, the separatrix and the asymptotic separatrices. As in the previous example $\alpha = 0$, we further introduce the marginally asymptotic trajectories tangent to g^η and the quasi-separatrix running into the discontinuity $(\frac{1}{2}, 0)$.

5.4.3 Classification of trajectories

There are two special trajectories less in the present example than in the case $\alpha = 0$: in the upper half-plane ($g > 0$), there is one $\beta_\lambda = 0$ asymptotic separatrix less and in the lower half-plane there is one marginally asymptotic trajectory less than for $\alpha = 0$. The topological structure (one vertex in the upper, none in the lower half-plane) is the same as in the previous example. Therefore the total number of global classes of societies is decreased by one in each half of phase space.

For $g < 0$ the absence of g_{de}^η entails that of class 13. Class 12 incorporates now all trajectories running left of the marginal asymptotic tangent to g_{ef}^η from the UV asymptotic $(\lambda^{(0)}, -\infty)$ to the IR one $(-\infty, -0)$. We will come back to this important example of how societies, cut to pieces by g^η in one gauge, may reproduce the behaviour of complete trajectories in another gauge in section 5.5.

In the upper half-plane, class 5 vanishes completely since the asymptotic $(\lambda_1^{(0)}, \infty)$ does not exist for $\alpha = 1$. Furthermore, the asymptotic separatrix approaching $(-\infty, 1/25)$ is complete, i.e. contrary to $\alpha = 0$ it does not run into g^η. Hence class 3 as defined for $\alpha = 0$ is absent. We define a class 3' instead, which shares the asymptotic behaviour of class 4 but consists of complete trajectories.

The complete global classification of trajectories is given in table 5.7. The complete, classified and rescaled phase space portrait is given fig. 5.8(a). A close up around the Gaussian and the non-Gaussian FP is provided in fig. 5.8(b).

5.5 Comparison of Portraits

We turn now to the comparison of the two phase space portraits with each other and a third one obtained with a sharp cutoff of type A in [108]. It is of special interest which global features are independent of the gauge fixing and the choice of cutoff function and which depend on it. The latter class can be identified as artificial. For phenomenological application of the Einstein–Hilbert flow equations, it is important to ascertain that the physical trajectory realised in Nature lies in a part of phase space reliably described in that approximation. Furthermore, we want to test whether the association procedure, introduced in section 5.1.2 and used subsequently in the classification nomenclature, is reflected by universal features of the flow.

5.5.1 Gauge dependence of portraits

We commence with a comparison of the two phase portraits of section 5.3 and 5.4. As already noted in section 5.4.3, the simpler structure of η's line of divergence for $\alpha = 1$ induces differences with respect to $\alpha = 0$. However, these differences can only lead to differences between local classifications of trajectories, since the global types of asymptotic behaviour are not governed by g^η but by the fixed lines of the couplings, g^λ, g^g. Hence these changes affect only the splitting of societies into associates. An exception are the global classes separated by marginally asymptotic trajectories, which are defined with respect to g^η.

(a)

(b)
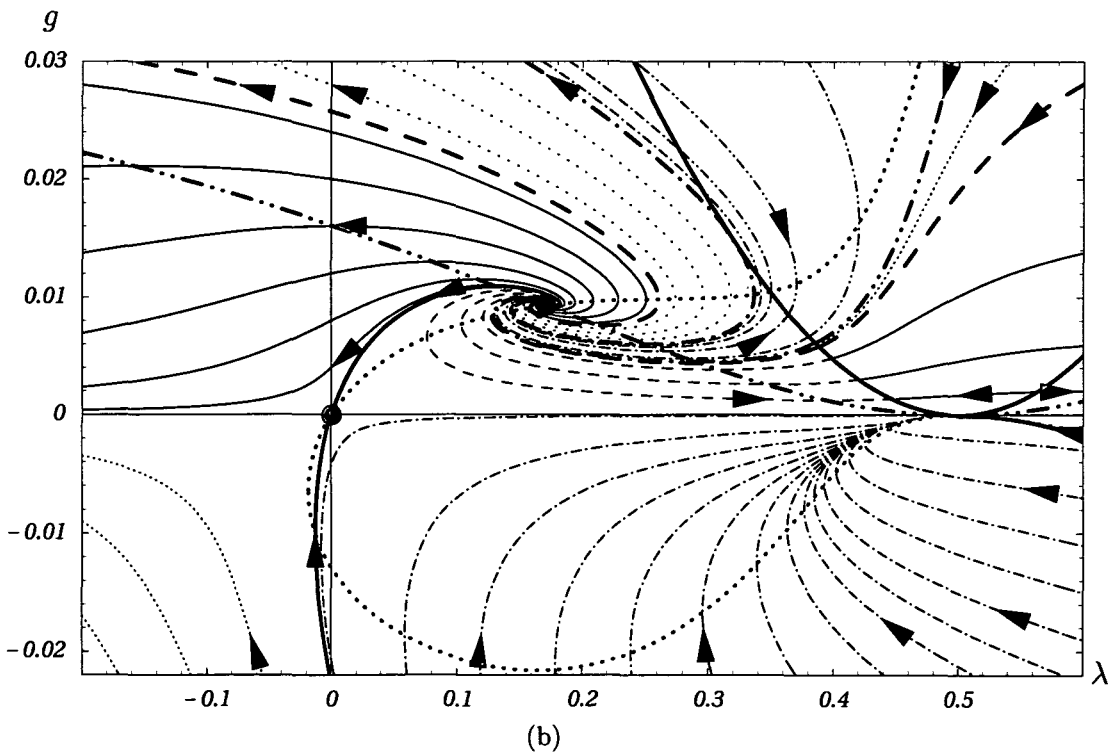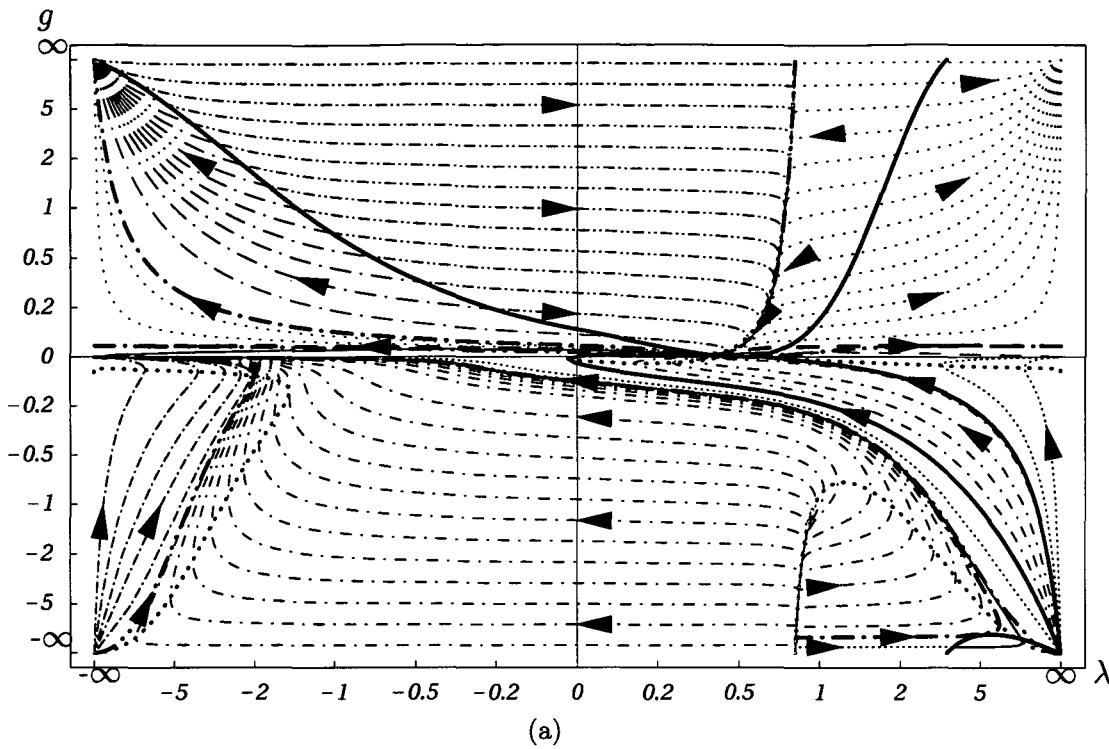
Figure 5.8: Globally classified trajectories for $d = 4, \alpha = 1$. Cf. the main text for discussion of this portrait. (a) Entire phase space with rescaled axis $x \rightarrow \frac{x}{1+|x|}$. (b) Close up around the FPs.

traj.	graphics	UV	IR
$1a$	– – –	$NG - FP$	g^η_{ab}
$1b$	——	g^η_{bc}	g^η_{ab}
$1c$	– – –	g^η_{bc}	$(+\infty, +0)$
$2a$	——	$NG - FP$	$(-\infty, +0)$
$3'a$	$\cdots$	$NG - FP$	$(-\infty, +\infty)$
$4a_1$	– · – · –	$NG - FP$	g^η_{ab}
4_b	– ·· – ··	g^η_{ab}	g^η_{ab}
$4a_2$	– · – · –	g^η_{ab}	$(-\infty, +\infty)$
$6a$	$\cdots$	$NG - FP$	g^η_{ab}
$6b$	$\cdots\cdots$	g^η_{bc}	g^η_{ab}
$6c$	$\cdots$	g^η_{bc}	$(+\infty, +\infty)$
$7e$	– · – · –	$(-\infty, -\infty)$	$(-\infty, -0)$
$8f$	– – –	g^η_{ef}	$(+\infty, -\infty)$
$8e$	– · – · –	g^η_{ef}	$?(\frac{1}{2}, -0)?$
$9f$	——	g^η_{ef}	$(+\infty, -\infty)$
$9e$	$\cdots\cdots$	g^η_{ef}	$(+\infty, -0)$
$10f$	——	g^η_{ef}	$(+\infty, -\infty)$
$10e$	$\cdots\cdots$	g^η_{ef}	$(-\infty, -0)$
$11e_1$	– – –	g^η_{ef}	$(-\infty, -0)$
$11f$	– ·· – ··	g^η_{ef}	g^η_{ef}
$11e_2$	$\cdots\cdots$	$(\lambda^{(0)}, -\infty)$	g^η_{ef}
$12e$	– · – · –	$(\lambda^{(0)}, -\infty)$	$(-\infty, -0)$

Table 5.7: Global classes of trajectories for the case $d = 4, \alpha = 1$, their labels, graphical representation and UV and IR endpoints.

This can be turned into an argument for the interpretation (ii) of association, given in section 5.1.2: the breakdown of the flow is not gauge independent, since g^η depends partly on α. But gauge dependent features should be considered as artifacts. Hence the breakdown of the truncation could itself be partly an artifact of the truncation.

This is underlined by the consequences of the absence of sector d for $\alpha = 1$. For negative g, the absence of its boundary g^η_{de} leads to the completeness of 7e-trajectories, as opposed to the splitting of societies of class 7 into associates of classes 7d and 7e for $\alpha = 0$. Furthermore, the complete class 12e contains all trajectories of the incomplete class 13 of $\alpha = 0$ (which is hence absent for $\alpha = 1$), since g^η_{de} is absent for $\alpha = 1$. Classes 12 and 13 have common UV and IR limits also for $\alpha = 0$, their separation was induced by the presence of g^η_{de}. All trajectories of UV and IR behaviour according to classes 7 and 12 are complete for $\alpha = 1$. Interpreting the gauge dependence of the presence of g^η_{de} as signalling its artificiality, one could opt for its removal and accordingly regard $\alpha = 1$ as the more physical case in this respect.

On the other hand, the other branches g^η_{ef}, g^η_{ab} and g^η_{bc} do not display such severe gauge dependence. Even though g^η_{ef} and g^η_{ab} show qualitatively different asymptotic behaviour, this affects the trajectories only at the local level. This is a reassuring observation, since the physical trajectory realised in our universe (see section 5.5.3) lies in this part of phase space. One local difference in gauge is, however, worth noting: whereas the only complete class for $\alpha = 0$ is class 2a, which connects the non-Gaussian UV FP with the asymptotic weak coupling limit $(-\infty, +0)$, for $\alpha = 1$ the incomplete class 3 of $\alpha = 0$ (contained in class 2 for $\alpha = 1$) is replaced by the new, complete class 3', which has a strong coupling IR limit $(-\infty, +\infty)$. Again, this can be interpreted as a sign that association across boundaries, though certainly unphysical locally, may nevertheless yield globally meaningful statements, in this case that there exist renormalisable theories with strong coupling behaviour at large scales.

Differences in the global structure of the phase portraits are determined by the limits of the zero lines of the couplings: the pole of g^λ at negative $\lambda_1^{(0)}$ found for $\alpha = 0$ is absent in the case $\alpha = 1$. Accordingly, the global class 5 does not exist for $\alpha = 1$. Following the principle that all gauge dependent qualitative features should be discarded as artifacts, we surmise this to be the case for the limit $(\lambda_1^{(0)}, +\infty)$. Interestingly, its pendant at $\lambda_2^{(0)}$ exists in both gauges. All other global characteristics are reproduces in both gauges. Especially the gauge universality of the four strong coupling limits in the four corners of phase space should be noted.

5.5.2 Cutoff dependence of portraits

So far we compared the two phase space portraits obtained in sections 5.3 and 5.4 with the optimised cutoff for two different gauges, searching for gauge independent features. A property must be cutoff independent to qualify as potentially universal. Hence portraits and classifications obtained from different cutoff functions have to be compared. Even if we trust the optimised cutoff most, the reproduction of certain features by other cutoffs would greatly enhance their trustworthiness.

Such an analogous phase space portraying and classification has been performed in

[108] for a *sharp cutoff* [80] of type A. The sharp cutoff is defined as

$$r^{\text{sc}}(z) = z^{-1} a \, \Theta(1 - z) \,, \qquad (5.37)$$

where the limit $a \to \infty$ has to be taken after insertion of (5.37) into the threshold functions (C.1). The threshold functions then take the form

$$\phi_n^p(w)^{\text{sc}} = \frac{1}{\Gamma[n]} \frac{1}{p-1} \frac{1}{(1+w)^{p-1}} \quad , \quad \tilde{\phi}_n^p(w)^{\text{sc}} = 0 \quad \text{for} \quad p > 1 \qquad (5.38)$$

$$\phi_n^1(w)^{\text{sc}} = -\frac{1}{\Gamma[n]} \ln(1+w) + c_n \quad , \quad \tilde{\phi}_n^1(w)^{\text{sc}} = \frac{1}{\Gamma[1+n]} \quad \text{for} \, p = 1 \,,$$

where c_n is a free parameter eventually fixed by demanding $\phi_n^1(0)^{\text{sc}}$ to equal the value of the threshold function for the modified exponential cutoff (B.1) with vanishing argument. The sharp cutoff yields analytic flow equations whose numerical solutions can studied. However, it is known to have worse stability than the smooth or the optimised cutoffs [83], and its singular nature may lead to spurious divergences.

In this case, the stability boundary lies at $\lambda = 1/2$ too. The β-functions display a genuine divergence at this boundary and flows cannot be continued across it. The η-divergence curve lies at $g^\eta = \text{const.} < 0$. The phase space portraits to be compared to our results are given in fig. 12 to 15 of [108], and the corresponding classification is performed in table III, ibidem. The sharp cutoff does not allow to investigate the region $\lambda > 1/2$ (cf. the $\ln(1 + w)$ term in (5.38), in particular), so the comparison of portraits has to be restricted to its complement. For the present purpose of comparison, we treat the stability boundary on the same ground as the η-boundary.

Trajectories were classified in [108] in a local way. The nomenclature used there consists of roman numerals labelling the "Types" of trajectories, followed by an "a" if the trajectories lie in the upper half plane and a "b" for the lower one. The possible asymptotic limits are two weak coupling $(-\infty, \pm 0)$ and one strong coupling $(-\infty, +\infty)$ ones. Note that our rescaled g is smaller by a factor $4\pi 6 \approx 75$ than the canonical one used in [108]. This is of course irrelevant for qualitative comparisons of the structures of phase portraits, but must be taken into account when comparing numerical values.

In order to get a first impression of the extent of cutoff dependence, we compare this "sharp" $\alpha = 1$ portrait with the "optimised" $\alpha = 1$ one generated and discussed in section 5.3. For negative gravitational coupling, both the local (η-boundary) and global (asymptotic limits) structure is rather different in the two cases. Since only one limit, $(-\infty, -0)$ is present in the sharp cutoff case, no complete trajectories or societies exist. Near the origin and the discontinuity $(1/2, -0)$ the local similarity of trajectories 10e and Type Ib and 8e and Type IIIb is remarkable. This behaviour seems to constitute a universal, gauge and cutoff independent feature. Since the discontinuity lies exactly on the stability boundary for the sharp cutoff, no new insights into it are obtained.

For positive g, the identical topological structure of sector a (to which we have to restrict this comparison) renders the portraits more similar. Both portraits have the same asymptotic limits and, accordingly, the same global classes. A mapping of classifications is given in table 5.8. (The seemingly missing Type IIa trajectory is the separatrix in [108].) The threefold degeneracy of Type IIIa with respect to the global

optimised	$1a$	$2a$	$3a'$	$4a_1$	$4a_2$	$6a$
sharp	$IIIa$	Ia	IVa	$IIIa$	Va	$IIIa$

Table 5.8: Dictionary between the classification of the $\alpha = 1$ optimised cutoff portrait with the one obtained with $\alpha = 1$ and the sharp cutoff [108] in sector a.

trajectory classification illustrates again the finer resolution of the latter scheme A purely local classification of trajectories would have given identical results for the two cutoffs. That both cutoffs give a qualitatively identical phase space portrait (at least in sector a) is very remarkable and further strengthens trust in the sector around the non-Gaussian FP.

Comparison of the $\alpha = 0$, optimised cutoff portrait with the sharp cutoff $\alpha = 1$ one confirms the previous findings. One finds both the differences, seen when comparing the two portraits generated for different gauges and identical cutoff and those seen in the comparison of the portraits for different cutoffs in harmonic gauge. In this sense, variation of cutoff functions and variation of gauge fixing have an orthogonal impact on the flow.

5.5.3 The physical trajectory in Einstein–Hilbert gravity

Only one RG trajectory of gravity can be realised in Nature. Assuming space-time to be macroscopically four-dimensional (as opposed to the alternatives presented in the RSII [12] or infinite-volume extra-dimensions models [14]), it is approximated best in the Einstein–Hilbert truncation by one of the trajectories in the four-dimensional phase-space portraits presented in the previous sections. Experiments tell us that this approximation is very good at all directly investigated scales, since no deviations from general relativity have been detected so far.

How can we determine which of these trajectories describes the scale dependence of the two coupling constants? This question has been discussed in depth in [130]. Given a set of flow equations, a trajectory is fixed by initial values of the couplings at an initial renormalisation scale. Newton's constant is accurately measured at scales ranging from a fraction of a millimetre to astrophysical scales. Assuming naive cutoff identification (which is well-justified because space-time is nearly flat on these scales) and fixing the initial scale at one metre, the dimensionless Newton's constant is found to be very tiny, $g(1m) \approx 10^{-70}$. However, the value of the cosmological constant is not measurable at these scales, neither in the laboratory nor at galactic scales. All that can be said with certainty is that it is much smaller than the corresponding mass-scales, since it would otherwise dominate already at these scales. Note that we cannot make use of its best-fit value in, e.g., the ΛCDM concordance model, since there is no *independent* determination of G_k at cosmological scales. At these scales, the cosmological constant is of the order of the Hubble scale, $\bar{\lambda}(H_0) \sim H_0^2$, where H_0 is the Hubble constant. Hence the dimensionless cosmological constant is of order unity, $\lambda(H_0) = +O(1)$. For the present purpose, the estimate $|\lambda(1m)| \ll 1$ is sufficient.

These two estimates yield an initial point of the physical trajectory in the upper half-

plane ($g > 0$) and very close to the origin. Hence, the physical trajectory can belong either to class 1a or 2a. The possibility of it belonging to 2a can be excluded on the ground that no trajectory of class 2a fulfils the two conditions $\lambda_{k_1} \ll 1$ and $\lambda_{k_2} = O(1)$ for $k_2 < k_1$. Accordingly, the physical trajectory must belong to class 1a, as concluded previously in [130] from slightly different arguments.

It shares the positive features of its class: (i) it has a well defined UV-limit in the non-Gaussian FP, (ii) sector a for $\lambda > 0$ is found to be universally described by different gauges and cutoffs in this section. On the other hand, it also suffers the breakdown of the truncation at g^{η}_{ab}. Since g is bound to stay very small, this breakdown occurs for $\lambda = 1/2$. Unfortunately, this lies in the range where the cosmological constant becomes cosmologically relevant. To solve this issue, either the methods used in deriving the flow equations (e.g., the weak-curvature expansion, cf. section 2.2.4, is a point worth of improvement in this context) or the truncation have to be modified. The second possibility implies the interesting consequence that the Einstein-theory of gravity, general relativity, is modified at cosmological scales. This would be of relevance to a hypothetical IR fixed point of gravity discussed in the literature [133], [131], [132], [126]. A third, albeit speculative, resolution could be based upon the association procedure introduced in this work: since the physical trajectory remains very close to the λ-axis, its associate of class 1b has to span a very short λ-interval between g^{η}_{ab} and g^{η}_{bc}. The UV-starting point of the third associate of class 1c receives only a very small set-off with respect to the IR-termination of the original physical trajectory. From the point of view of association, it could be conjectured that the physical trajectory is IR-completed by its 1c associate, leading to constant Newton and cosmological constant in the IR.

With the advent of models with extra dimensions of infinite size, [12], [14], IR complete trajectories of potential phenomenological relevance can also be discussed in higher dimensions. This will be done elsewhere.

In this chapter we have analysed the flow equations of Einstein–Hilbert gravity with the optimised cutoff (2.19). Their explicit form allowed a detailed analytical, general analysis and the construction of phase space portraits spanning the entire coupling space. For this cutoff, the stability boundary does not yield divergent flows, it can be crossed safely. The structure of non-perturbative divergences of the anomalous dimensions, however, proved important for the structure of the portraits. A procedure for connecting trajectories across these divergences was proposed. It was argued and illustrated by explicit examples that this procedure may indeed capture the qualitative behaviour of the exact flow. The explicit phase portraits were constructed for the two gauges $\alpha = 0, 1$ in four space-time dimensions. Detailed classification was given in order to extract the universal, i.e. gauge and cutoff independent, features in a comparison of these two portraits with each other and a third one previously published [108], which used the sharp cutoff function. The excellent concurrence of all three portraits in the physically relevant sector serves to underpin the reliability of the Einstein–Hilbert truncation.

Chapter 6

Conclusions and Outlook

6.1 Summary of Results

In this thesis non-Gaussian UV-attractive FPs of the RG equations of quantum gravity were studied in higher dimensions (section 3 and 4). According to the scenario of asymptotic safety, such a FP implies the non-perturbative renormalisability of the theory (section 1.4). These FPs are found in this work in all investigated dimensions 4 to 10 in the approximation of the Einstein–Hilbert truncation. If the UV FPs also exist in extended truncations, as is indicated by previous results in four dimensions (section 2.3), gravity is non-perturbatively renormalisable in higher dimensions. In that case, all physical quantities show scaling behaviour according to their canonical dimension in the far UV, FP-regime: Newton's constant, e.g., becomes asymptotically free. Previously discussed phenomenological implications in four dimensions are reviewed in section 2.4. Indications for those in the context of field-theoretic models with extra dimensions (section 1.2), which provide one of the main motivations for our investigations, are presented below in section 6.2.

What prevented previous investigations of higher-dimensional FPs to reach a definitive conclusion so far, was the cutoff dependence of the FPs existence and properties, which is caused by truncation. This spuriousness is overcome in this work by employing a stability optimisation criterion for the ERG flow (section 2.1.1). It singles out a subset of cutoff functions yielding the most stable flows. For these cutoffs, the UV FP exists independently of the type of cutoff function used. Universal quantities at the FP, foremost the eigenvalues of the stability matrix, coincide at the percent level for all functions (section 3).

A second, non-trivial test of the reliability of the obtained FP results, is their gauge fixing independence. Truncation induces a spurious sensitivity of universal quantities on the gauge fixing. In section 4 it is shown that the stability criterion leads to a reduction of this artificial dependence. The universal properties of the FP show quantitatively good independence of the choice of gauge fixing in all studied dimensions.

Throughout the FP studies, one optimised cutoff function leads to most stable flows at the FP. Since it also yields analytic flow equations, it is used in section 5 to investigate the entire phase space of solutions to the flow equations. After a general discussion

of the properties of the system of flow-equations, explicit phase space portraits are constructed and studied in four dimensions. This allows to ascertain that the physical trajectory (section 5.5.3) realised at large scales in Nature is connected to the UV FP, i.e. that four-dimensional gravity has a reliable, UV complete description in the present approximation.

6.2 Implications for the Phenomenology of Extra Dimensions

In order to illustrate the kind of implications for the phenomenology of models with large extra dimensions to be expected from an ERG description of high energy quantum effects in gravity, we shortly reconsider some quantitative results of these models in the light of the results presented here. These musings must be regarded as mere indications at the kind of changes induced by this approach to quantum gravity, at best of semi-qualitative relevance. Detailed investigations of these effects are certainly the topic of further work in the near future.

When giving the phenomenological motivation for field-theoretic approaches of quantum gravity in extra dimensions in section 1.2, we mentioned three processes explicitly: (i) production of gravitons [20], (ii) virtual graviton exchange mediated interaction [20], [136] and (iii) black hole production [4], [5]. Other effects have also been investigated; see for example [137], [138], [19], [15], [6], [139]. Let us briefly sketch in what manner the processes (i), (ii) and (iii) could get modified by the FP behaviour of the gravitational coupling above the fundamental, extra-dimensional Planck-mass, M_d. To this end we use naive cutoff identification (see section 2.4) $k \equiv \sqrt{s}$, where s is the centre-of-mass energy of the process squared.

(i) Cross sections for the production of gravitons h in leptonic collisions, $l\bar{l} \longrightarrow h\, X$ with X being a photon or Z-boson, have the general scaling behaviour [20]:

$$\sigma_{l\bar{l}\to h\, X}(s) \sim \frac{1}{s}\left(\frac{\sqrt{s}}{M_d}\right)^{d-2} . \tag{6.1}$$

The centre-of-mass energy occurs with positive exponent for dimensions higher than four. The corresponding cross section grows unbounded with energy. In the ERG description of quantum gravity, the value of the gravitational coupling depends on the typical energy of the process considered. For relevant energies sufficiently far above the Planck scale, it will be governed by the RG FP also in extra dimensions. The fundamental Planck mass shows a scaling behaviour, $M_d = m_*^d k$ in this UV regime, where m_*^d is a dimensionless constant following from g_*. Using the cutoff identification $k \to \sqrt{s}$, the RG-improved graviton emission cross section is given by

$$\sigma_{l\bar{l}\to h\, X}(s \gg M_d) \sim \frac{1}{s}\left(m_*^d\right)^{2-d} \tag{6.2}$$

in the FP regime. For these arbitrarily high energies, it decreases with s. A similar modification is likely to hold for hadronic processes too. Indeed this is a tautology of

being in the scaling, FP regime: energy $\sqrt{s}$ remains the only dimensionful scale. Hence cross sections, which have mass dimension -2, must behave as s^{-1}. Dimensional analysis allows for no other possibility. It is nevertheless illuminating to illustrate this tautology with the slightly more explicit argument above.

(ii) The UV divergences encountered in virtual graviton exchange already at treelevel [20] essentially result from the fact that momentum conservation at the vertice is required only for directions parallel to the brane. The remaining directions q_T give the UV-divergent contributions. The momentum-space scattering amplitude due to graviton exchange is given at treelevel [20] by

$$A \approx \mathcal{T} \frac{1}{M_d^{d-2}} \int^{\Lambda} d^{d-4} q_T \frac{1}{s - q_T^2} \, . \tag{6.3}$$

The factor $\mathcal{T}$ depends on the four-dimensional energy-momentum tensors of the scattering particles. The second part yields the divergent contribution, necessitating its regularisation, denoted by Λ. Let us consider the far UV, relevant to the UV-divergence only, where we RG-improve $M_d = m_d^* q_T$ as in the FP regime. This is assumed to hold true above some scale $\tilde{k}$, which can be determined from the full flow. The contributions to A from momenta below $\tilde{k}$ are finite. The RG-improved UV contribution $A^{\mathrm{RG\ UV}}$ can be estimated for $s \ll \tilde{k}$ as

$$A^{\mathrm{RG\ UV}} \approx \mathcal{T} \int_{\tilde{k}}^{\infty} d^{d-4} q_T \frac{(M_*^d(q_T))^{2-d}}{(s - q_T^2)^{d/2}} \approx -\mathcal{T} S_d (m_*^d)^{2-d} \int_{\tilde{k}}^{\infty} dq_T \, q_T^{d-5} \frac{1}{q_T^d}$$

$$= -\mathcal{T} S_d (m_*^d)^{2-d} \int_{\tilde{k}}^{\infty} dq_T \, q_T^{-5} < \infty \, , \tag{6.4}$$

where S_d is the appropriate surface of the unit-sphere resulting from the respective angular integrations. In contrast to (6.3), (6.4) is UV-finite, as must be the case for the RG-improved effective theory with finite UV limit. The effective, physical UV cutoff $\tilde{k}$ is not a free parameter: it can be read off from the solution of the flow equations as the scale where teh FP behaviour sets in.

(iii) A geometrical argument for the cross section of black hole production [4] and identifying its mass with the centre-of-mass energy available [4] yields the expression

$$\sigma_{\mathrm{BH}}(s) \approx \pi \, r_{\mathrm{BH}}^2 \sim \frac{1}{M_d^2} \left(\frac{\sqrt{s}}{M_d} \right)^{2/(d-3)} \, . \tag{6.5}$$

where r_{BH} is the Schwarzschild radius determined by M_d and the mass of the black hole, $\sqrt{s}$. In this example, there are two choices for naive cutoff identification: either $k \sim 1/r_{\mathrm{BH}}$ or $k \sim \sqrt{s}$. For trans-Planckian $\sqrt{s} \gg M_d(k = 0)$, the first possibility would leave M_d constant. This corresponds to the view that black hole formation at trans-Planckian energies is a classical process and will screen all trans-Planckian quantum effects. The second choice implies again $\sigma \sim s^{-1}$, the scaling FP result. This ambiguity in the interpretation reminds us that cutoff identification plays an important role in the application of RG results.

The above examples are, as stated above, only meant to give a first flavour of the kind of phenomenology possible with ERG-improved gravity endowed with a FP. Detailed studies, especially of the energy range around the fundamental Planck mass, would certainly prove very interesting. Unfortunately, this is beyond the scope of this thesis. We hope to return to this point elsewhere soon.

6.3 Directions for Future Research

The number of directions into which research opens from the present state of knowledge is very large. In this section we would like to indicate some of the most obvious ones.

That collider-phenomenological questions of models of large extra dimensions could now be tackled in a UV-complete way, at least in principle, has been illustrated in the previous section. This was meant to indicate how the questions raised in our motivation for ERG gravitational studies in extra dimensions in section 1.2 can be successfully addressed.

The most obvious step to accumulate further evidence for the asymptotic freedom of gravity in more than four dimensions is to repeat the analysis presented in this work for the higher truncations already available. This includes the R^2-truncation of [111], non-local truncations [115] and the inclusion of matter [113], [112]. The absence of qualitative differences between the four- and higher-dimensional behaviour demonstrated in this work for the Einstein–Hilbert truncation suggests that the same is likely to occur also for these higher truncations.

The strong dependence of the FP couplings on the gauge-fixing parameter α for large values, discussed in sections 4.1 and 4.3.3, suggests a yet uninvestigated extension of truncation in the gauge-fixing sector. For example, it may be hoped that these large α effects can be removed by renormalising the ghost fields too.

In obtaining the β-functions of the couplings by projecting the r.h.s. of the flow equation onto the l.h.s., a certain background (maximally symmetric space) was assumed, see section 2.2.4. Furthermore, this projection was done around zero curvature. Using different backgrounds and developing the operator expansion around non-zero curvature would allow a further non-trivial test of the universality of the previous results.

Keeping an external scale like the mean curvature in the flow would furthermore give a physical cutoff identification prescription. This would be important for obtaining unambiguous results for phenomenological applications in strongly curved space-times, see section 2.4. The impact of such strong curvature projections on the stability boundary, with all ensuing consequences, is an open and important issue.

The perhaps most ambitious class of extended truncations is the inclusion of interacting matter. Since this case is the one realised in Nature, a confirmation of the FP results in such a setting would greatly increase the physical significance of the previous results. Coupling QED and quantum gravity would allow us to investigate the quantum version of the classical mutual regularisation of divergences [35].

We can conclude this thesis by stating that much has been achieved, but far more awaits investigation. The field of non-perturbative RG studies of gravity is young yet.

The surprising successes, most prominently the indications for the asymptotic safety of gravity as a quantum field theory, certainly warrant further investigations. A word of caution is of course appropriate: so far only first steps on the way to renormalisable quantum gravity have been taken. If the asymptotic safety of gravity has been fully established, the resulting theory constitutes *one* possible UV-complete description, albeit a very simple one, getting by with the metric degrees of freedoms already present in low-energy general relativity. It might well be the case that another, more involved theory is the actual high-energy completion of gravity. In the end, only experiment can decide which description of Nature is the correct one. It can, however, be considered rather encouraging that a consistent framework for concrete, falsifiable predictions is at hand at all, especially in the field of quantum gravity.

Appendix A

Power Counting Non-Renormalisability

In this appendix an alternative, compact derivation of the power counting formula (1.2), which gives the maximal degree of UV-divergence at some order in perturbation theory, is giving. We do this for the case of one coupling g with finite mass dimension d_g. The generalisation to more than one coupling is straightforward.

Any contribution G_N^n at fixed perturbative order n to the full N-point correlation function G_N must share its mass dimension, since $G_N = \sum_{n=1}^{\infty} G_N^n$. Its Fourier transform is of the general form

$$\tilde{G}_N^n = g^n \left(\prod_i^I \int^\Lambda d^d q_i \right) f(m_i, p_i, q_i) \tag{A.1}$$

with generic masses m_i, external momenta p_i and loop momenta q_i. Since the r.h.s. of (A.1) is potentially UV-divergent, it is regulated by a common momentum cutoff Λ. The precise form of f is determined by the Feynman rules of the theory but is not further specified. Following the usual power counting argument, we approximate f by a product of monomials in the moduli of the (euclidean) loop momenta, neglecting all external scales (and all IR-issues):

$$\tilde{G}_N^n \approx \text{const.}\, g^n \prod_i^I \left(\int^\Lambda dq_i (q_i)^{n_i} \right) = \text{const.}\, g^n \Lambda^\Delta . \tag{A.2}$$

For power counting to be applicable, it is essential that this approximation is possible[1].

The usual power counting analysis would now proceed to determine the relations between the integers I, n_i, n, d and N, making use of diagrammatic, topological considerations, which will eventually yield the *superficial* degree of divergence Δ.

These intricacies can be shortcut by noting that the mass dimensions must be the same on the l.h.s. and r.h.s of (A.2). On the l.h.s., the mass dimension is a fixed number: $[\tilde{G}_N^n] \equiv [\tilde{G}_N] := c_N$, already introduced in (1.2). Hence, the superficial divergence must be $\Delta = c_N - n\, d_g$, which gives (1.2).

---

[1]This is not always the case: field theories on non-commutative space-times show UV-IR mixing, power-counting in its usual form is hence not applicable, cf. e.g. [140], [141], [142], [143]

Appendix B

Cutoff Functions

In this work five different cutoff functions are employed, see also [84].

The modified exponential cutoff is defined for $0 < b$ as

$$r_{\text{mexp}}(z) := \frac{b}{(b+1)^z - 1}, \tag{B.1}$$

the modified exponential cutoff with alternative normalisation for $0 < b$ as

$$r_{\text{mexp}}^{alt}(z) := \frac{b}{e^z - 1}, \tag{B.2}$$

the exponential cutoff for $1 \leq b$ as

$$r_{\text{exp}}(z) := \frac{1}{2^{z^b} - 1}, \tag{B.3}$$

the generalised optimised cutoff for $0 < b$ as

$$r_{\text{go}}(z) := b(\frac{1}{z} - 1)\Theta(1 - z), \tag{B.4}$$

the power-like cutoff for $1 \leq b$ as

$$r_{\text{pow}}(z) := z^{-b} \tag{B.5}$$

and the modified cutoff for $1 \leq b$ as

$$r_{\text{mix}}(z) := \left(2^{\left(z + (b-1)z^b\right)/b} - 1\right)^{-1}. \tag{B.6}$$

The cutoffs fulfil the necessary conditions $\lim_{z \to 0}(z\,r) > 0$ and $\lim_{1/z \to 0}(z\,r) \to 0$, which follow from (2.2) and (2.3). The modified exponential, modified and generalised optimised cutoffs are mass-like for all allowed values of b, i.e. $\lim_{z \to 0}(z\,r) < \infty$. The exponential and the power-like cutoffs are mass like only for $b = 1$, otherwise they are divergent, i.e. $\lim_{z \to 0}(z\,r) \to \infty$.

For $b \to \infty$ all cutoff functions approach the sharp cutoff (5.37). They are parametrised in such a way that the higher b is, the narrower and steeper is the slope between the flat

behaviour in the IR and UV. Accordingly, the range of momenta contributing to the threshold functions, which is determined by $\partial_z r(z)$, is narrower for the "harder" cutoffs with a high value of b. The smoother cutoffs with lower b are called "soft" ones, a wider range of momentum modes contributes at each infinitesimal step in the flow. The values of b for which C attains its optimised values of 2 are given in table 3.4. The respective optimised cutoffs are moderately hard.

Appendix C

Flow Equations of Gravity

C.1 Cutoffs Type A

In this appendix the abreviating functions used in (2.63) and (2.64) are provided. The scalar threshold functions are defined as (cf. [101])

$$
\begin{aligned}
\Phi_n^p(w) &:= \frac{1}{\Gamma(n)} \int_0^\infty dz\, z^{n-1} \frac{-z^2 r'(z)}{(z(1+r(z))+w)^p}, \\
\tilde{\Phi}_n^p(w) &:= \frac{1}{\Gamma(n)} \int_0^\infty dz\, z^{n-1} \frac{z r(z)}{(z(1+r(z))+w)^p},
\end{aligned}
\tag{C.1}
$$

for $n > 0$. The functions themselves are given by

$$
A_1(\lambda; d) := -2\lambda + \frac{g_k}{(4\pi)^{d/2-1}} \left(a_1(d)\Phi_{d/2}^1(-2\lambda) + a_3(d)\Phi_{d/2}^1(0) \right),
\tag{C.2}
$$

$$
A_2(\lambda; d) := \lambda_k - \frac{a_1(d)g_k}{2(4\pi)^{d/2-1}} \tilde{\Phi}_{d/2}^1(-2\lambda),
\tag{C.3}
$$

$$
\begin{aligned}
B_1(\lambda; d) := \frac{1}{3(4\pi)^{d/2-1}} \Big(& a_1(d)\Phi_{d/2-1}^1(-2\lambda) + a_2(d)\Phi_{d/2}^2(-2\lambda) \\
& + a_3(d)\Phi_{d/2-1}^1(0) + a_4(d)\Phi_{d/2}^2(0) \Big),
\end{aligned}
\tag{C.4}
$$

$$
B_2(\lambda; d) := -\frac{1}{6(4\pi)^{d/2-1}} \left(a_1(d)\tilde{\Phi}_{d/2-1}^1(-2\lambda) + a_2(d)\tilde{\Phi}_{d/2}^2(-2\lambda) \right),
\tag{C.5}
$$

where the coefficients are defined as

$$
a_1(d) := d(d+1), \quad a_2(d) := -6d(d-1), \quad a_3(d) := -4d, \quad a_4(d) := -24.
\tag{C.6}
$$

C.2 Cutoff Type B

For cutoffs of type B (general gauge fixing, see section 2.2.5 and [103]), the abbreviating functions read

$$
C_1(\lambda, g; \alpha, d) := -2\lambda + \frac{g}{(4\pi)^{d/2-1}} \Big(d(d-1)\Phi^1_{d/2}(-2\lambda) + 2d\Phi^1_{d/2}(-2\alpha\lambda)
$$

$$
-4d\,\Phi^1_{d/2}(0) \Big), \qquad (C.7)
$$

$$
C_2(\lambda, g; \alpha, d) := \lambda - \frac{g}{(4\pi)^{d/2-1}} \Big(\frac{d(d-1)}{2}\tilde{\Phi}^1_{d/2}(-2\lambda) + d\tilde{\Phi}^1_{d/2}(-2\alpha\lambda) \Big), \qquad (C.8)
$$

$$
D_1(\lambda; \alpha, d) := \frac{4}{(4\pi)^{d/2-1}} \Big(3\delta_{d,2} \Big[\frac{1}{1-2\lambda} - \frac{1}{1-2\alpha\lambda} \Big] + c_1(d)\Phi^1_{d/2-1}(-2\lambda)
$$

$$
+ c_3(d)\Phi^2_{d/2}(-2\lambda) + c_2(d)\Phi^1_{d/2-1}(-2\alpha\lambda) + c_4(d,\alpha)\Phi^2_{d/2}(-2\alpha\lambda)
$$

$$
-2c_2(d)\Phi^1_{d/2-1}(0) + c_5(d)\Phi^2_{d/2}(0) \Big), \qquad (C.9)
$$

$$
D_2(\lambda; \alpha, d) := -\frac{2}{(4\pi)^{d/2-1}} \Big(c_1(d)\tilde{\Phi}^1_{d/2-1}(-2\lambda) + c_2(d)\tilde{\Phi}^1_{d/2-1}(-2\alpha\lambda)
$$

$$
+ c_3(d)\tilde{\Phi}^2_{d/2}(-2\lambda) + c_4(d,\alpha)\tilde{\Phi}^2_{d/2}(-2\alpha\lambda) + \frac{3\delta_{d,2}1}{1-2\lambda} - \frac{3\delta_{d,2}}{1-2\alpha\lambda} \Big). (C.10)
$$

The coefficients appearing above are

$$
c_1(d) := \frac{d^3 - 2d^2 - 11d - 12}{12d - 12} \quad, \quad c_2(d) := \frac{d^2 - 6}{6d},
$$

$$
c_3(d) := -\frac{d^3 - 4d^2 + 7d - 8}{2d - 2} \quad, \quad c_4(d,\alpha) := -\frac{\alpha d(d-2) - d - 1}{d},
$$

$$
c_5(d) := -\frac{2d + 2}{d}. \qquad (C.11)
$$

and the scalar threshold functions are given in (C.1).

The anomalous dimension is given in this case by

$$
\eta_N(k) = \frac{g_k D_1(\lambda_k; \alpha, d)}{1 - g_k D_2(\lambda_k; \alpha, d)}. \qquad (C.12)
$$

The corresponding flow equations of g_k and λ_k for cutoffs of type B are

$$
\partial_t g_k = [d - 2 + \eta_N(k)]g_k, \qquad (C.13)
$$

$$
\partial_t \lambda_k = C_1(\lambda_k, g_k; \alpha, d) + \eta_N(k)C_2(\lambda_k, g_k; \alpha, d). \qquad (C.14)
$$

Bibliography

[1] S. Carlip, "Quantum gravity: A progress report," Rept. Prog. Phys. **64** (2001) 885 [arXiv:gr-qc/0108040].

[2] C. Rovelli, "Notes for a brief history of quantum gravity," arXiv:gr-qc/0006061.

[3] C. Kiefer, "Quantum gravity," Clarendon Press, Oxford 2004

[4] S. Dimopoulos and G. Landsberg, "Black holes at the LHC," Phys. Rev. Lett. **87** (2001) 161602 [arXiv:hep-ph/0106295].

[5] S. B. Giddings and S. Thomas, "High energy colliders as black hole factories: The end of short distance physics," Phys. Rev. D **65**, 056010 (2002) [arXiv:hep-ph/0106219].

[6] P. Kanti, "Black holes in theories with large extra dimensions: A review," Int. J. Mod. Phys. A **19**, 4899 (2004) [arXiv:hep-ph/0402168].

[7] V. A. Rubakov and M. E. Shaposhnikov, "Do We Live Inside A Domain Wall?," Phys. Lett. B **125** (1983) 136.

[8] G. R. Dvali and M. A. Shifman, "Domain walls in strongly coupled theories," Phys. Lett. B **396** (1997) 64 [Erratum-ibid. B **407** (1997) 452] [arXiv:hep-th/9612128].

[9] C. D. Hoyle, D. J. Kapner, B. R. Heckel, E. G. Adelberger, J. H. Gundlach, U. Schmidt and H. E. Swanson, "Sub-millimeter tests of the gravitational inverse-square law," Phys. Rev. D **70** (2004) 042004 [arXiv:hep-ph/0405262].

[10] J. Polchinski, "Lectures on D-branes," arXiv:hep-th/9611050.

[11] N. Arkani-Hamed, S. Dimopoulos and G. R. Dvali, "The hierarchy problem and new dimensions at a millimeter," Phys. Lett. B **429** (1998) 263 [arXiv:hep-ph/9803315].

[12] L. Randall and R. Sundrum, "An alternative to compactification," Phys. Rev. Lett. **83**, 4690 (1999) [arXiv:hep-th/9906064].

[13] L. Randall and R. Sundrum, "A large mass hierarchy from a small extra dimension," Phys. Rev. Lett. **83**, 3370 (1999) [arXiv:hep-ph/9905221].

[14] G. R. Dvali, G. Gabadadze and M. Porrati, "4D gravity on a brane in 5D Minkowski space," Phys. Lett. B **485** (2000) 208 [arXiv:hep-th/0005016].

[15] T. G. Rizzo, "Pedagogical introduction to extra dimensions," arXiv:hep-ph/0409309.

[16] T. R. Taylor and G. Veneziano, "Strings And D = 4," Phys. Lett. B **212** (1988) 147.

[17] K. R. Dienes, E. Dudas and T. Gherghetta, "Grand unification at intermediate mass scales through extra dimensions," Nucl. Phys. B **537** (1999) 47 [arXiv:hep-ph/9806292].

[18] N. Arkani-Hamed, H. C. Cheng, B. A. Dobrescu and L. J. Hall, "Self-breaking of the standard model gauge symmetry," Phys. Rev. D **62** (2000) 096006 [arXiv:hep-ph/0006238].

[19] G. Gabadadze, "ICTP lectures on large extra dimensions," arXiv:hep-ph/0308112.

[20] G. F. Giudice, R. Rattazzi and J. D. Wells, "Quantum gravity and extra dimensions at high-energy colliders," Nucl. Phys. B **544**, 3 (1999) [arXiv:hep-ph/9811291].

[21] W. Heisenberg, Zeitschrift.f.Ph. **110** 251 (1938)

[22] W. Heisenberg, Sovlay Berlin 1939, Kapitel 3, 4

[23] R. P. Feynman, "Quantum Theory Of Gravitation," Acta Phys. Polon. **24** (1963) 697.

[24] B. S. DeWitt, "Quantum Theory Of Gravity. II. The Manifestly Covariant Theory," Phys. Rev. **162**, 1195 (1967).

[25] G. 't Hooft, "An Algorithm For The Poles At Dimension Four In The Dimensional Regularization Procedure," Nucl. Phys. B **62** (1973) 444.

[26] G. 't Hooft and M. J. G. Veltman, "One Loop Divergencies In The Theory Of Gravitation," Annales Poincare Phys. Theor. A **20** (1974) 69.

[27] S. Deser and P. van Nieuwenhuizen, "One Loop Divergences Of Quantized Einstein-Maxwell Fields," Phys. Rev. D **10**, 401 (1974).

[28] S. Deser and P. van Nieuwenhuizen, "Nonrenormalizability Of The Quantized Dirac - Einstein System," Phys. Rev. D **10**, 411 (1974).

[29] M. H. Goroff and A. Sagnotti, "Quantum Gravity At Two Loops," Phys. Lett. B **160**, 81 (1985).

[30] M. H. Goroff and A. Sagnotti, "The Ultraviolet Behavior Of Einstein Gravity," Nucl. Phys. B **266**, 709 (1986).

[31] A. E. M. van de Ven, "Two loop quantum gravity," Nucl. Phys. B **378** (1992) 309.

[32] S. Sakata, H. Umezawa and S. Kamefuchi, "On The Structure Of The Interaction Of The Elementary Particles. I: The Prog. Theor. Phys. **7** (1952) 377.

[33] M. E. Peskin and D. V. Schroeder, "An Introduction to quantum field theory,"

[34] S. Weinberg, "The Quantum theory of fields. Vol. 1: Foundations,"

[35] S. Deser, "Quantum Gravity: Whence, Whither," 'Trends in Theoretical Physics', Ed. by Paul J. Ellis & Y.C. Tang, Addison-Wesley, 1989. In *Ellis, P.J. (ed.), Tang, Y.C. (ed.): Trends in theoretical physics, vol. 1* 175-191, BRX-TH-271

[36] S. Weinberg, "Phenomenological Lagrangians," Physica A **96** (1979) 327.

[37] S. Weinberg, "The quantum theory of fields. Vol. 2: Modern applications,"

[38] J. F. Donoghue, "Leading quantum correction to the Newtonian potential," Phys. Rev. Lett. **72**, 2996 (1994) [arXiv:gr-qc/9310024].

[39] J. F. Donoghue, "General relativity as an effective field theory: The leading quantum corrections," Phys. Rev. D **50**, 3874 (1994) [arXiv:gr-qc/9405057].

[40] J. F. Donoghue, "Introduction to the Effective Field Theory Description of Gravity," arXiv:gr-qc/9512024.

[41] N. E. J. Bjerrum-Bohr, "Quantum gravity, effective fields and string theory,", PhD thesis arXiv:hep-th/0410097.

[42] S. Weinberg, in *General Relativity: An Einstein centenary survey*, Eds. S. W. Hawking and W. Israel, Cambridge University Press (1979), p.790

[43] M. Gell-Mann and F. E. Low, "Quantum Electrodynamics At Small Distances," Phys. Rev. **95** (1954) 1300.

[44] E. C. G. Stueckelberg and A. Petermann, "Normalization Of Constants In The Quanta Theory," Helv. Phys. Acta **26** (1953) 499.

[45] E. Brezin and J. Zinn-Justin, "Renormalization Of The Nonlinear Sigma Model In 2 + Epsilon Dimensions. Phys. Rev. Lett. **36** (1976) 691.

[46] D. J. Gross and A. Neveu, "Dynamical Symmetry Breaking In Asymptotically Free Field Theories," Phys. Rev. D **10** (1974) 3235.

[47] K. Gawedzki and A. Kupiainen, "Renormalizing The Nonrenormalizable," Phys. Rev. Lett. **55** (1985) 363.

[48] B. Rosenstein, B. J. Warr and S. H. Park, "The Four Fermi Theory Is Renormalizable In (2+1)-Dimensions," Phys. Rev. Lett. **62**, 1433 (1989).

[49] K. G. Wilson, "Renormalization Group And Critical Phenomena. 1. Renormalization Group And The Kadanoff Scaling Picture," Phys. Rev. B **4** (1971) 3174.

[50] K. G. Wilson, "Renormalization Group And Critical Phenomena. 2. Phase Space Cell Analysis Phys. Rev. B **4** (1971) 3184.

[51] K. G. Wilson and J. B. Kogut, "The Renormalization Group And The Epsilon Expansion," Phys. Rept. **12** (1974) 75.

[52] K. G. Wilson, "The Renormalization Group: Critical Phenomena And The Kondo Problem," Rev. Mod. Phys. **47** (1975) 773.

[53] D. F. Litim, "Universality and the renormalisation group," arXiv:hep-th/0503096.

[54] C. Wetterich, "Average Action And The Renormalization Group Equations," Nucl. Phys. B **352** (1991) 529.

[55] L. P. Kadanoff, "Scaling Laws For Ising Models Near T(C)," Physics **2** (1966) 263.

[56] C. Wetterich, "Exact evolution equation for the effective potential," Phys. Lett. B **301** (1993) 90.

[57] J. Polchinski, "Renormalization And Effective Lagrangians," Nucl. Phys. B **231**, 269 (1984).

[58] C. Bagnuls and C. Bervillier, "Exact renormalization group equations: An introductory review," Phys. Rept. **348** (2001) 91 [arXiv:hep-th/0002034].

[59] D. F. Litim and J. M. Pawlowski, "Perturbation theory and renormalisation group equations," Phys. Rev. D **65** (2002) 081701 [arXiv:hep-th/0111191].

[60] D. F. Litim and J. M. Pawlowski, "Completeness and consistency of renormalisation group flows," Phys. Rev. D **66** (2002) 025030 [arXiv:hep-th/0202188].

[61] S. Bornholdt and C. Wetterich, "Average action for models with fermions," Z. Phys. C **58** (1993) 585.

[62] C. Wetterich, "The Average action for scalar fields near phase transitions," Z. Phys. C **57**, 451 (1993).

[63] B. Bergerhoff, F. Freire, D. Litim, S. Lola and C. Wetterich, "Phase diagram of superconductors," Phys. Rev. B **53** (1996) 5734 [arXiv:hep-ph/9503334].

[64] F. Hofling, C. Nowak and C. Wetterich, "Phase transition and critical behaviour of the d = 3 Gross-Neveu model," Phys. Rev. B **66**, 205111 (2002) [arXiv:cond-mat/0203588].

[65] C. Wetterich, "Bosonic effective action for interacting fermions," arXiv:cond-mat/0208361.

[66] V. Branchina, "RG generated fermion mass," Phys. Lett. B **549** (2002) 260 [arXiv:hep-ph/0101157].

[67] J. Jaeckel and C. Wetterich, "First order chiral phase transition from a six-fermion 'instanton' interaction," Nucl. Phys. A **733**, 113 (2004) [arXiv:hep-ph/0309101].

[68] D. Litim, C. Wetterich and N. Tetradis, "Nonperturbative analysis of the Coleman-Weinberg phase transition," Mod. Phys. Lett. A **12** (1997) 2287 [arXiv:hep-ph/9407267].

[69] M. Reuter and C. Wetterich, "Average action for the Higgs model with Abelian gauge symmetry," Nucl. Phys. B **391** (1993) 147.

[70] M. Reuter and C. Wetterich, "Running gauge coupling in three-dimensions and the electroweak phase transition," Nucl. Phys. B **408** (1993) 91.

[71] D. U. Jungnickel and C. Wetterich, "Effective action for the chiral quark-meson model," Phys. Rev. D **53**, 5142 (1996) [arXiv:hep-ph/9505267].

[72] J. Jaeckel, "Effective actions for strongly interacting fermionic systems," arXiv:hep-ph/0309090.

[73] H. Gies and J. Jaeckel, "Renormalization flow of QED," Phys. Rev. Lett. **93**, 110405 (2004) [arXiv:hep-ph/0405183].

[74] H. Gies and C. Wetterich, "Universality of spontaneous chiral symmetry breaking in gauge theories," Phys. Rev. D **69**, 025001 (2004) [arXiv:hep-th/0209183].

[75] H. Gies, J. Jaeckel and C. Wetterich, "Towards a renormalizable standard model without fundamental Higgs scalar," Phys. Rev. D **69**, 105008 (2004) [arXiv:hep-ph/0312034].

[76] M. C. Birse, B. Krippa, J. A. McGovern and N. R. Walet, "Pairing in many-fermion systems: An exact renormalisation group treatment," Phys. Lett. B **605** (2005) 287 [arXiv:hep-ph/0406249].

[77] J. P. Blaizot, R. M. Galain and N. Wschebor, "Non Perturbative Renormalization Group, momentum dependence of n-point functions and the transition temperature of the weakly interacting Bose gas," arXiv:cond-mat/0412481.

[78] U. Ellwanger and C. Wetterich, "Evolution equations for the quark - meson transition," Nucl. Phys. B **423**, 137 (1994) [arXiv:hep-ph/9402221].

[79] J. M. Pawlowski, D. F. Litim, S. Nedelko and L. von Smekal, "Infrared behaviour and fixed points in Landau gauge QCD," Phys. Rev. Lett. **93**, 152002 (2004) [arXiv:hep-th/0312324].

[80] J. Berges, N. Tetradis and C. Wetterich, "Non-perturbative renormalization flow in quantum field theory and statistical physics," Phys. Rept. **363** (2002) 223 [arXiv:hep-ph/0005122].

[81] C. Wetterich, "Effective average action in statistical physics and quantum field theory," Int. J. Mod. Phys. A **16** (2001) 1951 [arXiv:hep-ph/0101178];

[82] D. F. Litim, "Derivative expansion and renormalisation group flows," JHEP **0111** (2001) 059 [arXiv:hep-th/0111159].

[83] S. B. Liao, J. Polonyi and M. Strickland, "Optimization of renormalization group flow," Nucl. Phys. B **567** (2000) 493 [arXiv:hep-th/9905206].

[84] D. F. Litim, "Optimisation of the exact renormalisation group," Phys. Lett. B **486** (2000) 92 [arXiv:hep-th/0005245];

[85] D. F. Litim, "Mind the gap," Int. J. Mod. Phys. A **16** (2001) 2081 [arXiv:hep-th/0104221];

[86] D. F. Litim, "Optimised renormalisation group flows," Phys. Rev. D **64** (2001) 105007 [arXiv:hep-th/0103195].

[87] D. F. Litim, "Convergence and stability of the renormalisation group," arXiv:hep-th/0208117.

[88] D. F. Litim, "Critical exponents from optimised renormalisation group flows," Nucl. Phys. B **631** (2002) 128 [arXiv:hep-th/0203006].

[89] D. F. Litim and L. Vergara, "Subleading critical exponents from the renormalisation group," Phys. Lett. B **581** (2004) 263 [arXiv:hep-th/0310101].

[90] D. F. Litim and J. M. Pawlowski, "Flow equations for Yang-Mills theories in general axial gauges," Phys. Lett. B **435** (1998) 181 [arXiv:hep-th/9802064].

[91] D. F. Litim and J. M. Pawlowski, "On gauge invariance and Ward identities for the Wilsonian renormalisation group," Nucl. Phys. Proc. Suppl. **74** (1999) 325 [arXiv:hep-th/9809020].

[92] M. Reuter and C. Wetterich, "Effective average action for gauge theories and exact evolution equations," Nucl. Phys. B **417** (1994) 181.

[93] U. Ellwanger, M. Hirsch and A. Weber, "Flow equations for the relevant part of the pure Yang-Mills action," Z. Phys. C **69** (1996) 687 [arXiv:hep-th/9506019].

[94] D. F. Litim and J. M. Pawlowski, "On gauge invariant Wilsonian flows," Phys.Lett.B **435**, 181 (1998), [arXiv:hep-th/9901063].

[95] F. Freire, D. F. Litim and J. M. Pawlowski, "Gauge invariance and background field formalism in the exact renormalisation group," Phys. Lett. B **495** (2000) 256 [arXiv:hep-th/0009110].

[96] L. F. Abbott, "Introduction To The Background Field Method," Acta Phys. Polon. B **13** (1982) 33.

[97] A. Rebhan and G. Wirthumer, "On The Equivalence Of The Background Field Method," Z. Phys. C **28** (1985) 269.

[98] F. Freire and C. Wetterich, "The Ward Identity from the Background Field Dependence of the Effective Action," Phys. Lett. B **380** (1996) 337 [arXiv:hep-th/9601081].

[99] F. Freire, D. F. Litim and J. M. Pawlowski, "Gauge invariance, background fields and modified Ward identities," Int. J. Mod. Phys. A **16** (2001) 2035 [arXiv:hep-th/0101108].

[100] D. F. Litim and J. M. Pawlowski, "Wilsonian flows and background fields," Phys. Lett. B **546** (2002) 279 [arXiv:hep-th/0208216].

[101] M. Reuter, "Nonperturbative Evolution Equation for Quantum Gravity," Phys. Rev. D **57** (1998) 971 [arXiv:hep-th/9605030].

[102] S. Falkenberg and S. D. Odintsov, "Gauge dependence of the effective average action in Einstein gravity," Int. J. Mod. Phys. A **13** (1998) 607 [arXiv:hep-th/9612019].

[103] O. Lauscher and M. Reuter, "Ultraviolet fixed point and generalized flow equation of quantum gravity," Phys. Rev. D **65** (2002) 025013 [arXiv:hep-th/0108040].

[104] M. Reuter and C. Wetterich, "Exact evolution equation for scalar electrodynamics," Nucl. Phys. B **427** (1994) 291.

[105] P. B. Gilkey, "The Spectral Geometry Of A Riemannian Manifold," J. Diff. Geom. **10** (1975) 601; "Invariance theory, the heat equation and the Atiyah-Singer index theorem," CRC Press, Boca Raton 1995.

[106] J. W. York, Jr., "Conformal invariant orthogonal decomposition of symmetric tensors on Riemannian manifolds and the intial-value problem of general relativity," J. Math. Phys. **14**, 456 (1973)

[107] W. Souma, "Non-trivial ultraviolet fixed point in quantum gravity," Prog. Theor. Phys. **102** (1999) 181 [arXiv:hep-th/9907027].

[108] M. Reuter and F. Saueressig, "Renormalization group flow of quantum gravity in the Einstein-Hilbert truncation," Phys. Rev. D **65** (2002) 065016 [arXiv:hep-th/0110054].

[109] O. Lauscher and M. Reuter, "Is quantum Einstein gravity nonperturbatively renormalizable?," Class. Quant. Grav. **19** (2002) 483 [arXiv:hep-th/0110021].

[110] O. Lauscher and M. Reuter, "Towards nonperturbative renormalizability of quantum Einstein gravity," Int. J. Mod. Phys. A **17** (2002) 993 [arXiv:hep-th/0112089].

[111] O. Lauscher and M. Reuter, "Flow equation of quantum Einstein gravity in a higher-derivative truncation," Phys. Rev. D **66** (2002) 025026.

[112] L. N. Granda, "Nonperturbative renormalization group for Einstein gravity with matter," Europhys. Lett. **42** (1998) 487 [arXiv:hep-th/0501225].

[113] R. Percacci and D. Perini, "Constraints on matter from asymptotic safety," Phys. Rev. D **67** (2003) 081503 [arXiv:hep-th/0207033].

[114] R. Percacci and D. Perini, "Asymptotic safety of gravity coupled to matter," Phys. Rev. D **68** (2003) 044018 [arXiv:hep-th/0304222].

[115] M. Reuter and F. Saueressig, "A class of nonlocal truncations in quantum Einstein gravity and its renormalization group behavior," Phys. Rev. D **66** (2002) 125001 [arXiv:hep-th/0206145].

[116] M. Reuter and F. Saueressig, "Nonlocal quantum gravity and the size of the universe," Fortsch. Phys. **52** (2004) 650 [arXiv:hep-th/0311056].

[117] T. R. Taylor and G. Veneziano, "Quantum Gravity At Large Distances And The Cosmological Constant," Nucl. Phys. B **345**, 210 (1990).

[118] T. R. Taylor and G. Veneziano, "Quenching The Cosmological Constant," Phys. Lett. B **228**, 311 (1989).

[119] H. W. Hamber, "On the gravitational scaling dimensions," Phys. Rev. D **61**, 124008 (2000) [arXiv:hep-th/9912246].

[120] H. W. Hamber, "Scaling dimensions of lattice quantized gravity," arXiv:hep-th/0101175.

[121] H. W. Hamber and G. Kagel, "Exact Bianchi Identity in Regge Gravity," Class. Quant. Grav. **21**, 5915 (2004) [arXiv:gr-qc/0107031].

[122] H. W. Hamber and R. M. Williams, "Non-perturbative gravity and the spin of the lattice graviton," Phys. Rev. D **70**, 124007 (2004) [arXiv:hep-th/0407039].

[123] P. Forgacs and M. Niedermaier, "A fixed point for truncated quantum Einstein gravity," arXiv:hep-th/0207028.

[124] M. Reuter and H. Weyer, "Renormalization group improved gravitational actions: A Brans-Dicke approach," Phys. Rev. D **69** (2004) 104022 [arXiv:hep-th/0311196].

[125] A. Bonanno and M. Reuter, "Cosmology of the Planck era from a renormalization group for quantum gravity," Phys. Rev. D **65** (2002) 043508 [arXiv:hep-th/0106133].

[126] A. Babic, B. Guberina, R. Horvat and H. Stefancic, "Renormalization-group running cosmologies: A scale-setting procedure," arXiv:astro-ph/0407572.

[127] A. Bonanno and M. Reuter, "Cosmological perturbations in renormalization group derived cosmologies," Int. J. Mod. Phys. D **13** (2004) 107 [arXiv:astro-ph/0210472].

[128] A. Bonanno and M. Reuter, "Quantum gravity effects near the null black hole singularity," Phys. Rev. D **60** (1999) 084011 [arXiv:gr-qc/9811026].

[129] A. Bonanno and M. Reuter, "Renormalization group improved black hole spacetimes," Phys. Rev. D **62** (2000) 043008 [arXiv:hep-th/0002196].

[130] M. Reuter and H. Weyer, "Quantum gravity at astrophysical distances?," JCAP **0412**, 001 (2004) [arXiv:hep-th/0410119].

[131] M. Reuter and H. Weyer, "Running Newton constant, improved gravitational actions, and galaxy rotation curves," Phys. Rev. D **70**, 124028 (2004) [arXiv:hep-th/0410117].

[132] A. Bonanno and M. Reuter, "Cosmology with self-adjusting vacuum energy density from a renormalization group fixed point," Phys. Lett. B **527** (2002) 9 [arXiv:astro-ph/0106468].

[133] E. Bentivegna, A. Bonanno and M. Reuter, "Confronting the IR Fixed Point Cosmology with High Redshift Supernova Data," JCAP **0401**, 001 (2004) [arXiv:astro-ph/0303150].

[134] D. F. Litim, "Fixed points of quantum gravity," Phys. Rev. Lett. **92**, 201301 (2004) [arXiv:hep-th/0312114].

[135] H. Kawai and M. Ninomiya, "Renormalization Group And Quantum Gravity," Nucl. Phys. B **336** (1990) 115.

[136] G. F. Giudice and A. Strumia, "Constraints on extra-dimensional theories from virtual-graviton exchange," Nucl. Phys. B **663**, 377 (2003) [arXiv:hep-ph/0301232].

[137] G. F. Giudice, R. Rattazzi and J. D. Wells, "Transplanckian collisions at the LHC and beyond," Nucl. Phys. B **630**, 293 (2002) [arXiv:hep-ph/0112161].

[138] R. Rattazzi, "Transplanckian collisions at future accelerators," arXiv:hep-ph/0205265.

[139] G. F. Giudice, T. Plehn and A. Strumia, "Graviton collider effects in one and more large extra dimensions," Nucl. Phys. B **706** (2005) 455 [arXiv:hep-ph/0408320].

[140] S. Minwalla, M. Van Raamsdonk and N. Seiberg, "Noncommutative perturbative dynamics," JHEP **0002**, 020 (2000) [arXiv:hep-th/9912072].

[141] I. Chepelev and R. Roiban, "Convergence theorem for non-commutative Feynman graphs and renormalization," JHEP **0103**, 001 (2001) [arXiv:hep-th/0008090].

[142] H. Grosse and R. Wulkenhaar, "Renormalisation of phi**4 theory on noncommutative R**4 in the matrix base," arXiv:hep-th/0401128.

[143] V. Rivasseau, F. Vignes-Tourneret and R. Wulkenhaar, "Renormalization of noncommutative phi**4-theory by multi-scale analysis," arXiv:hep-th/0501036.

Lebenslauf

Dipl.Ing. Peter Leopold Fischer

Persönliche Daten

Geburtsdatum	22. Jänner 1978, Wien
Nationalität	Österreich
Familienstand	Verheiratet mit Hélène Augy-Fischer seit 31. Juli 2001
Kinder	Clemens Fischer, * 18. September 2003, Genf

Schulbildung

September 1984 – Juni 1988	Besuch der Volkschule in Wien
September 1988 – Juni 1996	Besuch des Realgymnasiums BRG 18 in Wien
Juni 1996	Matura mit ausgezeichnetem Erfolg bestanden

Präsenzdienst

Oktober 2001 – Mai 2002	Abgeleistet am Heeresdatenverarbeitungsamt

---

Studium

Oktober 1996 – Juni 2001	Diplomstudium der Technischen Physik, TU Wien
Juli, August 2000	CERN Sommer Student (PS div., Neutrino factory working group)
Juni 2001	2. Diplomprüfung mit Auszeichnung bestanden Diplomarbeit: Vertices in Spherically Reduced Quantum Gravity unter Betreuung von O.Univ.Prof.DI.Dr. W. Kummer
Juni – Dezember 2002	Forschung bei Univ.Prof.DI.Dr. M. Schweda im Rahmen des FWF Projektes P15463
Oktober 2002 – Juni 2005	Doktoratsstudium der technischen Wissenschaften an der TU Wien bei O.Univ.Prof.DI.Dr. W. Kummer
Jänner 2003 – Juni 2005	Forschung an der CERN Theory Division (Group) im Rahmen des Österreichischen CERN Doktoranden Programmes des Ministeriums für Wissenschaft, Bildung und Kultur unter lokaler Betreuung von Prof. G. Veneziano und Priv.Doz. D. Litim

---

LEHRTÄTIGKEIT
als Studienassistent (vorm. Tutor) an der TU Wien

Oktober 1998 – Februar 2000	Experimentelle Physik
März 2000 – Juni 2001	Theoretische Physik
Oktober – Dezember 2002	Theoretische Physik

PREISE UND LEISTUNGSTIPENDIEN

Mai 1995, 1996	Erster Platz der Wiener Physik-Olympiade
Juni 1996	Erster Platz der Österreichischen Physik-Olympiade
Juli 1996	Dritter Preis bei der
	27. Internationalen Physik-Olympiade in Oslo
1998, 1999, 2001	Erhalt des Leistungsstipendiums

Wien, 23. Mai 2004   Peter Fischer